

Office of the Secretary of Defense
Chief, RDD, ESD, WHS

5 USC Sec 552
and

#2

Date: 12 APR 2013 Authority: EO 13526

Declassify: X Deny in Full: _____

Declassify in Part: _____

Reason: _____

MDR: 12-M-3145

DECLASSIFIED IN FULL

Authority: EO 13526

Chief, Records & Declass Div, WHS

Date: APR 12 2013

~~CONFIDENTIAL~~

AD 346751

DEFENSE DOCUMENTATION CENTER

FOR

SCIENTIFIC AND TECHNICAL INFORMATION

CAMERON STATION ALEXANDRIA VIRGINIA



~~CONFIDENTIAL~~

RZ
12-M-3145

NOTICE: When government or other drawings, specifications or other data are used for any purpose other than in connection with a definitely related government procurement operation, the U. S. Government thereby incurs no responsibility, nor any obligation whatsoever; and the fact that the Government may have formulated, furnished, or in any way supplied the said drawings, specifications, or other data is not to be regarded by implication or otherwise as in any manner licensing the holder or any other person or corporation, or conveying any rights or permission to manufacture, use or sell any patented invention that may in any way be related thereto.

NOTICE:

~~THIS DOCUMENT CONTAINS INFORMATION
AFFECTING THE NATIONAL DEFENSE OF
THE UNITED STATES WITHIN THE MEAN-
ING OF THE ESPIONAGE LAWS, TITLE 18,
U.S.C., SECTIONS 793 and 794. THE
TRANSMISSION OR THE REVELATION OF
ITS CONTENTS IN ANY MANNER TO AN
UNAUTHORIZED PERSON IS PROHIBITED
BY LAW.~~

Page determined to be Unclassified
Reviewed Chief, ROD, WHS
IAW EO 13526, Section 3.5
Date: APR 12 2013

346751

346751

ALVIN C. B. JUC
S. H. R. J.





ELECTRONICS DIVISION

This document consists of 184 pages,
and is number 26 of 45 copies,
series A and the following 0
attachments.

TWELFTH QUARTERLY
PROGRESS REPORT

ON

DISSEMINATION OF SOLID
AND LIQUID BW AGENTS

(Unclassified Title)

For Period March 4, 1963 - June 4, 1963
Contract No. DA-18-064-CML-2745

Prepared for:

U. S. Army Biological Laboratories
Fort Detrick, Maryland

JAN 31 1964

Submitted by:

G. R. Whitnah
G. R. Whitnah
Project Manager

Report No: 2411
Project No: 82408
Date: July 10, 1963

Approved by:

S. P. Jones
S. P. Jones, Director
Aerospace Research

AEROSPACE RESEARCH
2295 Walnut Street
St. Paul 13, Minnesota

~~CONFIDENTIAL - SECURITY INFORMATION~~
~~ALL INFORMATION CONTAINED HEREIN IS UNCLASSIFIED~~
~~DATE 10-10-2013 BY 60322~~

~~CONFIDENTIAL~~

~~CONFIDENTIAL - SECURITY INFORMATION~~
~~ALL INFORMATION CONTAINED HEREIN IS UNCLASSIFIED~~
~~DATE 10-10-2013 BY 60322~~

DECLASSIFIED IN FULL
Authority: EO 13526
Chief, Records & Declass Div. WHS
Date: APR 12 2013

FOREWORD

Staff members of the Aerospace Research Department and Engineering Department who have participated in directing or performing the work reported herein include Messrs. S. P. Jones, Jr., G. Whitnah, M. Sandgren, A. Anderson, R. Lindquist, J. McGillicuddy, J. Upton, C. Hagberg, W. L. Torgeson, S. Steinberg, P. Stroom, G. Morfitt, A. T. Bauman, T. Petersen, D. Harrington, R. Ackroyd, D. Kedi, B. Schmidt, G. Lunde, R. Dahlberg, R. Kendall, E. Knutson, J. Unga, D. Stender, J. Pilney, A. Johnson, G. Leiter, C. A. Morris, and O. Durigan.

Page determined to be Unclassified
Reviewed Chief, RDD, WHS
IAW E.O. 13526, Section 3.5
Date:

APR 12 2013

~~CONFIDENTIAL~~

ABSTRACT

This Twelfth Quarterly Progress Report presents the results of work conducted at General Mills, Inc. under Contract DA-18-064-CML-2745, "Dissemination of Solid and Liquid BW Agents" during the period from March 4 to June 4, 1963.

In reporting on the continuing study of the mechanics of dry powders, data are presented which were obtained with the improved multipurpose test unit in which shear strength, tensile strength and bulk density are measured within the confines of a single isolator lab. Initial findings are discussed for an investigation of three supposedly identical Sm samples which exhibit distinctly different compaction characteristics. Particle-size distributions (Whitby) are included, which show a smaller MMD for saccharin after compaction to a compressive stress of 2.84×10^4 dynes/cm². Tests showing that the addition of Cab-o-Sil to powders increases the stress required to produce a given bulk density are described.

Experiments with beds of fluidized powders are discussed in which bed depth, degree of agglomeration, amount of segregation or attrition, and amount of carry-over were investigated.

A specific surface area of $1.53 \text{ m}^2/\text{g} \pm 7$ percent and a rugosity of 2.2 are reported for saccharin from measurements made by the BET gas adsorption method.

Results are given from experiments in which the effect of positive ions on aerosol decay was investigated in the aerosol chamber.

An investigation of the effectiveness of graphite in reducing side-wall friction of compacted powders sliding in cylinders is reported. A 50-percent reduction in the force required to eject the compacted powder has been observed when graphite is used as compared to the force required using a bare aluminum surface.

~~CONFIDENTIAL~~

~~CONFIDENTIAL~~

Wind-tunnel studies are discussed for two areas of investigation. Simulant Sm was efficiently deagglomerated at an air velocity of Mach number 0.3 and at bulk densities ranging from 0.33 to 0.52 g/cm³. Storage of compacted Sm at -2 C or -23 C for periods up to 30 days has no significant detrimental effect on deagglomeration efficiency or viability.

Progress on the fabrication of the second E-41 spray tank is discussed. Minor design changes in the E-41 are described. Plans to flight test the E-41 at Eglin AFB on the F-100D and the F-105 are mentioned.

The status of planning and preparing for flight testing the E-41 spray tank on the AO-1 Mohawk airplane is reported.

iv

~~CONFIDENTIAL~~

DECLASSIFIED IN FULL
Authority: EO 13526
Chief, Records & Declass Div, W-13
Date:

APR 12 2013

CONFIDENTIAL

TABLE OF CONTENTS

Section	Title	Page
1	INTRODUCTION	1-1
2	STUDIES OF THE MECHANICS OF DRY POWDERS	2-1
2.1	Behavior of Powders in the Compacted State	2-1
2.1.1	Shear Strength of Compacted Powders	2-1
2.1.2	Tensile Strength of Compacted Powders	2-6
2.1.3	Compaction Characteristics of 3 Sm Samples	2-16
2.1.4	Fracture of Particles during Compaction	2-18
2.1.5	Effect of Cab-o-Sil on Energy of Compaction	2-22
2.1.6	Wall-Stress Distribution	2-22
2.2	Behavior of Powders in the Uncompacted State	2-24
2.2.1	The Fluidisation Process	2-24
2.2.2	Apparatus	2-25
2.2.3	Experimental Procedure and Results	2-27
2.2.4	Conclusions and Future Work	2-32
3	PHYSICAL AND CHEMICAL CHARACTERISTICS OF THE POWDER PARTICLE	3-1
3.1	Total Surface Area	3-1
3.1.1	Total Surface Area of Saccharin	3-1
3.1.2	Analysis of Experimental Errors in the Gravimetric BET Method of Measuring Surface Areas	3-6
3.1.3	A Typical Error Analysis to Determine Controlling Errors	3-14
3.1.4	Application of the Error Analysis	3-19
3.2	Particle Shape	3-19
3.3	Agglomerate Strength	3-32
3.4	Powder-to-Metal Friction	3-32
3.5	Particle-Size Analysis of the Swirl Disperser's Output	3-32
4	AEROSOL STUDIES	4-1
4.1	Description and Operating Characteristics of the Corona-Point Ion Generator	4-1
4.2	Procedure for Electrostatic Charge Runs	4-6

CONFIDENTIAL

DECLASSIFIED IN FULL
Authority: EO 13526
Chief, Records & Declass Div, WHS
Date: APR 12 2013

~~CONFIDENTIAL~~

TABLE OF CONTENTS (continued)

Section	Title	Page
4.3	Experimental Results	4-8
4.3.1	Talc Aerosols	4-8
4.3.2	Saccharin Aerosols	4-8
4.4	Sampling of Swirl Dispenser's Output	4-11
5	EXPERIMENTS USING GRAPHITE TO REDUCE SIDE-WALL FRICTION OF COMPACTED POWDER SLIDING IN CYLINDERS	5-1
5.1	Procedure	5-1
5.2	Results	5-4
5.3	Conclusions	5-9
6	DISSEMINATION AND DEAGGLOMERATION STUDIES	6-1
6.1	General Approach	6-1
6.2	Dissemination at Low Flight Speeds	6-1
6.3	Efficient Deagglomeration with the E-41 Aircraft Disseminator	6-2
6.4	Dissemination of Stored <u>Sm</u> in the Compacted Condition	6-8
6.4.1	Wind-Tunnel Deagglomeration Tests	6-8
6.4.2	Storage Viability Tests	6-9
7	E-41 SPRAY TANK	7-1
7.1	Fabrication of the Second E-41 Spray Tank	7-1
7.2	Improved Arrangement of Components within Discharge Shroud	7-1
7.3	Removal of Heater and Low-Pressure Switch	7-2
7.4	Addition of Filling Holes in Pistons and End Plates	7-2
7.5	Flight Tests at Eglin Air Force Base	7-4
8	PREPARATIONS FOR FLIGHT TESTS OF THE E-41 SPRAY TANK ON THE MOHAWK AIRCRAFT	8-1

~~CONFIDENTIAL~~

DECLASSIFIED IN FULL
Authority: EO 13526
Chief, Records & Declass Div, WNS
Date: APR 12 2013

~~CONFIDENTIAL~~

TABLE OF CONTENTS (continued)

Section	Title	Page
9	SUMMARY AND CONCLUSIONS	9-1
10	REFERENCES	10-1
APPENDIX A.	LOAD AND STRESS ANALYSIS, E-41 SPRAY TANK	
APPENDIX B.	OPTIONAL FOUR-FINNED TAIL SECTION DRAWING SK 29100-1305	

~~CONFIDENTIAL~~

DECLASSIFIED IN FULL
Authority: EO 13526
Chief: Records & Declass Div, WHS
Date: APR 12 2013

~~CONFIDENTIAL~~

LIST OF ILLUSTRATIONS

Figure	Title	Page
2-1	Multipurpose Test Unit	2-2
2-2	Close-Up of Multipurpose Test Unit Components	2-3
2-3	Main Units for Determination of Shear Strength, Tensile Strength, and Bulk Density	2-4
2-4	Close-Up of Improved Shear Strength Apparatus	2-5
2-5	Shear Strength of Talc	2-7
2-6	Shear Strength of Ground Saccharin	2-8
2-7	Shear Strength of Ground Powdered Milk	2-9
2-8	Shear Strength of Cornstarch	2-10
2-9	Comparative Shear Strength of Compacted Powders	2-11
2-10	Bulk Tensile Strength Versus Bulk Density for Powdered Sugar	2-12
2-11	Bulk Tensile Strength Versus Bulk Density for Cornstarch	2-13
2-12	Sketch of Instron Tensile Powder Sample	2-15
2-13	Compaction Stress Versus Bulk Density for <u>Sm</u>	2-17
2-14	Compaction Stress Versus Bulk Density for <u>Sm</u> (Dried)	2-19
2-15	Particle Size Distribution of Saccharin Samples	2-20
2-16	Illustrations of Deviations from Log-Log Plot of Compressive Stress Versus Density	2-21
2-17	Sketch of Apparatus for Measurement of Wall Stresses	2-23
2-18	Fluidized Bed Apparatus	2-26
2-19	Change in Fluid Velocity with ΔP in the Fluid Bed	2-28
2-20	Equilibration of Fluid Beds at Various Flow Rates	2-30

~~CONFIDENTIAL~~

DECLASSIFIED IN FULL
Authority: EO 13526
Chief, Records & Declass Div, WHS
Date: APR 12 2013

~~CONFIDENTIAL~~

LIST OF ILLUSTRATIONS (continued)

Figure	Title	Page
3.1	Saccharin Behavior	3-3
3.2	N ₂ Adsorption on Saccharin as a Function of Degassing Condition	3-4
3.3	N ₂ Adsorption by Saccharin after Various Degassing Conditions at Room Temperature	3-5
3.4	N ₂ Adsorption Isotherm on Saccharin	3-7
3.5	Uncertainty in BET Plot of N ₂ Adsorption by Saccharin	3-20
3.6	Micrograph 63-2-71, Ground Talc	3-21
3.7	Micrograph 63-4-5, Ground Talc	3-22
3.8	Micrograph 63-4-43, Ground Talc	3-23
3.9	Micrograph 63-4-44, Ground Talc	3-24
3.10	Micrograph 63-4-52, Ground Saccharin	3-25
3.11	Micrograph 63-4-48, Ground Egg Albumin	3-26
3.12	Micrograph 63-4-51, Ground Powdered Milk	3-27
3.13	Micrograph 63-4-59, <u>Sm</u> (Pool No. 7)	3-28
3.14	Micrograph 63-B-11, <u>Sm</u> (Pool No. 7)	3-29
3.15	Micrograph 63-A-31, Powdered Sugar	3-30
3.16	Micrograph 63-B-14, Unground Cornstarch	3-31
4.1	Corona-Point Ion Generator	4-1
4.2	Characteristics of the Corona-Discharge Ion Generator	4-3
4.3	Position of Ion Gun with Respect to Dispersing Gun in the Aerosol Chamber	4-4
4.4	Map of Ion Current Densities in Aerosol Chamber	4-5

~~CONFIDENTIAL~~

~~CONFIDENTIAL~~

LIST OF ILLUSTRATIONS (continued)

Figure	Title	Page
4.5	Modes of Ion Injection	4-7
4.6	Half Lives, Initial Amplitudes, and Prevailing Humidity for Talc Aerosol Electrostatic Charge Runs	4-9
4.7	Half Lives, Initial Amplitude, and Prevailing Humidity for Saccharin Aerosol Electrostatic Charge Runs	4-10
4.8	Gas Flow Characteristics of the Swirl Disperser	4-12
5.1	Schematic Diagram of Arrangement Used to Compact Powder into a Cylinder and to Determine the Force Required to Translate the Compacted Powder through the Cylinder	5-3
5.2	Comparison of Force to Eject Compacted Talc from a 6-Inch Diameter Aluminum Cylinder with and without Graphite	5-5
5.3	Comparison of Force to Eject Compacted Powdered Sugar from a 6-Inch Diameter Aluminum Cylinder with Graphite and a 7.5-Inch Diameter Aluminum Cylinder without Graphite	5-6
5.4	Comparison of Force to Eject Compacted Talc from a 6-Inch Diameter Aluminum Cylinder for Various Methods of Applying Graphite for Lubrication	5-7
6.1	Concentration of Fine Sm Aerosol Cloud in Wind Tunnel as a Function of Bulk Density (Airstream Mach Number 0.3; Sampling Probe Positioned 0.5 Inch from Wall)	6-3
6.2	Concentration of Fine Sm Aerosol Cloud in Wind Tunnel as a Function of Bulk Density and Airstream Mach Number (Sampling Probe Positioned 0.5 Inch from Wall)	6-4
6.3	Flight Speed Required for Dissemination of Dry, Compacted Sm Simulant (Lot S1-Sm-342) at Approximately 90 Percent Deagglomeration Efficiency	6-6
6.4	Energy Required to Compact Sm (Lot S1-Sm-342)	6-7
7.1	Housing for Components within the Discharge Shroud	7-3

x

~~CONFIDENTIAL~~

DECLASSIFIED IN FULL
Authority: EO 13526
Chief, Records & Declass Div, WHS
Date:

APR 12 2013

~~CONFIDENTIAL~~

TWELFTH QUARTERLY PROGRESS REPORT
ON
DISSEMINATION OF SOLID AND LIQUID BW AGENTS

1. INTRODUCTION

This is the twelfth of a series of quarterly progress reports which have been submitted to the Biological Laboratories as documentation of the work being performed by General Mills, Inc. under Contract DA-18-064-CML-2745. This work pertains to the dissemination of solid and liquid BW agents, and ranges from experimental and theoretical studies of the properties of finely-divided solids to the fabrication and field testing of full-scale disseminators. Much of the work is of a continuing nature, and reference to previous quarterly progress reports is necessary to provide the complete coverage of the subject.

A primary objective was to develop a spray tank to be carried as an external store for line-source dissemination of dry BW agents from aircraft flying at high subsonic speeds. The E-41 spray tank was developed to satisfy this objective, and flight trials have demonstrated that the tank performs very well at a speed of Mach 0.7. Tests are now planned in which the E-41 will be flown on the AO-1 Mohawk aircraft at a speed of 200 knots (Mach 0.3). Dissemination and deagglomeration studies conducted in the blow-down wind tunnel during the past quarter have demonstrated that compacted Sm can be efficiently aerosolized at this low flight speed if its bulk density does not exceed 0.52 g/cm^3 .

~~CONFIDENTIAL~~

DECLASSIFIED IN FULL
Authority: EO 13526
Chief, Records & Declass Div, WHS
Date: APR 12 2013

2. STUDIES OF THE MECHANICS OF DRY POWDERS

A program of study is underway to characterize the behavior of powders in the uncompacted state, their behavior during compaction, and their behavior in the compacted state. Such a study should yield information relative to the manufacture, handling, compaction, and dissemination of bulk powders. During the current quarter, we have utilized our improved multipurpose test unit and the energy-of-compaction apparatus to obtain fundamental information on a number of powders. In addition, we are looking very closely at three "similar" Sm samples to determine what characteristics are responsible for their different compaction properties. Studies are also underway to determine whether powder particles are fractured during compaction and to determine the effect of the addition of small amounts of Cab-o-Sil upon the compaction characteristics of powders. Fluid-bed experiments were conducted to determine the length of time required for a fluid bed to equilibrate, the extent of product loss during fluidization, and whether particle-size segregation results during the fluidization process.

2.1 Behavior of Powders in the Compacted State

Our completed multipurpose test unit is shown in Figures 2.1, 2.2, 2.3, and 2.4. This unit is used to measure shear strength, tensile strength, and bulk density within the confines of a single isolator lab. The newest addition, the improved sliding-disk shear-strength unit (Figure 2.4) is being used to obtain data reported in the following sections.

2.1.1 Shear Strength of Compacted Powders

To measure shear strength in the compacted state utilizing the sliding-disk method, the powder must first be compacted at a given compressive load and then sheared at some lighter load. The mechanics of this process of weight changing were sufficiently complicated to make it difficult to obtain reproducible

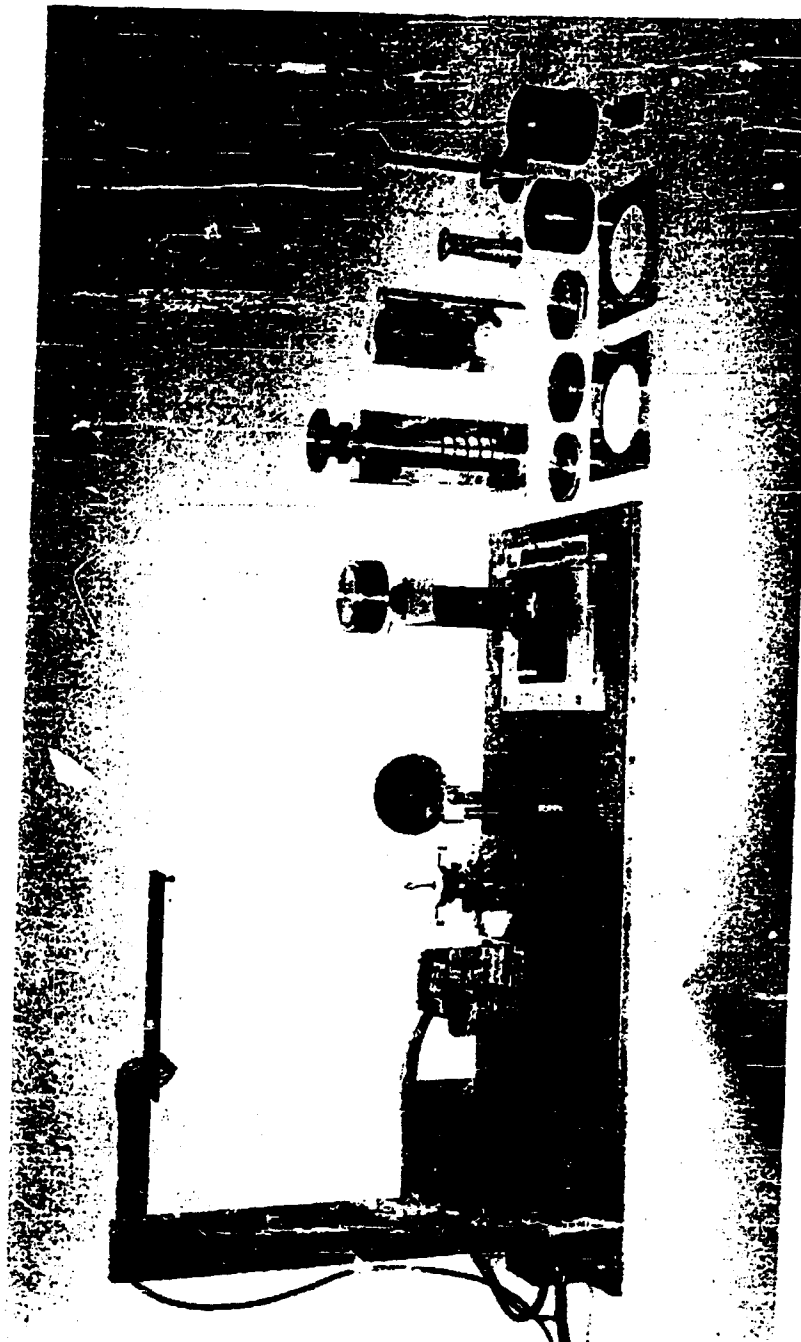


Figure 2.1 Multipurpose Test Unit

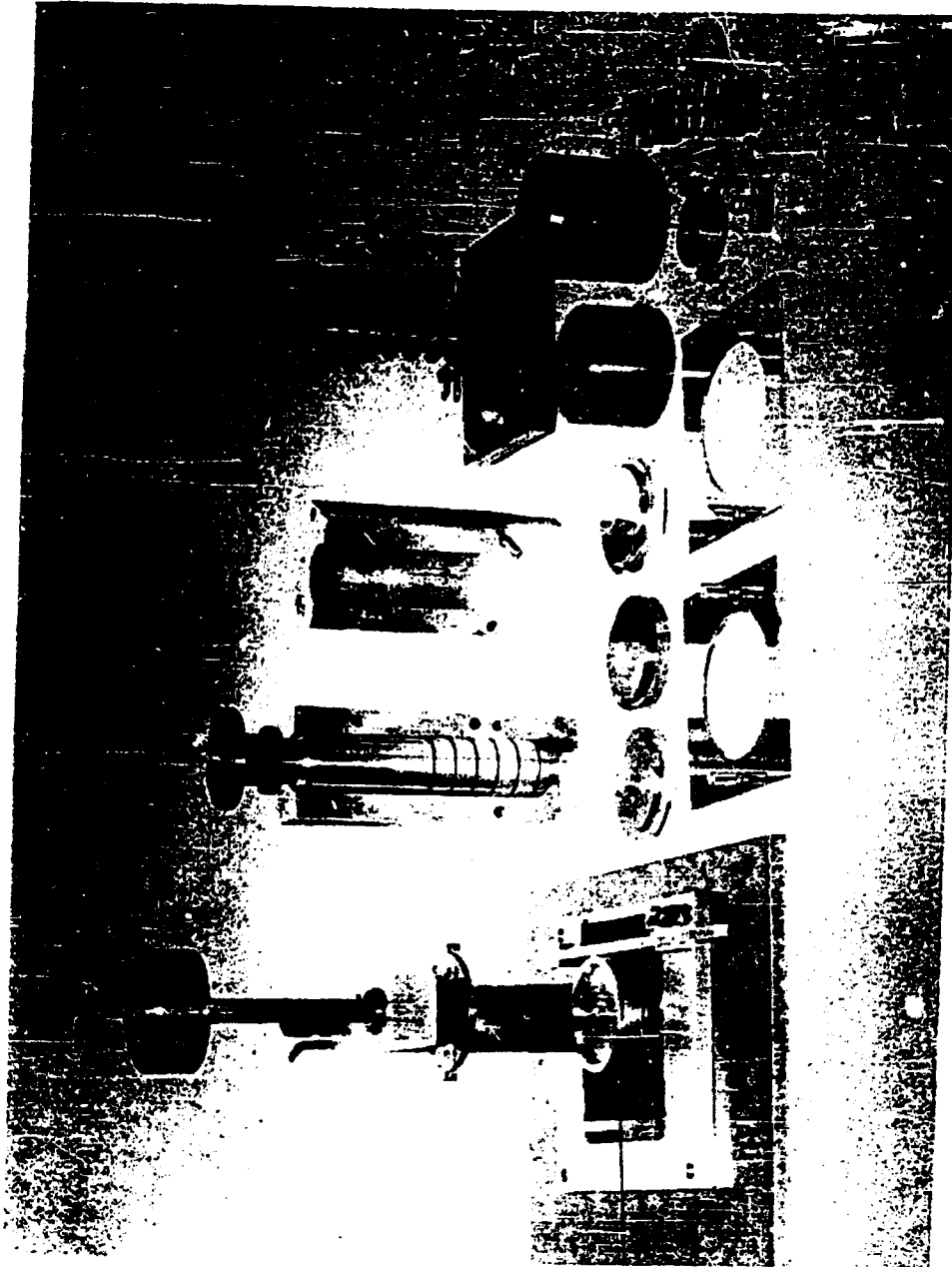


Figure 2.2 Close-up of Multipurpose Test Unit Components

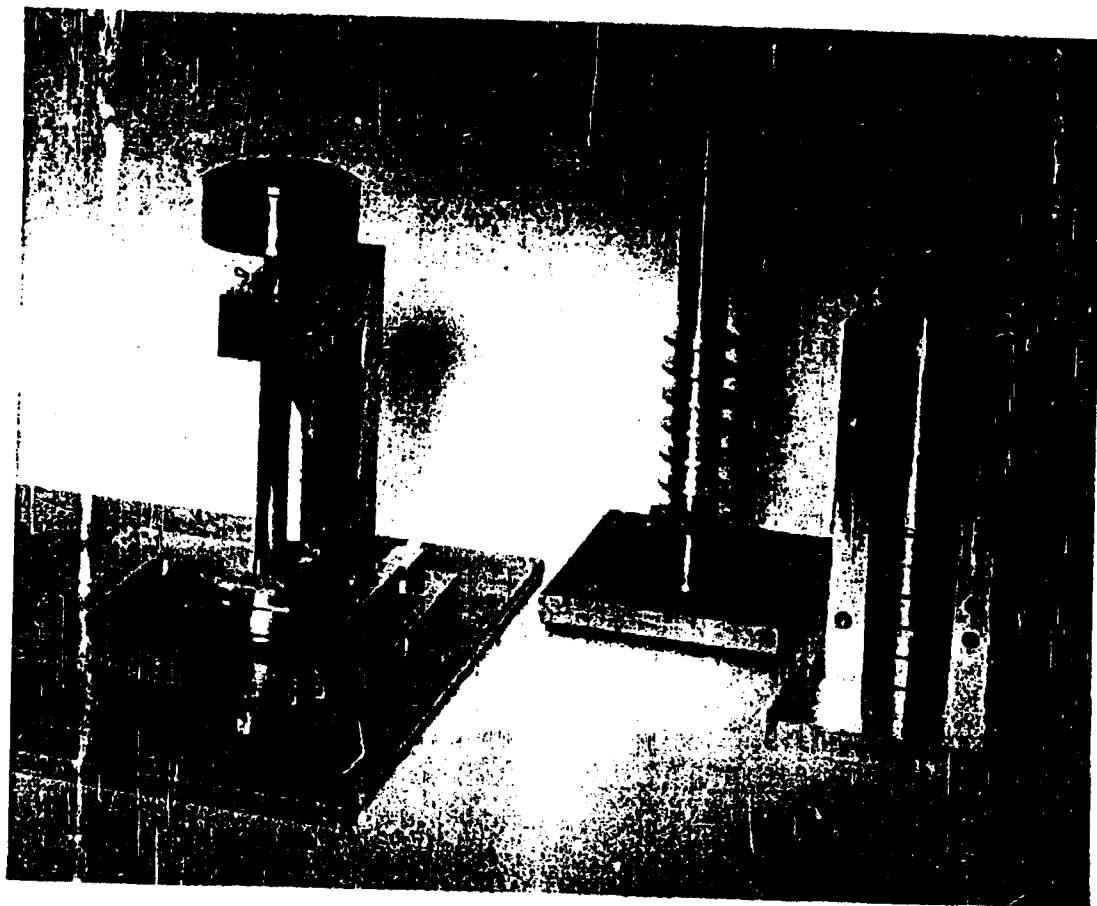


Figure 2.3 Main Units for Determination of Shear Strength, Tensile Strength, and Bulk Density

2-4

Page determined to be Unclassified
Reviewed On: ROD, VHS
IAW E.O. 13526, Section 3.5
Date: APR 12 2013

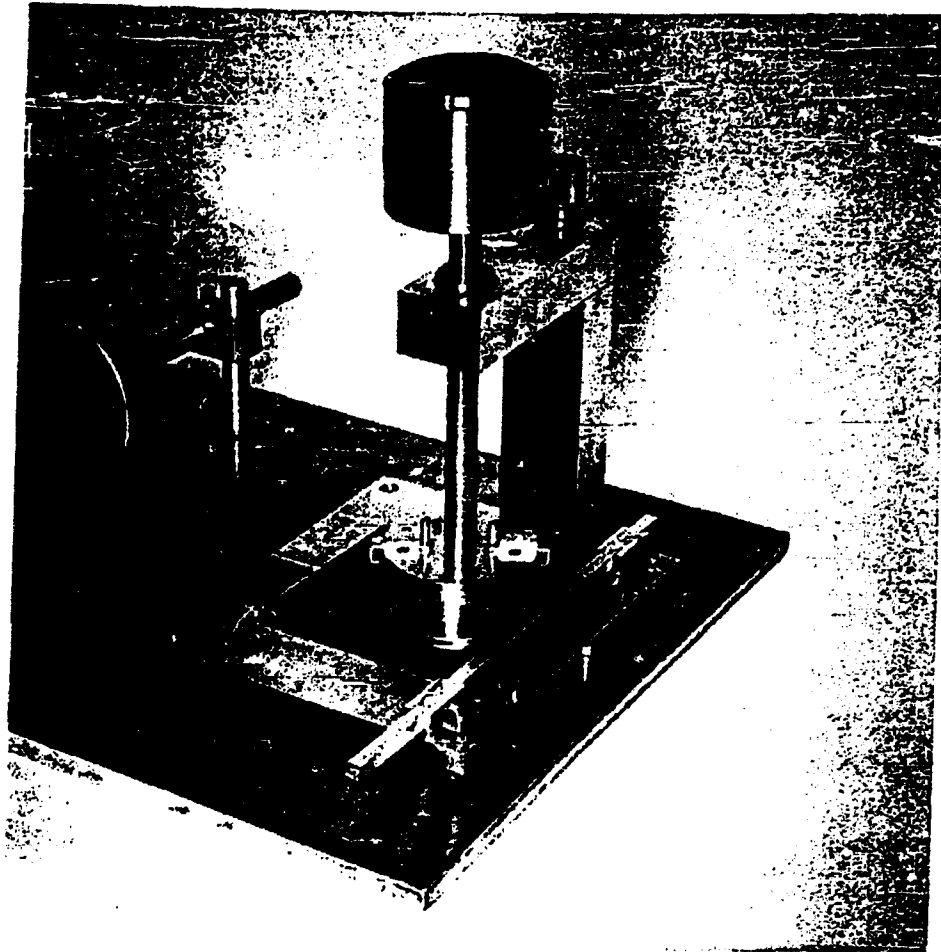


Figure 2.4 Close-up of Improved Shear Strength Apparatus

(1)
data at the lower stress levels. The improved shear-strength unit (Figure 2.4) has been completed to eliminate these difficulties, as illustrated in Figures 2.5 through 2.9. Each point plotted represents the average value for three determinations. For purposes of comparison, data for four representative powders are presented in Figure 2.9 by the method of least squares.

2.1.2 Tensile Strength of Compacted Powders

Tensile strength remains the one powder property most difficult to measure. The determination of the tensile strength is, however, of such significance to the total development of the technology of powders that the time and effort spent on its determination is well justified. We are currently investigating the segmented column and Instron triaxial tensile methods.

2.1.2.1 Segmented Column Method

The recent addition of a low-speed synchronous motor to replace the hand crank mechanism permits tensile failure of the compacted powder to take place at a more uniform rate. Because of the accuracy possible with this change in apparatus design, we feel that the data obtained are the best available from this method. Representative graphs are shown in Figures 2.10 and 2.11. Future work will include powders with diameters in the 5-micron range, such as ground egg albumin, ground powdered sugar, and Sm.

2.1.2.2 Triaxial Tensile Method

A continuing effort has been made to improve the triaxial tensile test technique that can be carried out in the Instron test machine.⁽¹⁾ Difficulties in sample preparation have retarded attempts to carry out a programmed series of tensile tests. However, several tests were conducted using powdered sugar with average densities from 0.85 to 1.02 g/cm³. Failure was found to occur in the center section where the cross-sectional area is smallest.

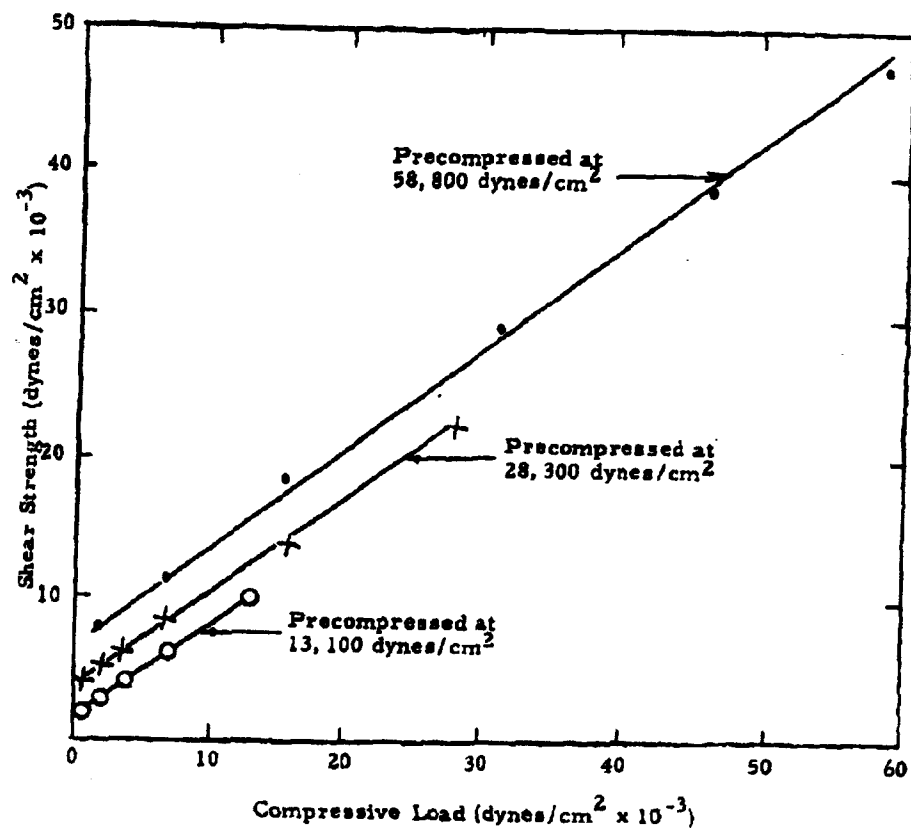


Figure 2.5 Shear Strength of Talc

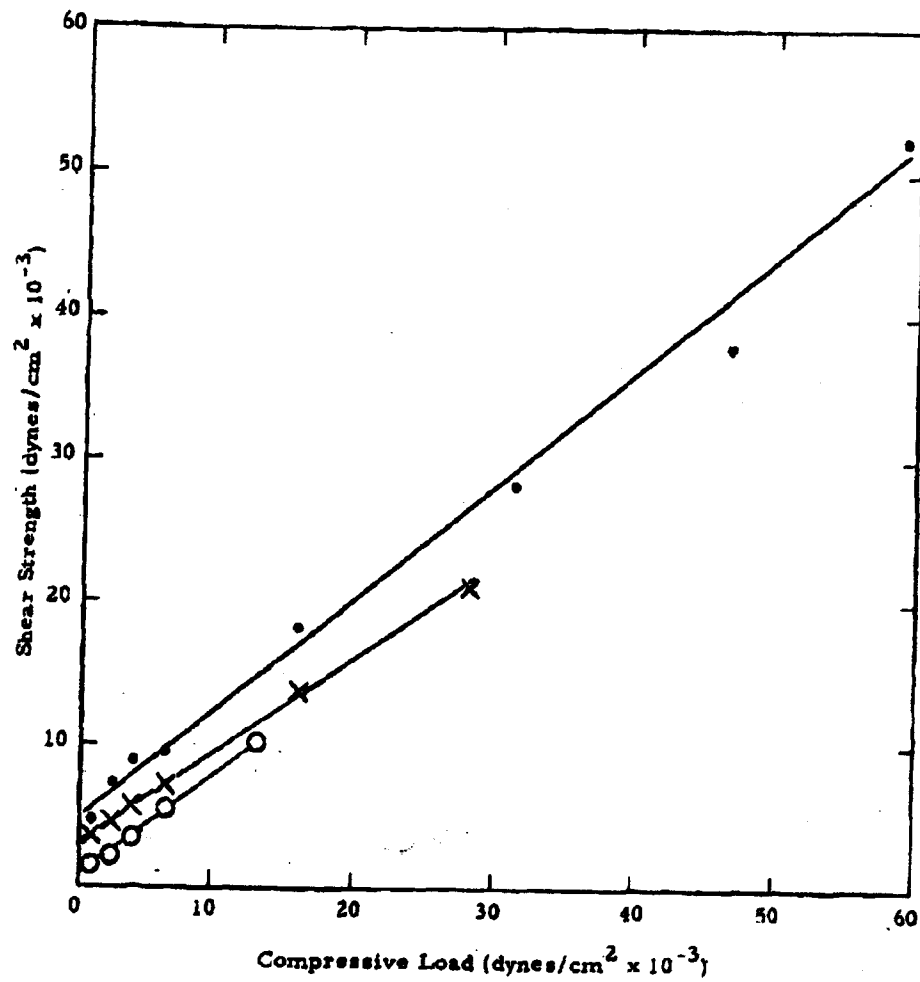


Figure 2.6 Shear Strength of Ground Saccharin

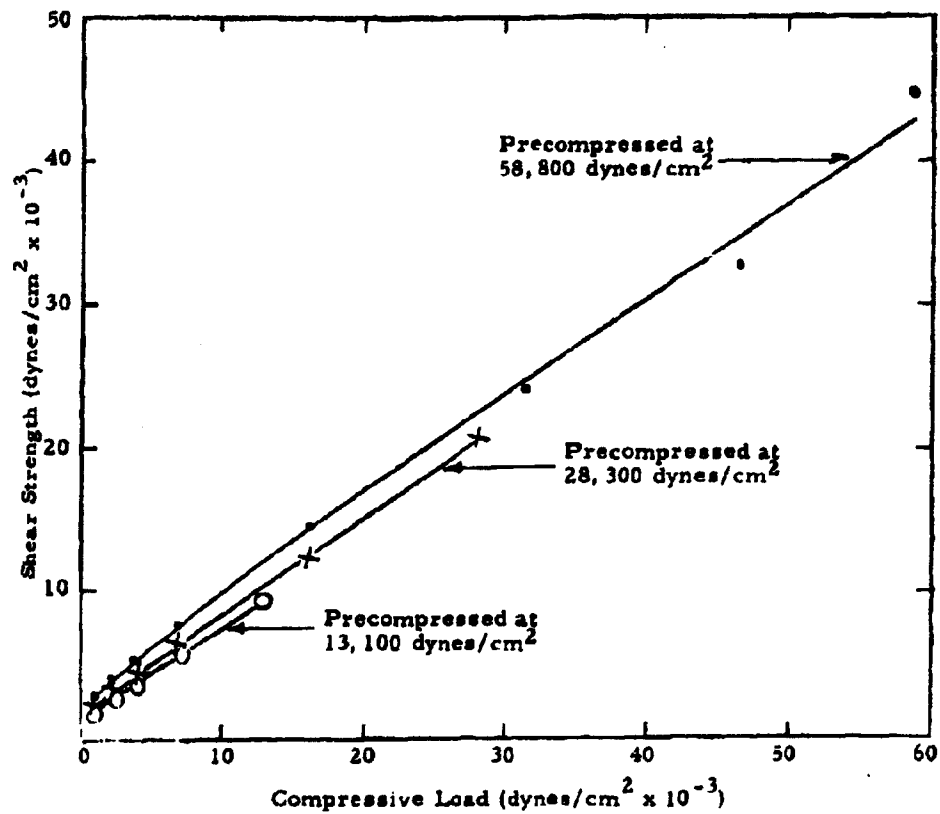


Figure 2.7 Shear Strength of Ground Powdered Milk

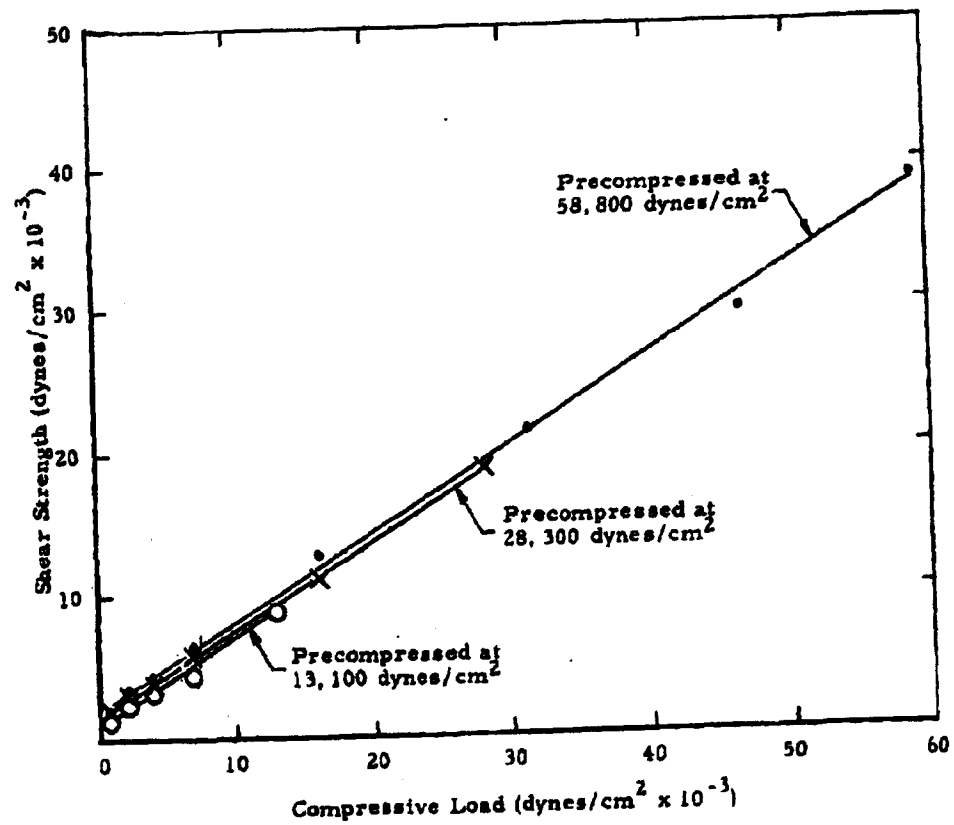


Figure 2.8 Shear Strength of Cornstarch

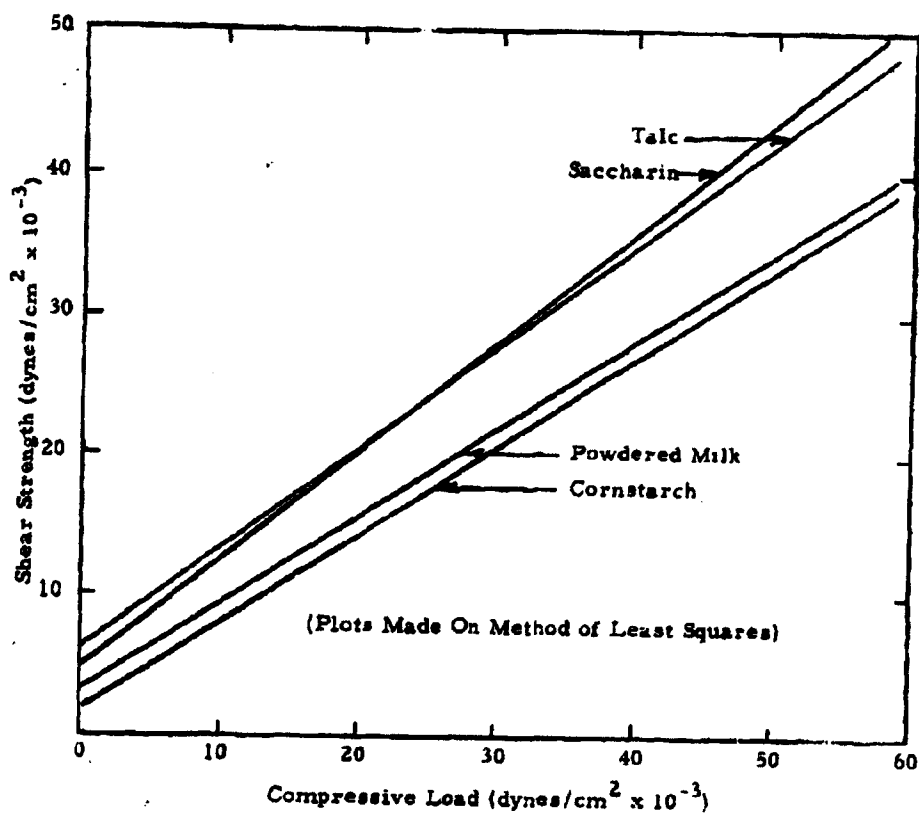


Figure 2.9 Comparative Shear Strength of Compacted Powders
(Precompressed at 58,800 dynes/cm²)

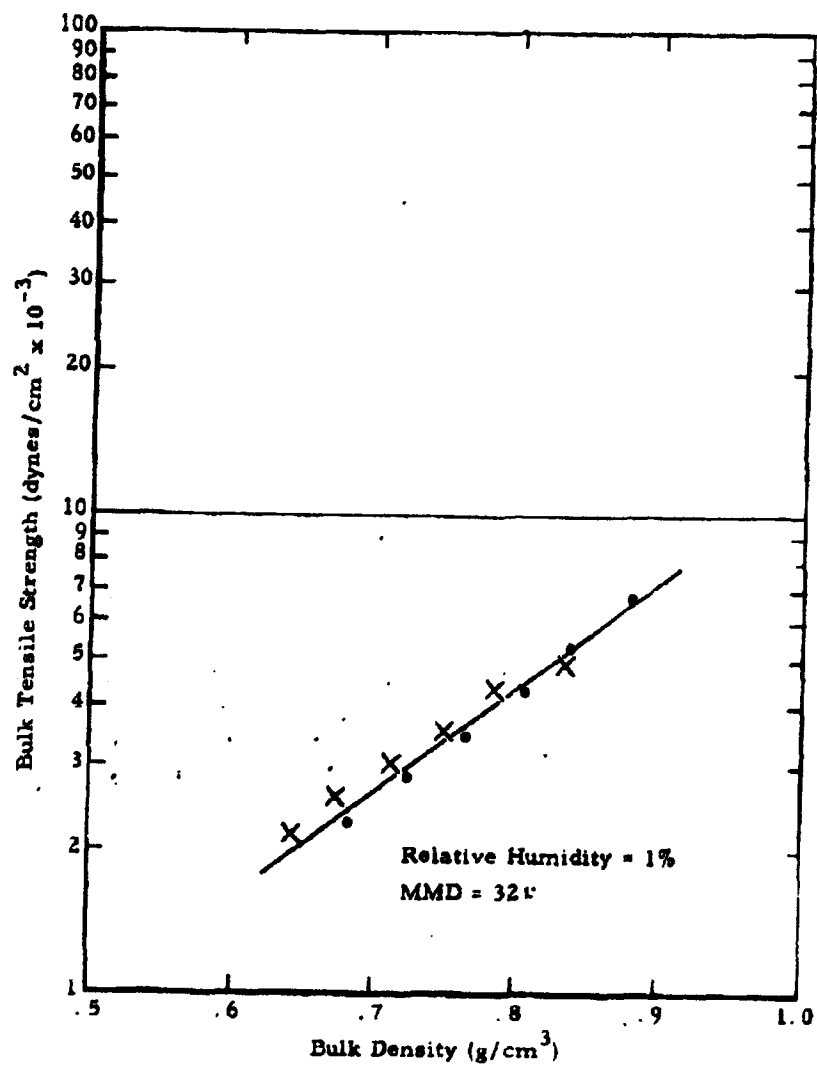


Figure 2.10 Bulk Tensile Strength Versus Bulk Density for Powdered Sugar

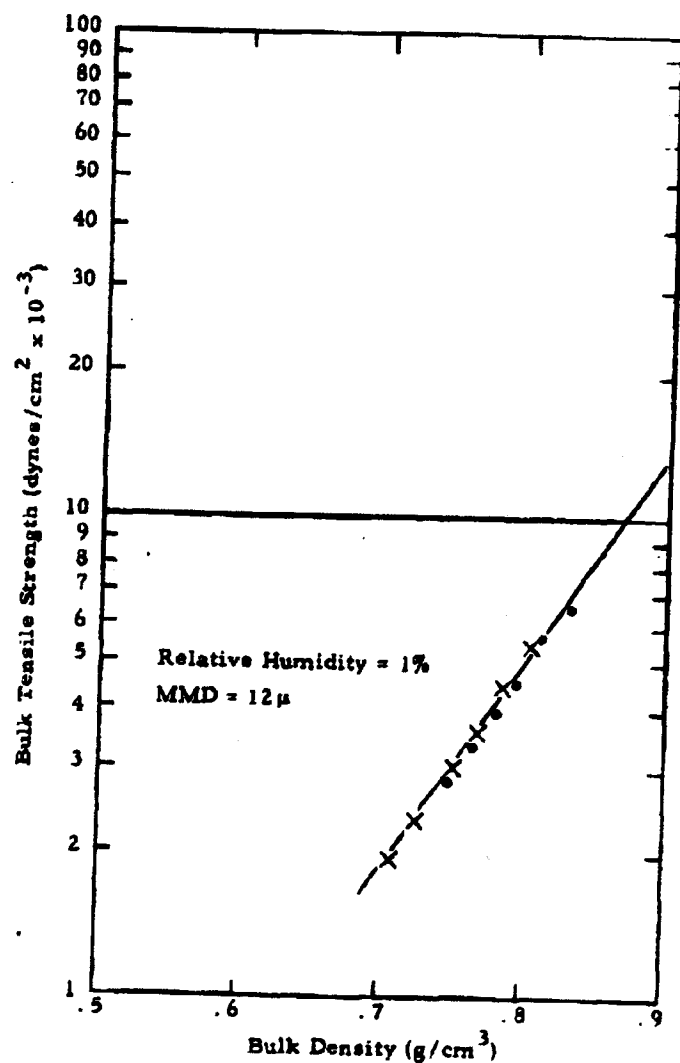


Figure 2.11 Bulk Tensile Strength Versus Bulk Density for Cornstarch

Sample-preparation procedure was varied to find the best method. "Rulon liquid", a slip and antistick agent, and graphite were separately tested for use on the inner wall of the apparatus. Both the graphite and Rulon allowed the flared trisection to be removed without damage to the powdered-sugar specimen. In addition to this, an increase in the tensile strength of powdered sugar at a given density was found when graphite was used.

The accepted method of sample preparation finally adopted was to place this powder sample into the graphite-coated apparatus and to compress the powder simultaneously from both ends by means of two 1.2-inch diameter pistons to which equal loads are applied. The density was found to be highest in the end cylinders and lowest in the center section. The density of the center section increased with time of compaction. Density and tensile tests on powdered sugar revealed that an eighteen-hour period of compaction was sufficient to produce a state of equilibrium in the powdered-sugar specimen.

The procedure followed for testing the specimen in the Instron machine during this quarter was the same as that previously reported.

The densities of the powdered sugar specimens in the region of failure were determined by carefully dissecting them after failure (Figure 2. 12). Preliminary results by this method yielded tensile strengths which lie between 0.9 to 1.6×10^4 dynes/cm² for densities of 0.85 to 1.02 g/cm³ using Rulon. However, when graphite was used, tensile strengths as high as 5.6×10^4 dynes/cm² were obtained for the same density range. This range of bulk-tensile strengths was approximately the same as that determined by the segmented-column tensile test for powdered sugar (see Figure 2. 23, Ref. 1).

It would appear that many problems can be eliminated by increasing the diameter of the 2.5-in. long "necked-down" center sections.

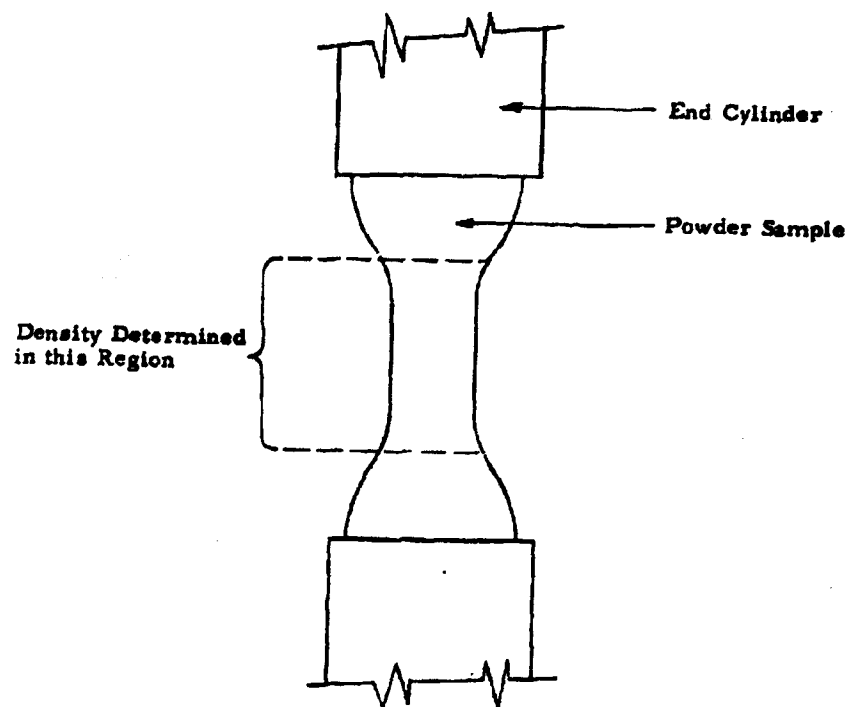


Figure 2. 12 Sketch of Instron Tensile Powder Sample

2.1.3 Compaction Characteristics of 3 Sm Samples

Three Sm samples (S1-SM-342, 352, and Pool #7) currently under investigation display distinctly different compaction characteristics. Because these samples are supposed to be identical, it is of fundamental importance to determine what property and/or properties contribute to this difference. We should ultimately be able to trace the difference to variations in methods of manufacture and/or difference in processing of the samples since manufacture.

Samples of each were taken from a deep freeze in sealed jars and placed in a dry box with a relative humidity less than 2 percent. After allowing sufficient time for the samples to reach room temperature, the compaction unit was carefully filled with each powder, sealed into a 2-mil polyethylene bag, and removed from the dry box for testing in the Instron unit. At no time prior to the filling of the compaction unit were the sealed jars opened.

The piston of the compaction unit was then advanced at a constant rate of 0.02 in./min until a load of 2000 lb was reached for each test with Sm. After each test, the compaction unit was removed from its polyethylene bag and returned to the dry box.

Compaction force is plotted against density in Figure 2.13 for all three samples of Sm. Each sample was tested in duplicate with good agreement. But although the compaction curves for the three samples have approximately the same slope, the individual curves are offset with respect to one another, indicating a scale shift. This means that the stress required to compact each of the three samples to a given density is quite different.

Several tests have been initiated to explain the scale shift for the three Sm samples. These are tests for particle-size distribution, particle density, and moisture content. Moisture contents of the three samples, determined by a standard technique, ⁽¹⁰⁾ are indicated on Figure 2.13. As can readily be seen from this information, moisture content alone does not explain the relative positions of the curves. Previous work with egg albumin ⁽²⁾ has shown a shift to the right with increasing particle size. And we therefore expect that particle-size distributions and particle-density tests (not yet completed) will shed some light on this scale shift.

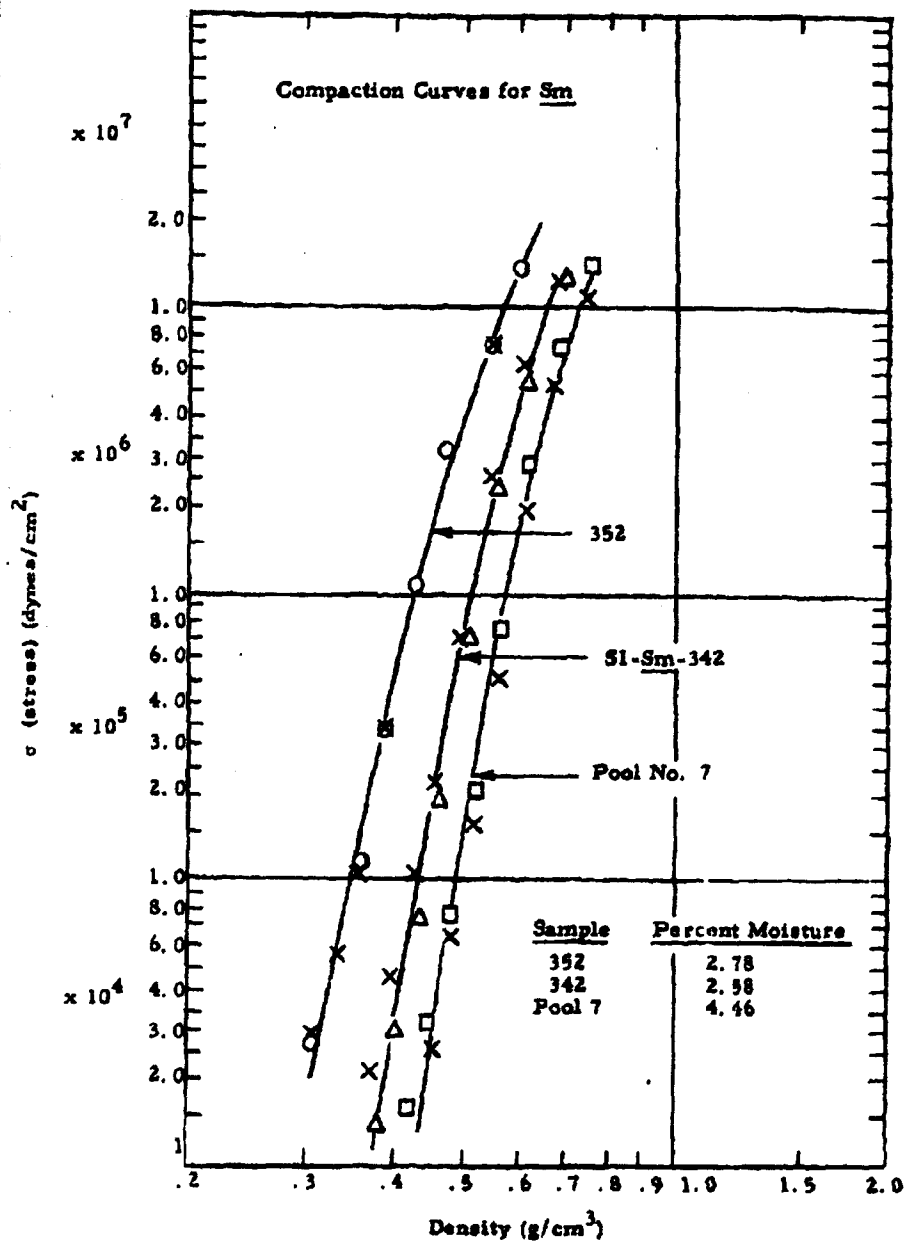


Figure 2.13. Compaction Stress Versus Bulk Density for Sm

To eliminate differences due to adsorbed moisture, the three Sm samples were dried by the same technique as that used for the moisture determinations. Compaction curves were again determined for the three dried samples, and results are presented in Figure 2. 14. During these tests, no attempt was made to break up agglomerates produced by drying.

Compaction curves for the dried Sm samples S1-SM-342 and 352 are (for all practical purposes) the same and are nearly coincident with the compaction curve for S1-SM-342 at 2.78 percent moisture (Figure 2. 13). The compaction curve for the dried Pool #7 sample lies to the right of its curve at 4.41 percent moisture.

It is thus evident that changes in moisture content alone do not account for scale shift. In addition to work already underway, studies of deagglomeration and changes in viability will be included to further explore this problem.

2. 1. 4 Fracture of Particles during Compaction

A study is currently underway to determine the extent of particle fracture represented by changes in particle-size distribution that occur during the compaction of a powder sample. We are determining experimentally the changes in Whitby particle-size distributions of a saccharin sample under a compressive stress of 2.84 dynes/cm^2 .

Considering the transmission of applied stress through a bed of powder by means of interparticle contacts, the interparticle contact area in a plane normal to the compressive stress is less than the total cross-sectional area, and the stress in the bed would therefore be larger than the applied stress. If this stress in the bed is sufficient to cause failure, then the size distribution will be changed.

Saccharin with an MMD of 6.9 microns and a standard deviation of 1.48 was compressed in the compaction apparatus⁽³⁾ by the Instron test machine to a compressive stress of $2.84 \times 10^4 \text{ dynes/cm}^2$. Saccharin samples of approximately a milligram quantity were then withdrawn from the 2 1/2-in. diameter

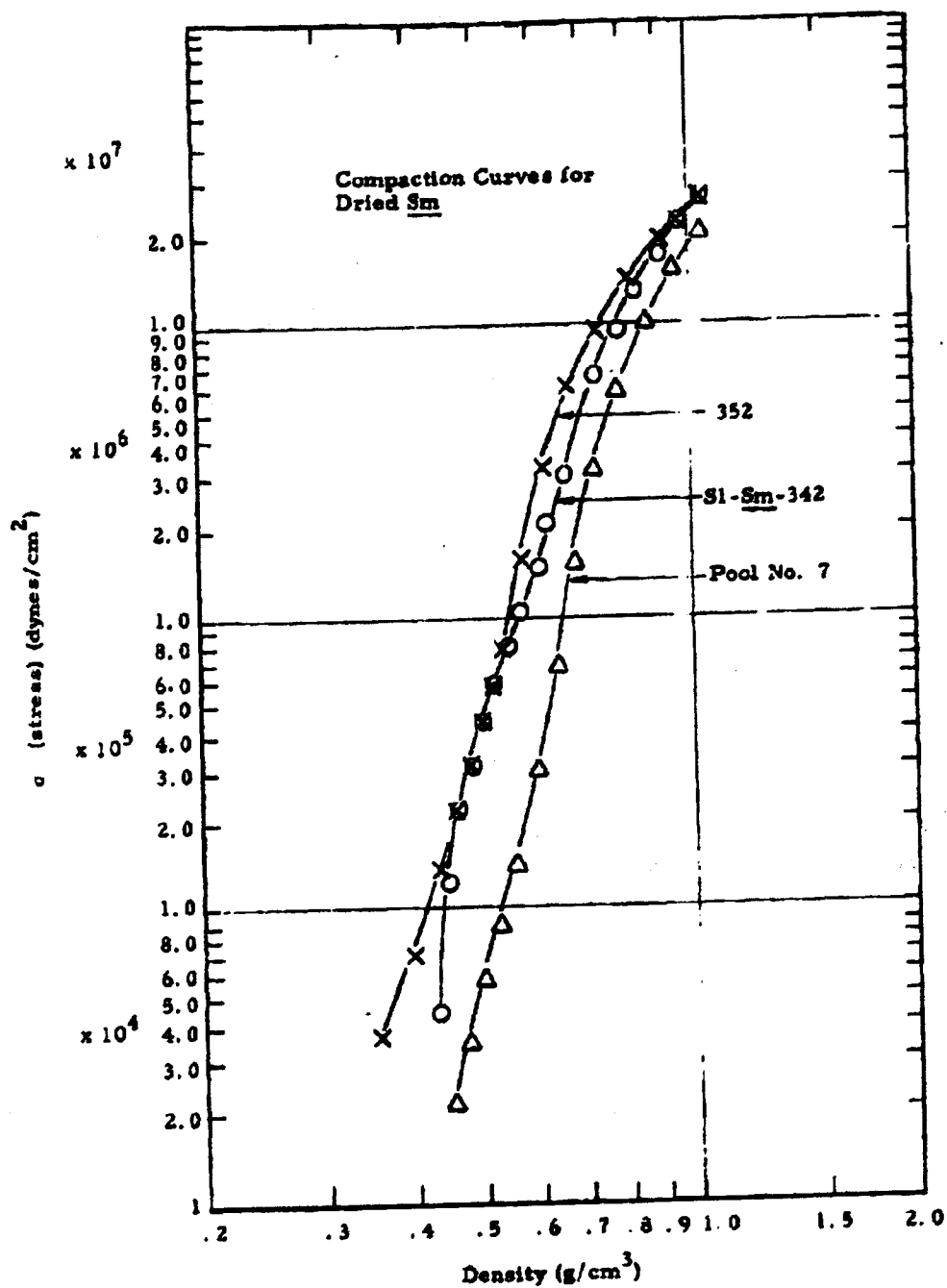


Figure 2.14. Compaction Stress Versus Bulk Density for Sm (Dried)

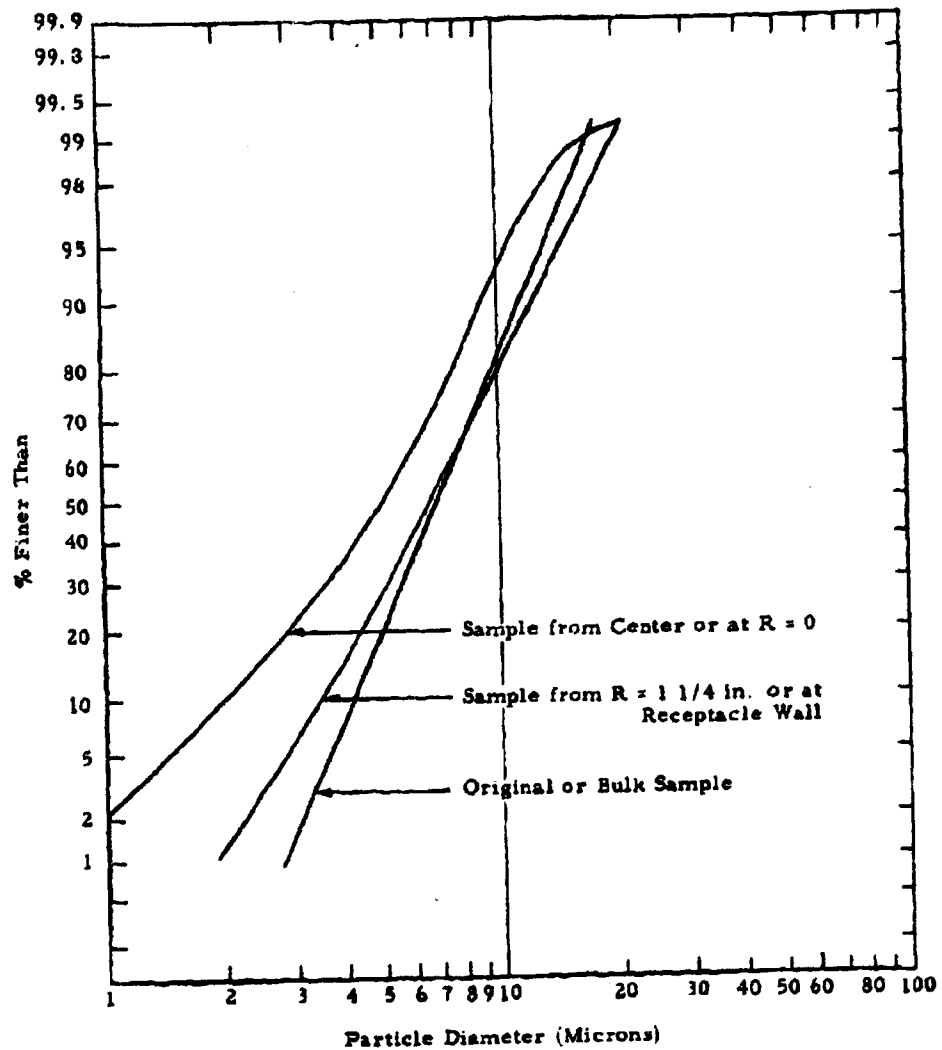


Figure 2.15 Particle Size Distribution of Saccharin Samples

powder receptacle, and its position from the center was recorded. Size analyses of the samples were performed, typical results of which are presented in Figure 2.15. It is evident that a change in particle-size distribution has occurred. Admittedly, this test was performed at a high stress level, which may exaggerate the effect. But it should be informative to make a quick check through a wider range of compressive stresses and with different powders to determine whether significant changes in size distribution result from the compaction process. Particular attention should be paid to powders with compaction curves whose slopes decrease at their upper portions (see Figure 2.16). This deviation from a straight line on the log-log plot of compaction stress versus density might indicate that particle failure is occurring, thus allowing density to increase more rapidly with stress. Sm would be a good sample for this test. See the compaction curves for Sm (Figures 2.13 and 2.14) in this report and note the changes in slope in the vicinity of $\sigma = 2.8 \text{ dynes/cm}^2$.

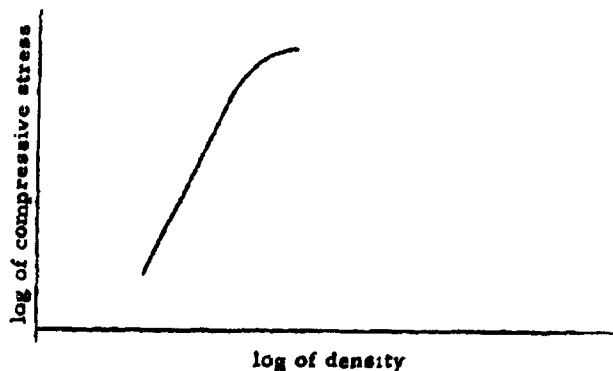


Figure 2.16 Illustration of Deviations from Log-Log Plot of Compressive Stress versus Density

2-21

Page determined to be Unclassified
Reviewed Chief, RDD, WHS
IAW EO 13526, Section 3.5
Date:

APR 12 2013

2.1.5 Effect of Cab-o-Sil on Energy of Compaction

A number of fundamental studies carried out in this laboratory⁽³⁾ have shown that Cab-o-Sil type additives can be used to measure flowability and dispersibility of powdered materials. These experiments were carried out on uncompacted powders. Although the use of additives with BW materials is not currently being stressed, we felt that the possibility of these principles being applied to dissemination of compacted powders warranted investigation.

Powder samples were mixed with 0.25 to 5.0 percent Cab-o-Sil by weight by processing through a modified fluid-energy mill. Energy-of-compaction data obtained from these samples indicated that much greater stresses were required to compact the Cab-o-Sil altered samples than to compact the unaltered powders to the same bulk densities. We have thus made a preliminary observation that the desirable properties which result from the addition of Cab-o-Sil will be obtained at the expense of greater difficulty in compacting the sample.

2.1.6 Wall-Stress Distribution

We are designing and building a piston-cylinder apparatus that will be capable of measuring stress at the cylinder wall created by the powder undergoing compaction. The measurement will be made as a function of a number of variables including type of powder, applied stress, and wall friction. This information will be of both theoretical and practical value. Details of this study will be presented in our next quarterly report.

A sketch of the piston-cylinder unit of the apparatus appears in Figure 2.17. The thin brass sleeve was rigidized by the outer heavy-walled aluminum sleeve. Holes drilled through the aluminum sleeve permit strain gauges to be placed upon diaphragm-like segments of the inner brass sleeve. Preliminary tests show that these gauged areas are very sensitive to changes in wall stress. The system of strain gauges is currently being connected to an automatic switching and recording system to permit efficient and accurate data collections.

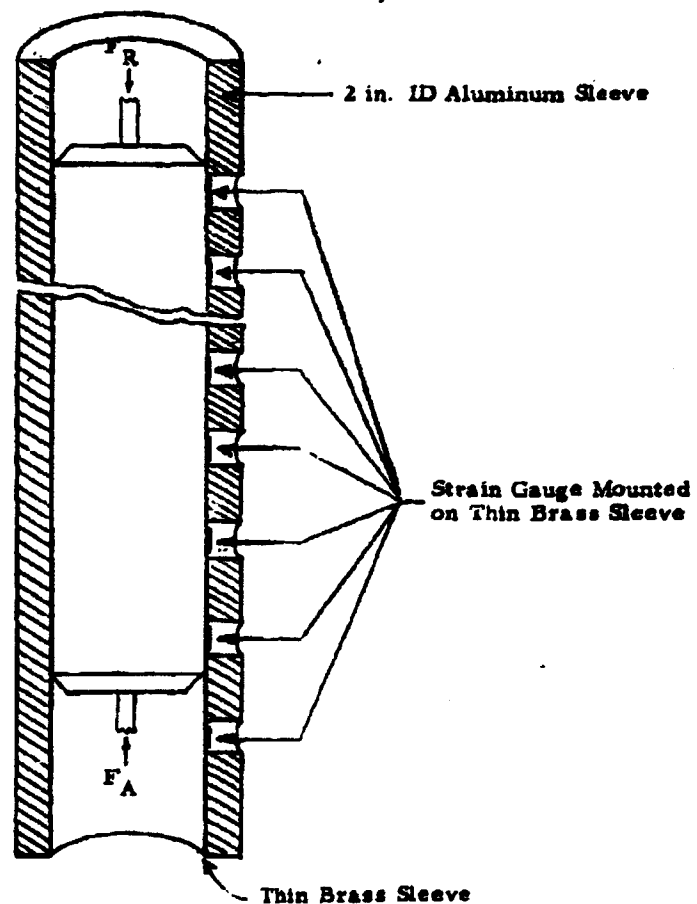


Figure 2.17 Sketch of Apparatus for Measurement of Wall Stresses

2.2 Behavior of Powders in the Uncompacted State

Our current objective in this area of study is to determine the behavior of fine powders undergoing fluidization. Studies are being made to determine the length of time required for equilibration of the fluid bed, the percentage of mass lost by a powder undergoing fluidization, and the extent of particle-size segregation during fluidization.

2.2.1 The Fluidization Process

A fluidized bed is a fluid-solid system in which a bed of finely divided solid particles is lifted by a stream of fluid.

When a fluid is passed through a bed of solid granular material, one of two things can occur. If particulate fluidization takes place, there will be a uniform expansion of the bed, in which the increasing spaces between particles allow greater ease of passage of the fluid. If aggregative fluidization takes place, there will be a bed expansion accompanied by the formation of large bubbles that is analogous to the upward flow of gas through a column of liquid. Whether a fluid-solid system will exhibit particulate or aggregative fluidization depends on the ratio of particle density to fluid density, and (to a lesser extent) on particle size. Particulate fluidization generally occurs when the fluid is a liquid, and aggregative fluidization most often occurs when the fluid is a gas.

Consider a bed of particles resting on a fine mesh screen. As the fluid velocity through the bed is increased, the pressure drop across the bed increases until it equals the weight of the bed per unit area of the grid plate. This is the point of incipient fluidization, which is defined as the lowest superficial fluid velocity at which the pressure drop across the bed (at its lowest density) equals the weight of the bed charge. ⁽⁴⁾

When the point of incipient fluidization is reached, continued increase of fluid velocity produces no further increase in pressure drop, but results in an expansion of the bed, in which the void spaces between the particles are increased, and the individual particles rest more upon a cushion of the fluid than directly upon each other.

Slugging and channeling are the two major problems encountered in fluidized bed experiments. If either is present, it must be eliminated before meaningful results can be obtained.

Channeling is a condition in which fluid passes through a bed of particles along a preferred path. Once started, channeling tends to grow worse until almost all the fluid is passing through the channel instead of being distributed evenly throughout the bed. One of the causes of channeling is a poor distribution of the solid material in the bed before fluidization. If the initial packing is such that a partial channel exists, the fluid will tend to follow this path of least resistance. It is also very important for the fluid to be well distributed over the entire area of the bed by the grid plate. A large number of small holes are preferred to a few large ones.

Slugging results when a bubble increases in size until its diameter equals that of the tube. It then carries a slug of powder with it as it rises. Fluid velocity is an important factor in the rate of bubble growth. For a given rate of bubble growth, slugging can be eliminated by using a tube with a length-to-diameter ratio that allows the bubble to escape before attaining the diameter of the tube.

2.2.2 Apparatus

Having completed a preliminary study on the problems of fluidization of fine powders (described in the previous report), a more permanent and exacting experimental system was designed and constructed. This system is presented in Figure 2.18.

The fluidization chamber is composed of a glass tube and nylon base. The length of the glass tube will vary depending on the work being done, but its mean inside diameter is 2.59 cm. The base, machined from a solid nylon rod, is constructed in three sections for ease in cleaning and assembly. The grid plate used for the present series of tests is a fine screen with openings of about 169 microns.

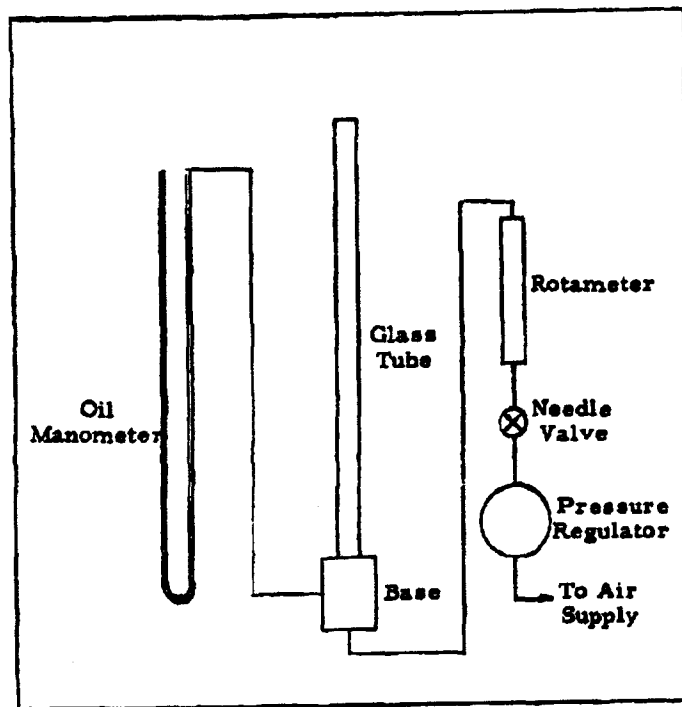


Figure 2.18 Fluidized Bed Apparatus

An oil manometer measures the pressure drop across the powder bed and grid plate through a pressure tap on the side of the base. Silicone oil with a density of 1.066 g/cm^3 is used in the manometer.

The fluidizing media (air is currently being used) enters the base just below the grid plate. The flow rate is measured by a rotameter and is controlled by a $0\text{-}2 \text{ lb/in.}^2$ pressure regulator. Fine adjustments in flow rate can be made with a 20-turn needle valve.

In discussing flow rates in connection with fluidized beds, it is convenient to use fluid velocity because this takes tube diameter into account. Velocities up to about 20 cm/sec are possible with the present apparatus.

2.2.3 Experimental Procedure and Results

A series of experimental studies using granulated sugar was carried out using the new experimental arrangement. The pressure drop (Δp) was studied as a function of fluid velocity (v) for bed depths of 6, 15, and 25 cm.

A set of typical results is shown in Figure 2.19. It is seen that in each case there is a peak before the curve levels off. This is a result of the condition of the bed before fluidization. If a bed has maximum void volume, $\ln \Delta p$ will increase linearly with $\ln v$ until incipient fluidization velocity is reached, and will then level off. Any other packing will result in the peak displayed here.

Within experimental error, the incipient fluidization velocities of the three bed depths agree quite well, as do their slopes before incipient fluidization:

<u>Bed Depth</u>	<u>Incipient Fluidization Velocity</u>	<u>Slope</u>
6 cm	2.55 cm/sec	3.81
15 cm	3.10 cm/sec	3.65
25 cm	2.60 cm/sec	3.78

2.2.3.1 Fluidized Bed Tests - Talc

In the fluidized bed tests reported in the 11th quarterly report, we noted that talc tends to agglomerate quite badly when it is fluidized. This effect has been observed before with small particles of high material density.⁽⁵⁾ As a result of this agglomeration, the bed's depth does not remain constant, but steadily decreases with time even though the fluid's velocity remains constant. The present series of tests was conducted to determine how much time the bed requires to reach equilibrium.

Channeling problems during the tests were corrected by the addition of a small vibrator to the glass tube. With 22 g of talc, it was then possible to obtain fairly good fluidization. Seventy-five minute fluidization studies were made under fluid velocities of 4, 8, and 12 cm/sec. These will be referred to as samples 1, 2, and 3.

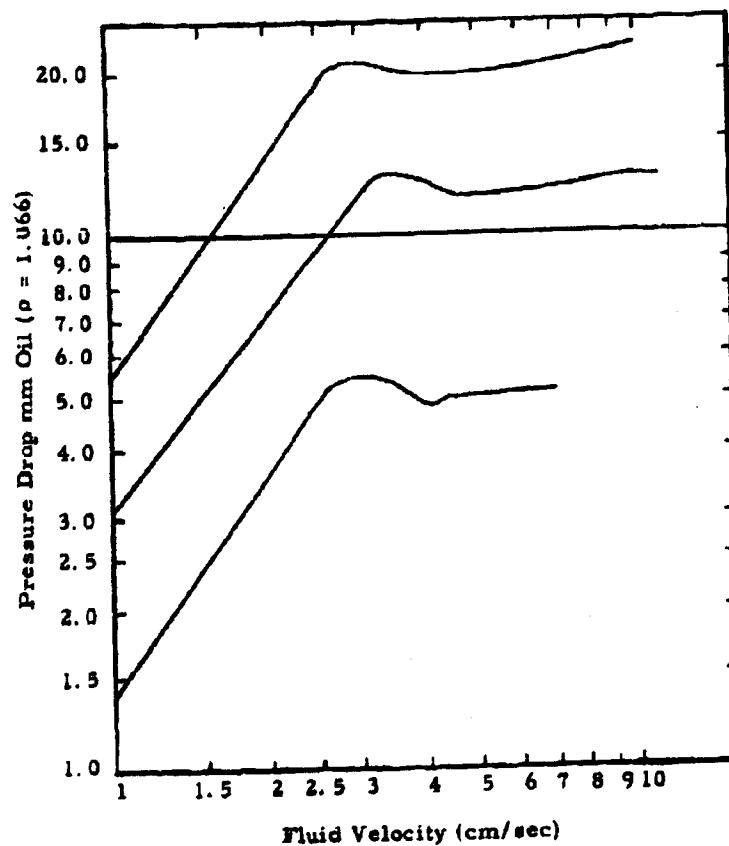


Figure 2.19 Change in Fluid Velocity with ΔP in the Fluid Bed

After the bed was prepared, a pressure regulator was adjusted to give the desired fluid velocity, and a timer was started. Minor random corrections were necessary to maintain proper fluid flow. Periodic measurements of bed depth and pressure drop were made and recorded. Three runs were made at each of the three fluid velocities, using fresh powder samples each time. Reproducibility of results was satisfactory.

One run at each of the flow rates is presented in Figure 2.20. Bed depth is plotted against time for a bed fluidized at 4, 8, and 12 cm/sec. At the end of the 75-minute run, the bed depth at 4 cm/sec is 28.7; at 8 cm/sec it is 24.5; and at 12 cm/sec it is 22.0. This might be taken as an indication that the lower flow rate actually fluidizes the bed better than the higher. This results from the fact that the higher flow rates agglomerate the powder more, resulting in a lower bed depth after flow is stopped. The following table illustrates the point.

<u>Sample</u>	<u>Bed Depth, No Flow</u>	<u>Bed Depth, Fluidized</u>	<u>Percent of Expansion by Fluidization at Prescribed Flow Rates</u>
1	27.4	28.7	4.8
2	20.3	24.5	20.7
3	17.9	22.0	22.9

Sample 1 was fluidized at 4 cm/sec for 75 minutes. At the end of this time, the bed depth was 28.7 cm. When fluid velocity was reduced to zero the bed depth was 27.4. This means it was expanded 4.8 percent when fluidized. The same reasoning on Sample 2 (8 cm/sec) and Sample 3 (12 cm/sec) reveals that the higher velocities do expand the bed by a greater percentage than the lower velocities.

In the 11th quarterly report, it was noted that when a bed of talc was fluidized, the slope of the curve for bed depth vs fluid velocity decreased with each successive expansion. This was due to the fact that the powder was still agglomerating each time the bed was fluidized. During the recent tests, powder was fluidized for a 75-minute period. After each of these tests,

2-30

Page determined to be Unclassified
Reviewed Chmrl. RDD, WMS
IAW EO 13526, Section 3.5
Date: APR 12 2013

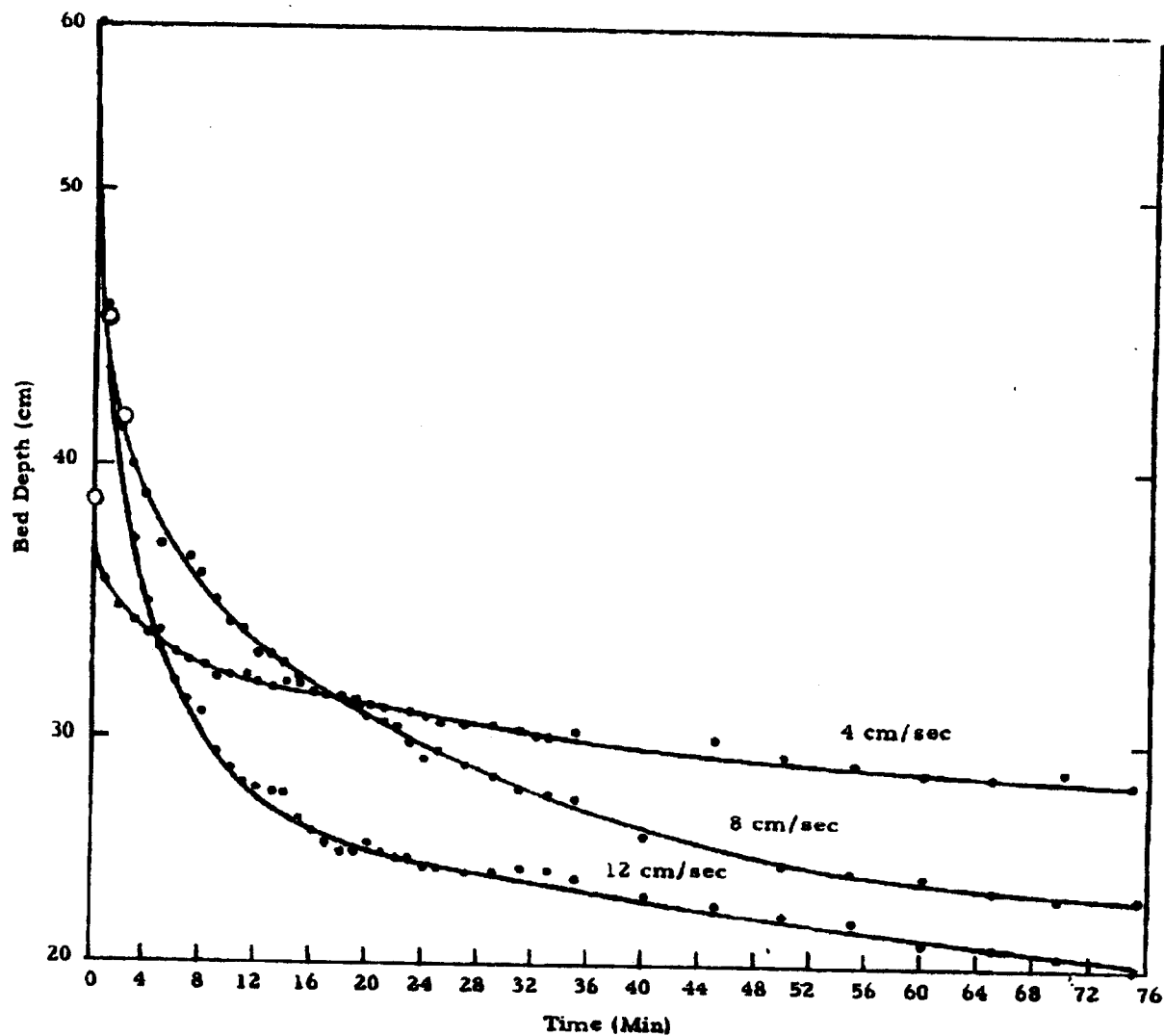


Figure 2.20 Equilibration of Fluid Beds at Various Flow Rates

four successive expansions were made without otherwise disturbing the bed. It was found that for all four expansions the curve of bed depth vs fluid velocity followed the same path (within experimental error) for both the 8 and 12 cm/sec treated samples. The 4 cm/sec sample did show some deviations, particularly at velocities above 4 cm/sec.

One would expect the agglomerates in the 12 cm/sec sample to be largest, and the 4 cm/sec sample to be smallest. This was confirmed by the incipient fluidization velocity for the three samples.

<u>Sample</u>	<u>Incipient Fluidization Velocity</u>
1	0.6 cm/sec
2	1.2 cm/sec
3	4.0 cm/sec

At fluid velocities of 8 and 12 cm/sec, good aggregative fluidization was obtained throughout the bed. But at 4 cm/sec, we found that fluidization took place in the upper portion of the bed while the lower portion was not fluidized. This effect has been observed before for heavy-particle systems, and results from the expansion of the fluid as it passes from the bottom to the top of the bed.

2.2.3.2 Powder Lost by Entrainment

Because the velocities used exceed the terminal velocities for many of the particles, it is obvious that a certain amount of the material will be carried out of the bed and be lost by entrainment. At 4 cm/sec there was no noticeable loss. At 8 cm/sec and 12 cm/sec, loss was visually detectable. This rate of loss decreased as the powder agglomerated. Measured losses are given below.

<u>Fluid Velocity</u>	<u>Powder Lost</u>
4 cm/sec	No measurable loss
8 cm/sec	0.6 g or 2.8 percent
12 cm/sec	1.2 g or 5.6 percent

2.2.3.3 Particle Segregation and Particle Attrition

After a bed had been fluidized during a 75-minute run, samples were taken from the top and bottom of the bed. The samples were subjected to size analyses by the Whitby technique. There were six samples (top and bottom for 4, 8, and 12 cm/sec runs), and all were found to have identical size distributions. The values obtained also agreed with those for unfluidized talc. It appears that there has been little, if any, segregation or attrition during the current experiments.

2.2.4 Conclusions and Future Work

We have shown that under properly controlled conditions, powders with diameters in the 5-micron range can be satisfactorily fluidized with only limited loss of product from the bed. Agglomeration does occur but without particle-size segregation within the bed.

Future work will include the fluidization of other types of powders, and attempts will be made to conduct "viscosity" measurements in the fluid bed. In addition, experiments will be performed in beds of bulk powder to determine interparticle resistance to flow and resistance to flow imposed by various geometric shapes.

3. PHYSICAL AND CHEMICAL CHARACTERISTICS OF THE POWDER PARTICLE

Behavior of particulate material is fundamentally determined by the nature of the intermolecular forces (physical and chemical) existing at the contact areas between particles. The number and character of these contacts is directly related to the nature of the surfaces of the powder particles. To study this problem, we are comparing the experimentally determined external surface of a particle with a calculated theoretically spherical particle surface to obtain a measure of the roughness of an external surface. The use of electron and light microscopy is providing excellent supplementary particle-shape information. The problem of measuring the strengths of agglomerates and the problem of powder-to-metal friction are currently being investigated.

3.1 Total Surface Area

The BET gas adsorption method (named for Brunauer, Emmett, and Teller, its developers) is being used to determine the total surface area of various powders. By this method, the quantity of gas necessary to form a monomolecular layer on the surface of the particle is determined. By assuming a value for the area covered by a single molecule, we are able to calculate the area covered by the adsorbed gas. During the preceding quarter, the total surface area of talc was determined. Talc particles are jagged, irregular, porous platelets (see electron micrographs in section 3.2) whereas saccharin has a relatively smooth, nonporous surface. We investigated the surface structure of saccharin for comparison during this quarter.

3.1.1 Total Surface Area of Saccharin

The total surface area of saccharin samples has been measured, and a procedure has been developed to cope with the problem of sublimation or other types of decomposition. A significant difference between the total surface areas of saccharin and talc was observed. Uncertainties in total surface measurements were analyzed in an error analysis of the BET method as applied to the gravimetric system.

In the application of surface-area measurements to powders (e. g., catalytic materials) there is no doubt about the stability of the powder under test conditions. The only concern is the removal of adsorbed contaminants, and degassing conditions are controlled by the nature of the contaminant.

However, in the case of saccharin, the stability of the powder is the controlling factor for degassing conditions. Saccharin sublimes readily at temperatures about 50 F above room temperature at pressures of approximately 5×10^{-5} mm Hg. At room temperature, its sublimation rate is negligible, permitting degassing at this temperature.

A degassing procedure of evacuation at a pressure less than 5×10^{-5} mm Hg at 76 F for 2 days will provide the "degassed state". The degassed state is defined as the state where further degassing will not produce any increase in surface area. If there are any contaminants remaining, they may be in one sense considered part of the structure, since to remove them one would have to decompose the powder. In this case, decomposition means sublimation.

The degassing temperature was decreased until sublimation occurred at a negligible rate. At high temperature (160 F) saccharin was observed to condense above the heating zone. At lower temperatures (96 F) saccharin was shown to be subliming by the fact that surface area increased with time of evacuation (Figure 3.1 and 3.2). Figure 3.2 shows the isotherms as the surface area increased from $0.8 \text{ m}^2/\text{g}$ to $2.32 \text{ m}^2/\text{g}$ and as temperature and degassing time were increased for the same sample. Figure 3.3 and Figure 3.1 show isotherms for degassing at room temperature. The surface areas of two samples are reproducible for much different evacuation times, and for the same powder the area does not increase with evacuation time. Measurement of the total surface area under conditions of powder stability has thus been accomplished.

Applying the BET equation to the adsorption data,^(c) we obtain a specific surface for saccharin of $1.53 \text{ m}^2/\text{g} \pm 7$ percent. The specific surface from the surface mean diameter, calculated from the MMD of 6.9 microns, is $0.71 \text{ m}^2/\text{g}$. The rugosity defined as

$$\frac{\text{BET Surface Area}}{\text{Surface area from MMD (Whitby)}} \text{ is } 2.2.$$

Figure 3.1 Saccharin Behavior

Run	Degassing Conditions				Comment
	Temperature	Time (hr)	Pressure (mm Hg)	Area (m ² /g)	
1	76 F	16	$< 5 \times 10^{-5}$	0.8	Runs 1-4 are the same sample.
2	96 F	+26	$< 5 \times 10^{-5}$	1.28	
3	96 F	+16	$< 5 \times 10^{-5}$	1.89	Plus time is that in addition to previous run.
4	85 F	+19	$< 5 \times 10^{-5}$	2.32	
5	76 F	113	$< 5 \times 10^{-5}$	1.53	Runs 6-8 are the same sample.
6	76 F	18	1×10^{-3}	1.32	
7	76 F	+30	$< 5 \times 10^{-5}$	1.59	Plus time is that in addition to previous run.
8	76 F	+19	$< 5 \times 10^{-5}$	1.42	

APR 15 2013

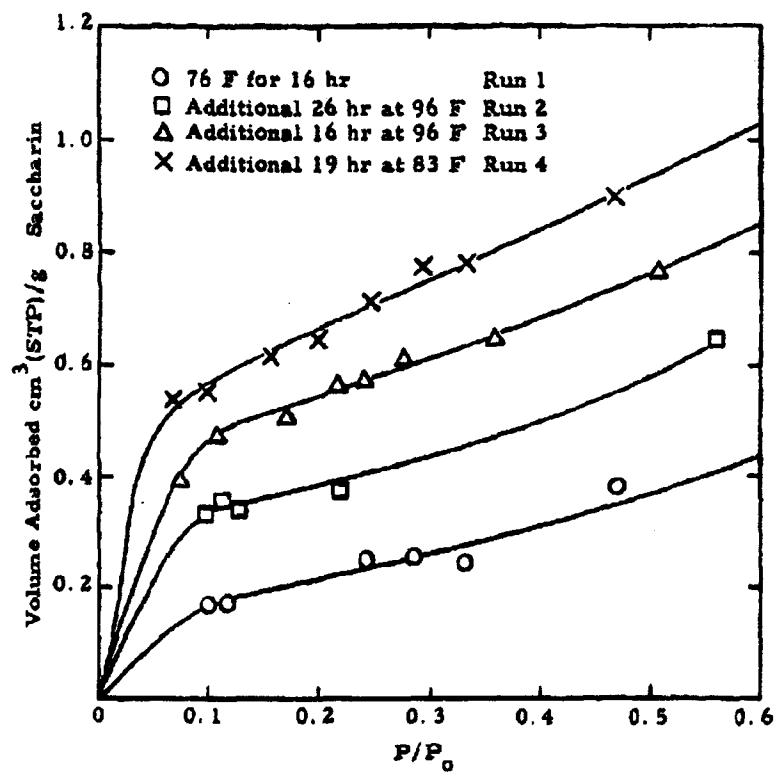


Figure 3.2 N₂ Adsorption on Saccharin as a Function of Degassing Condition

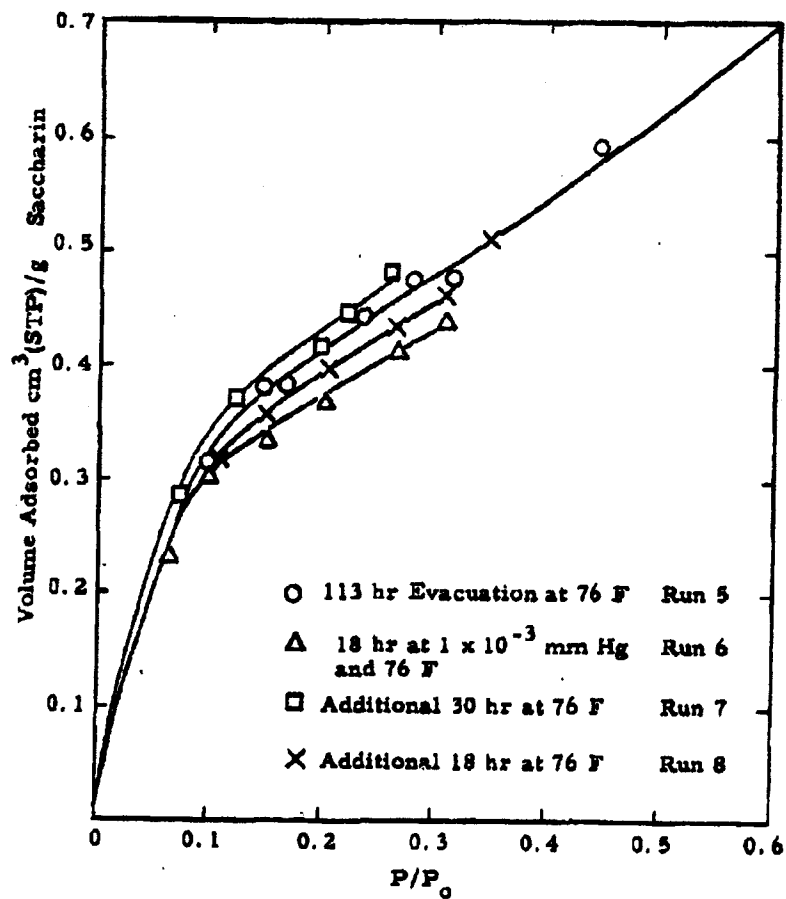


Figure 3.3 N₂ Adsorption by Saccharin after Various Degassing Conditions at Room Temperature

From the complete isotherm (Figure 3.4), we see that saccharin exhibits no hysteresis. This indicates that saccharin has little or no internal surface or pore structure. This is in marked contrast to talc,⁽¹⁾ which exhibits definite hysteresis. The rugosity of 2.2 indicates that a small amount of internal surface exists. This can be seen by comparing to one "roughness factor" defined as

$$\frac{\text{BET Surface Area}}{\text{Electron-microscope Area}}$$

Numerous powders exhibited roughness factors of 1 to 1.5.⁽⁷⁾ Surface areas based on MMD by the Whitby method are usually a little larger than those based on electron-microscope determinations.⁽⁸⁾ Therefore, the rugosity factor will be somewhat less than the roughness factor for a given powder.

3.1.2 Analysis of Experimental Errors in the Gravimetric BET Method of Measuring Surface Areas

The BET equation used to determine surface areas by adsorption is

$$\frac{P/P_0}{V(1 - P/P_0)} = \frac{1}{V_m C} + \frac{C-1}{V_m C} P/P_0 \quad (1)$$

where

V = Volume adsorbed (STP) at pressure P

P_0 = Vapor pressure of gas at adsorption temperature

C = Constant

V_m = Volume required to form monolayer

From a plot of

$$\frac{P/P_0}{V(1 - P/P_0)} \text{ vs } \frac{P}{P_0} \quad (2)$$

the slope S and intercept I are calculated, and are in turn used to calculate V_m by the equation

$$V_m = \frac{1}{S + I} \quad (3)$$

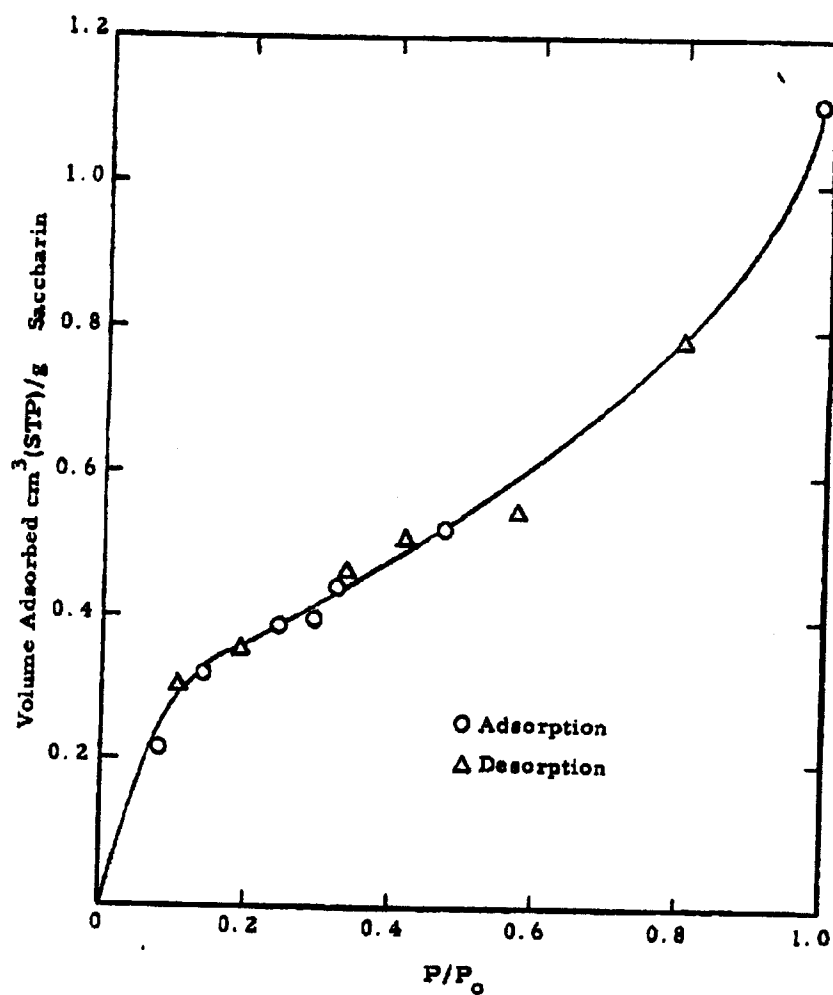


Figure 3.4 N₂ Adsorption Isotherm on Saccharin

Experimental errors or uncertainties affect the quantities

$$F_1 = \frac{P/P_o}{V(1 - P/P_o)}, \text{ and} \quad (4)$$

$$F_2 = P/P_o. \quad (5)$$

The errors in F_1 and F_2 are composed of the errors in each of the elements P , P_o , and V .

The errors in F_1 and F_2 are related to the errors in P , P_o , and V by the equation

$$d F_1 = \left\{ \left(\frac{\partial F_1}{\partial P} dP \right)^2 + \left(\frac{\partial F_1}{\partial P_o} dP_o \right)^2 + \left(\frac{\partial F_1}{\partial V} dV \right)^2 \right\}^{1/2} \quad (6)$$

$$d F_2 = \left\{ \left(\frac{\partial F_2}{\partial P} dP \right)^2 + \left(\frac{\partial F_2}{\partial P_o} dP_o \right)^2 \right\}^{1/2} \quad (7)$$

In other words, the square of the error is equal to the sum of the squares of errors contributed by each element.

Substituting Equations (4) into (6) and (5) into (7), we obtain

$$d F_1 = \frac{P/P_o}{V(1 - P/P_o)} \left\{ \frac{(dP/P)^2 + (dP_o/P_o)^2}{(1 - P/P_o)^2} + \left(\frac{dV}{V} \right)^2 \right\}^{1/2}$$

$$d F_2 = P/P_o \left\{ \left(\frac{dP}{P} \right)^2 + \left(\frac{dP_o}{P_o} \right)^2 \right\}^{1/2}$$

Converting to percent of error,

$$\frac{dF_1}{F_1} = \left\{ \frac{(dP/P)^2 + (dP_o/P_o)^2}{(1 - P/P_o)^2} + \left(\frac{dV}{V} \right)^2 \right\}^{1/2} \quad (8)$$

$$\frac{dF_2}{F_2} = \left\{ \left(\frac{dP}{P} \right)^2 + \left(\frac{dP_o}{P_o} \right)^2 \right\}^{1/2} \quad (9)$$

In the outline below, we determine individually by the technique above the uncertainty due to each element.

3.1.2.1 Error in P and P_o

The error in P and P_o is due to reading error:

$$dP = (\text{error in reading each manometer leg})\sqrt{2} \quad (10)$$

3.1.2.2 Error in Volume Adsorbed

The volume of gas adsorbed is obtained from the weight adsorbed, by the ideal gas law:

$$V = \frac{W_a RT}{M P}$$

The percent of error in V is

$$\frac{dV}{V} = \frac{dW_a}{W_a} \quad (11)$$

where W_a = weight adsorbed.

W_a is related to experimental data for gravimetric methods by

$$W_a = \frac{W_{sp} + W_{Bf}}{W_s}$$

The percent of error in W_a due to error in each component is

$$\frac{dW_a}{W_a} = \left\{ \frac{(dW_{sp})^2 + (dW_{Bf})^2}{(W_{sp} + W_{Bf})^2} + \left(\frac{dW_s}{W_s} \right)^2 \right\}^{1/2} \quad (12)$$

where

W_{sp} = weight change recorded by spring

W_{Bf} = buoyant force

W_s = weight of sample.

3.1.2.2.1 Error in Weight Change

Error in weight change as measured by spring displacement W_{sp} is determined by the equation

$$W_{sp} = D_f / K.$$

The percent of error is

$$\frac{dW_{sp}}{W_{sp}} = \left\{ \left(\frac{dD_f}{D_f} \right)^2 + \left(\frac{dK}{K} \right)^2 \right\}^{1/2} \quad (13)$$

where

D_f = displacement read by filar eye piece

K = sensitivity of spring, filar units/unit weight.

The error in D_f is

$$dD_f = (\text{error in making each ready}) \sqrt{2} \quad (14)$$

The error in K is due to calibration errors and uncertainty of spring temperature. The sensitivity is determined by the calibration equation,

$$K = \frac{D_{fcal}}{M_{cal}}$$

and the percent of error is

$$\frac{dK}{K} = \left\{ \left(\frac{d D_{fcal}}{D_{fcal}} \right)^2 + \left(\frac{d M_{cal}}{M_{cal}} \right)^2 \right\}^{1/2} \quad (15)$$

where

D_{fcal} = displacement read by filar eye piece in calibration

M_{cal} = weight used to calibrate the eye piece.

Error in K for quartz springs due to temperature uncertainty is given by, (11)

$$\frac{\partial \ln K}{\partial T} = -1.23 \times 10^{-4}$$

$$\frac{\partial K}{\partial T} dT = -1.23 \times 10^{-4} K dT \quad (16)$$

where

T = temperature of spring

dT = temperature uncertainty

The percent of error in K due to temperature and calibration uncertainty is

$$\frac{dK}{K} = \left\{ \left(\frac{d D_{fcal}}{D_{fcal}} \right)^2 + \left(\frac{d M_{cal}}{M_{cal}} \right)^2 + (1.23 \times 10^{-4} dT)^2 \right\}^{1/2} \quad (17)$$

Percent of error in W_{sp} due to each experimental error is found by substituting Equation (17) into Equation (13):

$$\frac{dW_{sp}}{W_{sp}} = \left\{ \left(\frac{d D_f}{D_f} \right)^2 + \left(\frac{d D_{fcal}}{D_{fcal}} \right)^2 + \left(\frac{d M_{cal}}{M_{cal}} \right)^2 + (1.23 \times 10^{-4} dT)^2 \right\}^{1/2} \quad (18)$$

3.1.2.2.2 Error in Buoyant Force

Buoyant forces are calculated by

$$W_{Bf} = V_T \rho_g$$

and percent of error by

$$\frac{d W_{Bf}}{W_{Bf}} = \left\{ \left(\frac{d V_T}{V_T} \right)^2 + \left(\frac{d \rho_g}{\rho_g} \right)^2 \right\}^{1/2} \quad (19)$$

where

V_T = total volume of sample plus quartz bucket and fiber

ρ_g = gas density.

The total volume is given by

$$V_T = V_q + V_s$$

and the percent of error by

$$\frac{d V_T}{V_T} = \left\{ \frac{(d V_q)^2 + (d V_s)^2}{(V_q + V_s)^2} \right\}^{1/2} \quad (20)$$

where

V_q = volume of quartz

V_s = volume of sample.

The percent of error for the quartz volume is

$$\frac{d V_q}{V_q} = \left\{ \left(\frac{d W_q}{W_q} \right)^2 + \left(\frac{d \rho_q}{\rho_q} \right)^2 \right\}^{1/2} \quad (21)$$

where

W_q = weight of quartz

ρ_q = density of quartz

and the percent of error for the sample volume is

$$\frac{d V_s}{V_s} = \left\{ \left(\frac{d W_s}{W_s} \right)^2 + \left(\frac{d \rho_s}{\rho_s} \right)^2 \right\}^{1/2} \quad (22)$$

where

$d W_s = \sigma_g$ from least squares line for relating spring deflection to weight

W_s = sample weight

ρ_s = sample density.

The density of the vapor was calculated by the Biethelot equation⁽¹²⁾

$$V = \frac{RT}{P} \left[1 + \frac{9}{128} \frac{P_R}{T_R} \left(1 - \frac{6}{T_R^2} \right) \right] \quad (23)$$

where

V = molal volume

R = gas constant

T_R = reduced temperature at temperature T

P_R = reduced press at pressure P

T = temperature of adsorption

P = pressure of adsorption.

If we assume that the Birtelot equation gives exact results, the percent of error in the gas density ρ_g is given by,

$$\frac{d \rho_g}{\rho_g} = \left\{ \frac{(d P/P)^2 + \left[1 + \frac{81}{64} \frac{P_R}{T_R} \right]^2 \left(\frac{dT}{T} \right)^2}{\left[1 + \frac{9}{128} \frac{P_R}{T_R} \left(1 - \frac{6}{T_R^2} \right) \right]^2} \right\}^{1/2} \quad (24)$$

The temperature was determined by interpolating between values of vapor pressure versus temperature by*

$$\log \frac{P}{P_0} = (0.05113) (T - T_0), \text{ and}$$

the percent of error in temperature is.

$$dT = \frac{2.303}{0.05113} \frac{dP_0}{P_0}. \quad (25)$$

3.1.3 A Typical Error Analysis to Determine Controlling Errors

3.1.3.1 Error in P and P₀

The uncertainty is due to the uncertainty in reading the manometer leg with the cathetometer which is 0.1 mm Hg. Therefore,

$$dP = dP_0 = 0.1 \sqrt{2} \quad (26)$$

3.1.3.2 Error in V

3.1.3.2.1 Error in Weight

Error in weight is given by Equation (18):

*From critical tables, the equation relating vapor pressure to temperature is

$$\log P_{mm} = \frac{-334.6376}{T} + 7.5777 - (0.00476) T$$

By taking ratios at the adsorption temperature and the normal boiling point and if the adsorption temperature is close to the normal boiling point, the working equation can be derived.

$$\frac{d W_{sp}}{W_{sp}} = \left\{ \left(\frac{d D_f}{D_f} \right)^2 + \left(\frac{d D_{fcal}}{D_{fcal}} \right)^2 + \left(\frac{d M_{cal}}{M_{cal}} \right)^2 + (1.23 \times 10^{-4} dT)^2 \right\}^{1/2}$$

The uncertainty in reading the filar eye piece is one unit. The uncertainty $d D_f = 1 \sqrt{2}$ since the displacement is the difference between two readings. In the calibration, a 10.02 ± 0.01 mg weight was used and produced a spring displacement of 821 filar eye-piece units.

$$\frac{d D_{fcal}}{D_{fcal}} = \frac{1 \sqrt{2}}{821} = 1.73 \times 10^{-3}$$

and
$$\frac{d M_{cal}}{M_{cal}} = \frac{0.01}{10.02} = 1 \times 10^{-3}$$

The uncertainty in the temperature of the column water was measured at 0.05 C.

$$1.23 \times 10^{-4} (0.05) = 6.15 \times 10^{-6}$$

Because spring deflections of 821 filar eye-piece units never occur, and because most deflections are usually an order of magnitude less, the controlling error in weight change as measured by the spring is the error due to reading the eye piece

$$\frac{d W_{sp}}{W_{sp}} \approx \frac{d D_f}{D_f}$$

(27)

or
$$d W_{sp} = \frac{d D_f}{K}$$

This means that the error in W_{sp} is constant for any given spring.

3.1.3.2.2 Error in Buoyant Force

Errors in total volume are given by Equation (20):

$$\frac{d V_T}{V_T} = \left\{ \frac{(d V_q)^2 + (d V_s)^2}{(V_q + V_s)^2} \right\}^{1/2}$$

3-15

The usual case is that the volume of the sample is 10 times as large as the volume of quarts. Therefore, errors in the sample volume would predominate:

$$\frac{d V_T}{V_T} \approx \frac{d V_s}{V_s} \quad (28)$$

Errors in volume of the sample are determined by Equation (22):

$$\frac{d V_s}{V_s} = \left\{ \left(\frac{d W_s}{W_s} \right)^2 + \left(\frac{d \rho_s}{\rho_s} \right)^2 \right\}^{1/2}$$

From least squares analysis,

$$d W_s = \sigma_g = 0.36.$$

The error in the true density is approximately 2 percent:

$$\frac{d \rho_s}{\rho_s} = 0.02$$

$$\frac{d V_s}{V_s} = \left\{ \left(\frac{0.36}{600} \right)^2 + (0.02)^2 \right\}^{1/2}$$

From this we see that the error in density of the sample predominates, or

$$\frac{d V_s}{V_s} \approx \frac{d \rho_s}{\rho_s}. \quad (29)$$

The error in the density of gas is provided by Equations (24) and (25):

$$\frac{d \rho_g}{\rho_g} = \left\{ \frac{\left(d P/P \right)^2 + \left[1 + \frac{81}{64} \frac{P_R}{T_R} \right]^2 \left[\frac{2.303}{0.05113} \frac{d P_o}{P_o} \frac{1}{T} \right]^2}{\left[1 + \frac{9}{128} \frac{P_R}{T_R} \left(1 - \frac{6}{T_R^2} \right) \right]^2} \right\}^{1/2}$$

At the normal boiling point of nitrogen, $P_R = 6.5 \times 10^{-3}$ and $T_R = 0.6$; and substituting above we get

$$\frac{d \rho_g}{\rho_g} = \frac{\left(\frac{d P}{P}\right)^2 + 1.05 \left(\frac{d P_o}{P_o T}\right)^2}{0.98}$$

The percent of error in P_o is always much less than P ; and dividing by T , the temperature of adsorption, makes

$$\frac{d P}{P} \gg 1.05 \frac{d P_o}{P_o T}$$

Therefore,

$$\frac{d \rho_g}{\rho_g} \approx \frac{d P}{P} \quad (30)$$

The error in the buoyant force is given by Equation (19):

$$\frac{d W_{Bf}}{W_{Bf}} = \left\{ \left(\frac{d V_T}{V_T} \right)^2 + \left(\frac{d \rho_g}{\rho_g} \right)^2 \right\}^{1/2}$$

Substitute Equation (28), (29), and (30) into Equation (9), and we obtain

$$\frac{d W_{Bf}}{W_{Bf}} = \left\{ \left(\frac{d \rho_s}{\rho_s} \right)^2 + \left(\frac{d P}{P} \right)^2 \right\}^{1/2}$$

Since $d P = 0.1 \sqrt{2}$ mm Hg and P is always greater than 50 mm Hg,

$$\frac{d \rho_s}{\rho_s} \ll \frac{d P}{P}$$

Therefore,

$$\frac{d W_{Bf}}{W_{Bf}} \approx \frac{d \rho_s}{\rho_s} \quad (31)$$

The error in the volume adsorbed is determined by Equations (11) and (12):

$$\frac{dV}{V} = \left\{ \frac{(dW_{sp})^2 + (dW_{Bf})^2}{(W_{sp} + W_{Bf})^2} + \left(\frac{dW_s}{W_s} \right)^2 \right\}^{1/2}$$

Because the error in the density of the sample was shown to obscure the error due to weighing the sample (see the analysis of errors in the buoyant force), derivation of Equation (29) is

$$\frac{dV}{V} = \left\{ \frac{(dW_{sp})^2 + (dW_{Bf})^2}{(W_{sp} + W_{Bf})^2} \right\}^{1/2}$$

Substituting Equation (31) and Equation (27) into the above equations provides

$$\frac{dV}{V} = \left\{ \frac{\left(\frac{dD_f}{K} \right)^2 + \left[W_{Bf} \frac{d\rho_s}{\rho_s} \right]^2}{(W_{sp} + W_{Bf})^2} \right\}^{1/2} \quad (32)$$

The error in the function F_1 is arrived at through Equation (8):

$$\frac{dF_1}{F_1} = \left\{ \frac{(dP/P)^2 + (dP_o/P_o)^2}{(1 - P/P_o)^2} + \left(\frac{dV}{V} \right)^2 \right\}^{1/2}$$

Because the error due to the density of the sample obscured the error due to pressure in the buoyant-force error analysis, derivation of Equation (31) can approximate the error in F_1 by

$$\frac{dF_1}{F_1} = \frac{dV}{V}$$

and substituting Equation (32), we get

$$\frac{d F_1}{F_1} = \left\{ \frac{\left[\frac{d D_f}{K} \right]^2 + \left[W_{Bf} \frac{d \rho_s}{\rho_s} \right]^2}{(W_{sp} + W_{Bf})^2} \right\}^{1/2} \quad (33)$$

For the same reason, we can say that the error in F_1 is much greater than the error in F_2 and that in plots only the error in F_1 need be considered.

3.1.4 Application of the Error Analysis

In Figure 3.5, the results of the error analysis are applied to the saccharin data, with the uncertainty of each point plotted as an "error bar". The solid line is the average line depicting the area for saccharin of $1.53 \text{ m}^2/\text{g}$. The dashed lines are the envelopes of the most probable slopes drawn through any set of data. They were drawn to include 2/3 of the error bars in each run. (5) The areas calculated from these envelopes represent an uncertainty of 7 percent. The envelope include about 2/3 of the points, giving credence to the concept that 1.53 is the most probable value, with 7 percent being the standard deviation.

3.2 Particle Shape

Electron and light microscopes have been used to obtain very useful particle-shape information on many of the powders currently under study. Figures 3.6 through 3.16 contain micrographs of talc, saccharin, egg albumin, powdered milk, Sm, powdered sugar, and cornstarch. Although the micrographs "speak for themselves", it is interesting to note the unique, jagged, plate-like structure of talc because compacted talc displays much greater elasticity than any of the other powders under study. The micrographs indicate a complete range of shape characteristics from the irregular structure of talc to the smooth, nearly spherical structure of cornstarch. Figure 3.13 dramatizes the wide range of particle sizes found typically in Sm samples.

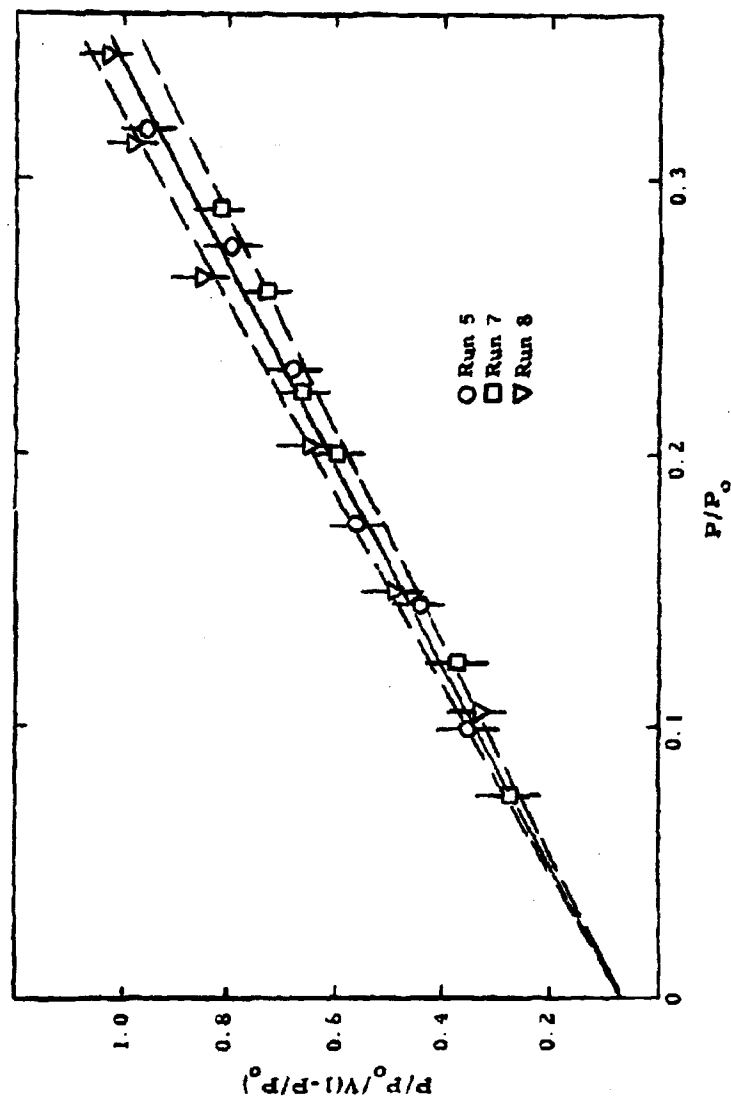


Figure 3.5 Uncertainty in BET Plot of N_2 Adsorption by Saccharin



Figure 3.6

Powder Ground Talc MMD (Whitby) 1.75 microns
Method of Dispersion Aerosol cloud formed by hand syringe.
Gravitational settling of powders upon a specimen grid.
Magnification 30,000X (microscope), 2.5X (enlargement); 75,000X total
Micrograph No. 63-2-71



Figure 3.7

Powder Ground Talc MMD (Whitby) 1.75 microns

Method of Dispersion Gravitational settling in an aerosol chamber upon a specimen grid. Aerosol formed by hand syringe.

Magnification 30,000X (microscope); 2.5X (enlargement); 75,000X total

Micrograph No. 63-4-5

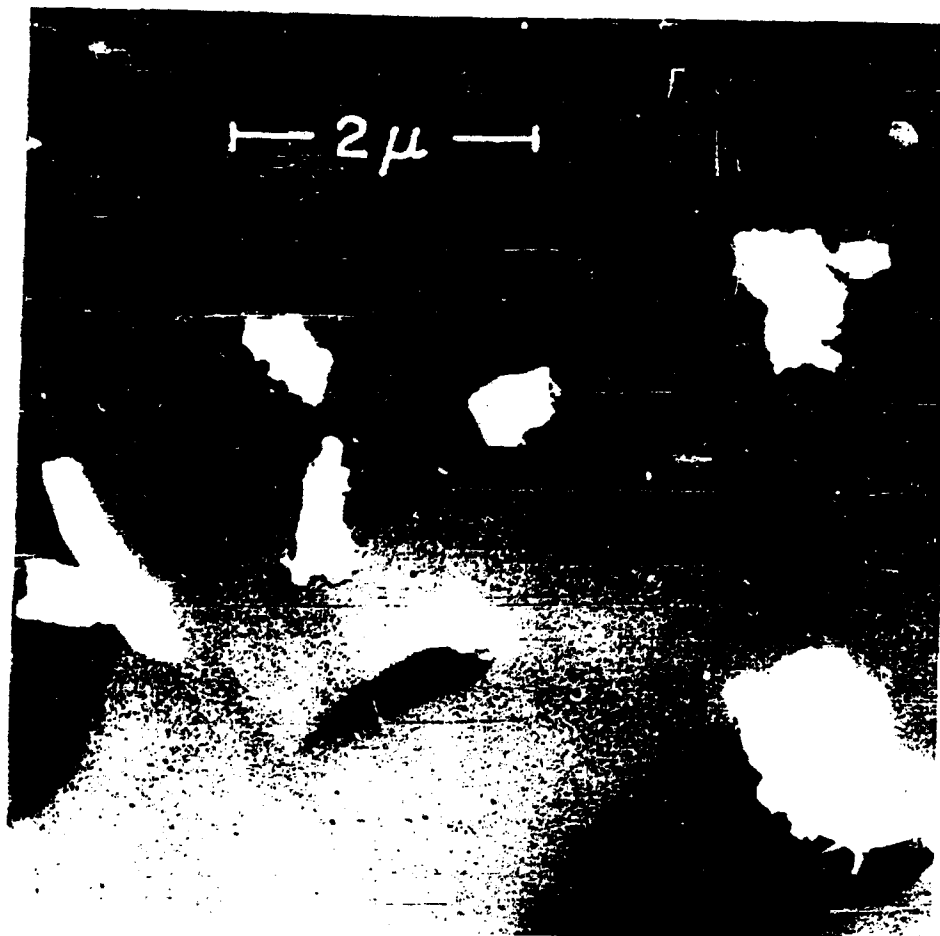


Figure 3.8

Powder Ground Talc **MMD (Whitby)** 1.75 microns
Method of Dispersion Particles dispersed in liquid naphtha. Suspension
liquid sprayed on specimen grid with Raasch Type VL Airbrush.
Magnification 10,000X (microscope); 2.5X (enlargement); 25,000X total
Micrograph No. 63-4-43
 (specimen grid shadow cast with chromium at a 5 to 5
 height to length ratio)

3-23

Page determined to be Unclassified
 Reviewed Chief, RDD, WHS
 IAW EO 13526, Section 3.5
 Date: **APR 15 2013**

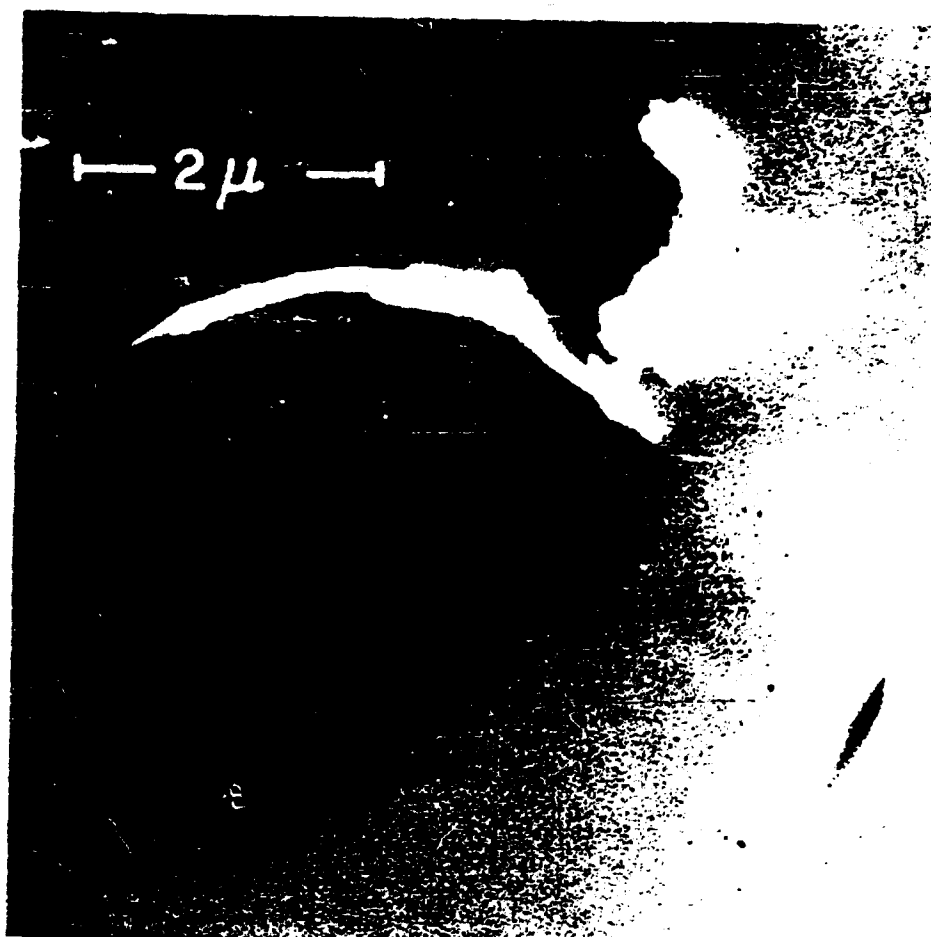


Figure 3.9

Powder Ground Talc MMD (Whitby) 1.75 microns
 Method of Dispersion Naphtha dispersed suspension sprayed on specimen
grid with Paasch Type VL Airbrush (15 mm. at 10 psi).
 Magnification 10,000X (microscope); 2.5X (enlargement); 25,000X total
 Micrograph No. 63-4-44
 (Specimen grid shadow cast with chromium at a 3:0.5 height
 to length ratio.)

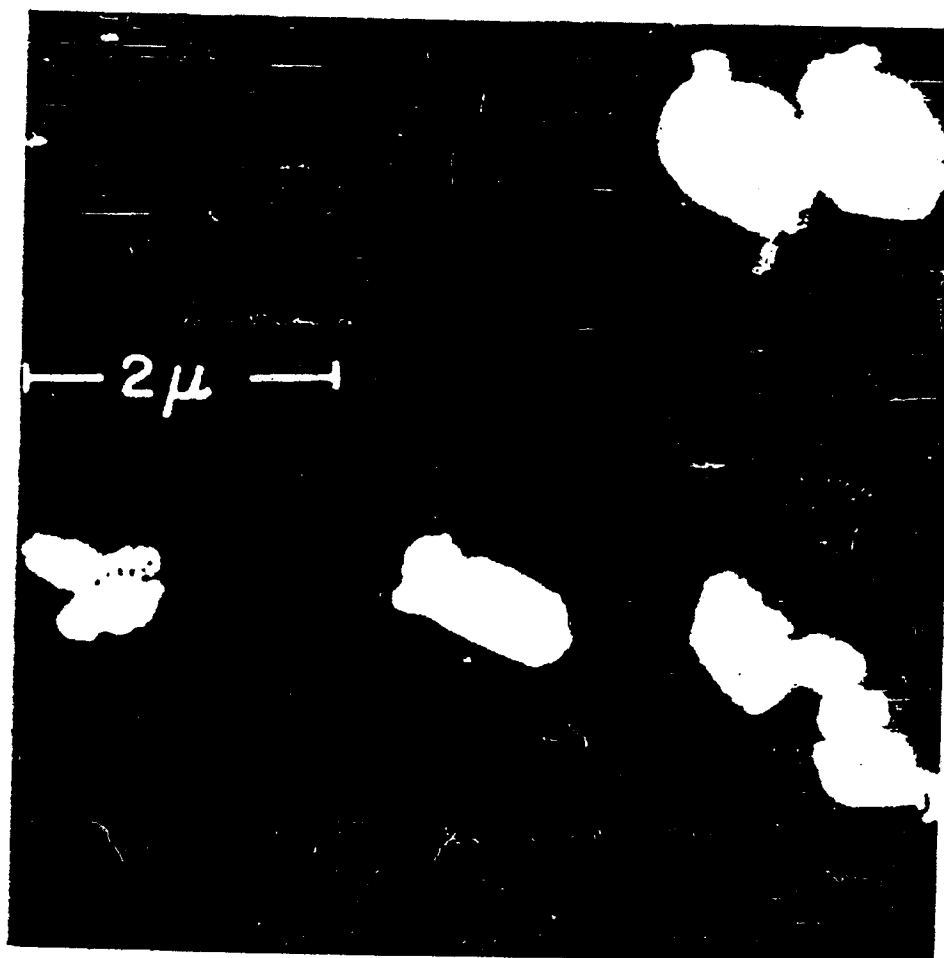


Figure 3.10

Powder Ground Saccharin MMD (Whitby) 6.9 microns
 Method of Dispersion Dispersed in naphtha; sprayed on grid with a
Paasche Type VL Airbrush (15 in. and 10 psi)
 Magnification 10,000X (microscope); 2.5X (enlargement); 25,000X total
 Micrograph No. 63-4-52
 (Specimen grid shadow cast with chromium at a 3 to 5 height
 to length ratio.)

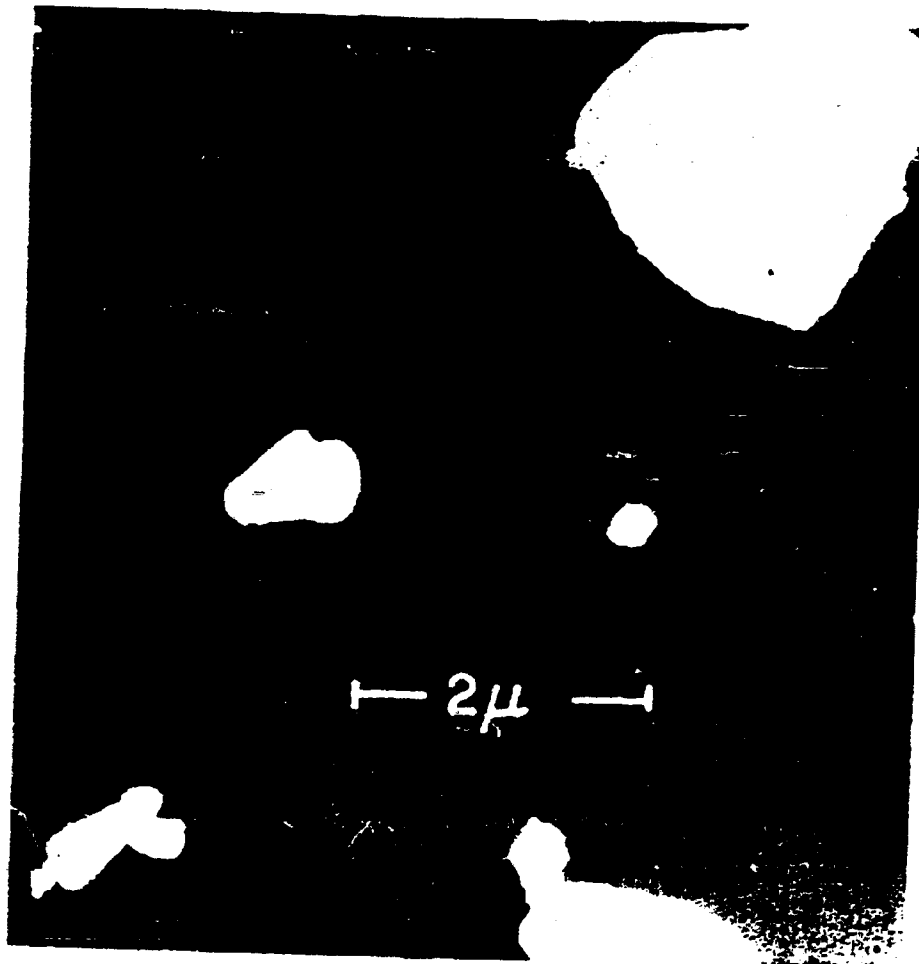


Figure 3.11

Powder Ground Egg Albumin MMD (Whitby) 4.8 microns

Method of Dispersion Dry powder dispersed on specimen grid with a
Paasche Type VM Airbrush (15 in and 40 psi).

Magnification 10,000X (microscope); 2.5X (enlargement); 25,000X total

Micrograph No. 63-4-48

(Specimen grid shadow cast with chromium at a 3 to 5 height
to length ratio.)

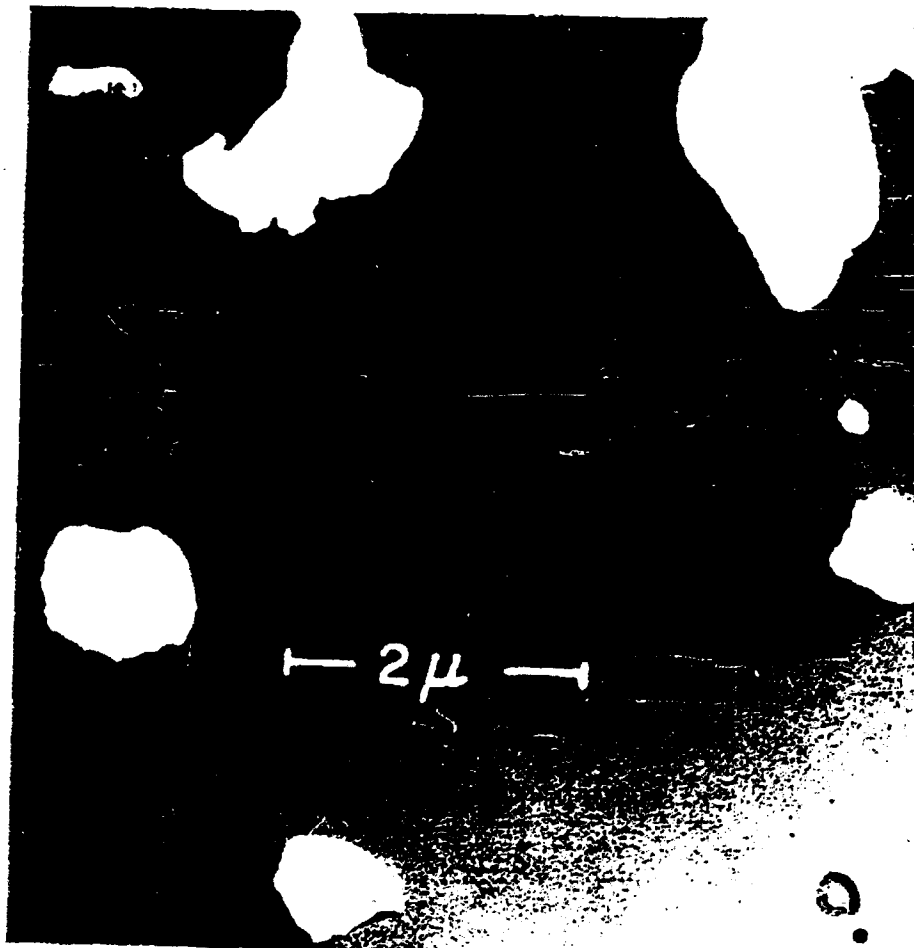


Figure 3.12

Powder Ground Powdered Milk MMD (Whitby) 7.0 microns
 Method of Dispersion Dispersed in naphtha; sprayed on grid with a Paasche
Type VL Airbrush (15 in. and 40 psi).
 Magnification 10,000X (microscope); 2.5X (enlargement); 25,000X total
 Micrograph No. 63-4-51
 (Specimen grid shadow cast with chromium at a 3 to 5 height
 to length ratio.)



Figure 3.13

Powder Sm (Pool # 7) _____ MMD (Whitby) 6.4 microns
Method of Dispersion Dispersed in naphtha; sprayed on specimen grid with a
Paasche Type VL Airbrush (15 in. and 40 psi).
Magnification 3,000X (microscope); 2.5X (enlargement); 75,000X total
Micrograph No. 63-4-59



Figure 3.14

Powder Sm (Pool # 7) MMD (Whitby) 6.4 microns
Method of Dispersion Dispersed in butyl alcohol; sprayed on glass slide
with airbrush (15 in. and 40 psi).
Magnification 400X (light microscope); 2.5X (enlargement); 1,000X total
Micrograph No. 63-B-11



Figure 3.15

Powder Powdered Sugar MMD (Whitby) 34.5 microns
Method of Dispersion Dispersed in butyl alcohol; sprayed on glass slide
with a Faasche Type VL Airbrush (15 in. 40 psi).
Magnification 400X (light microscope); 2.5X (enlargement); 1,000X total
Micrograph No. 63-A-31

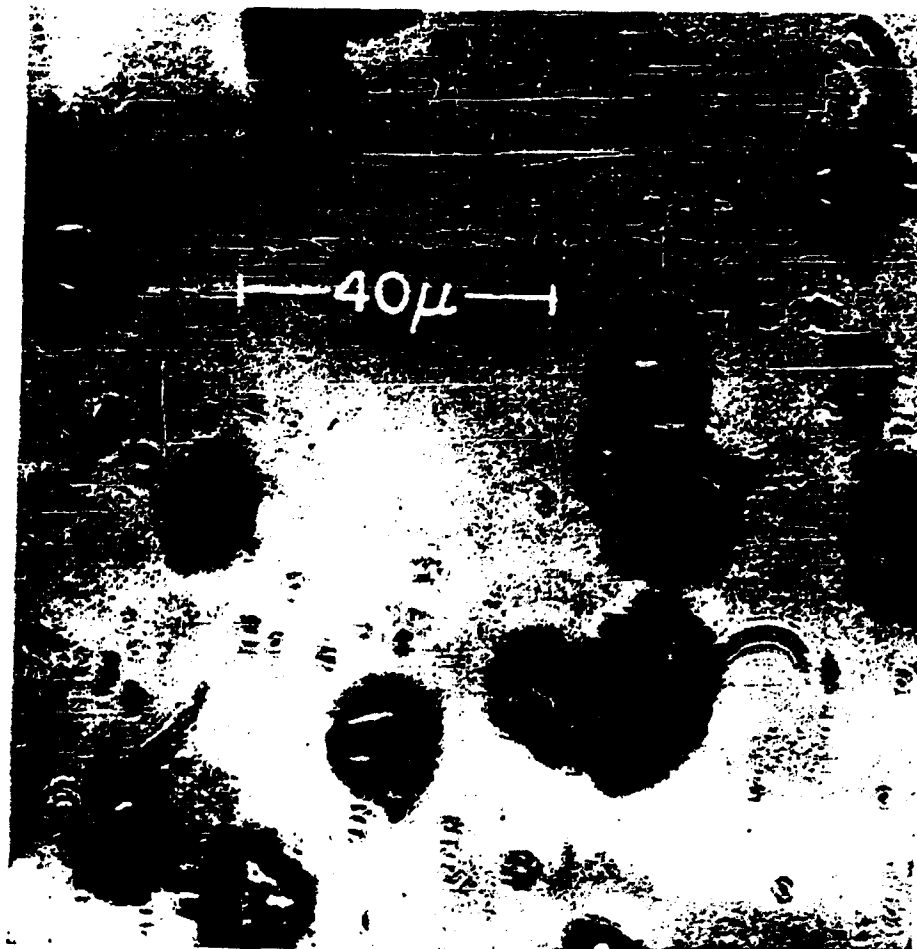


Figure 3.16

Powder Unground Cornstarch MMD (Whitby) 12.2 microns
Method of Dispersion Dispersed in butyl alcohol; sprayed on a glass slide
with a Paasche Type VL Airbrush (15 in. and 40 psi).
Magnification 400X (light microscope); 2.5X (enlargement); 1,000X total
Micrograph No. 63-B-14

3.3 Agglomerate Strength

We reported previously ⁽⁹⁾ that the energy-of-compaction apparatus was being used in an attempt to measure the strength of agglomerates in a powder bed. The results to date are not encouraging. Experimental conditions sensitive enough to measure agglomerate strengths also pick up background noise, vibrations, and minor powder bed nonuniformities, thus obscuring the desired information.

3.4 Powder-to-Metal Friction

The use of graphite to reduce powder-to-metal friction is discussed in various sections in this report. Graphite or graphite-like materials seem to be unique in their ability to reduce greatly this frictional force. A study will soon be made to determine criteria for methods of application and the smoothness of metal surfaces necessary to optimize this property.

3.5 Particle-Size Analysis of the Swirl Dispenser's Output

To determine if grinding of powders is taking place in the swirl dispenser used in the aerosol studies (see Section 4.4 of this report), Whitby size analyses were determined on representative samples obtained from the dispenser.

The method of sampling consists of coupling a 5-liter flask to the output of the swirl dispenser by means of a short tube. The tube extends into the flask and is immersed in a settling liquid about two inches deep. The settling medium used is the same as that used in the Whitby technique for the powder in question. The swirl dispenser was operated at 250 psi of nitrogen applied to the gas inlets for 5 seconds.

After a run, the settling medium containing the powder was concentrated by centrifugal force. The supernatant liquid was decanted and the remainder was diluted with naptha to a predetermined ratio. The mixture was then used as the feeding liquid for Whitby size analysis.

The results obtained were as follows:

	<u>Original Sample</u>		<u>Dispersed Sample</u>	
	<u>MMD</u>	<u>Std. Dev.</u>	<u>MMD</u>	<u>Std. Dev.</u>
Saccharin	6.7 μ	1.50	6.7 μ	1.47
Powdered Sugar	32 μ	2.07	32 μ	1.60

We determined from these analyses that little, if any, grinding is taking place in the disperser.

4. AEROSOL STUDIES

During this period, a program of research was initiated to study the effects of atmospheric charge conditions on aerosol decay. Ion concentration in the aerosol chamber was varied by introducing large quantities of positive ions at selected times in an aerosol's history by means of a corona-discharge ion generator. Other tests were conducted in addition to the electrostatic-charge runs and are discussed later in this section.

4.1 Description and Operating Characteristics of the Corona-Point Ion Generator

The general operating characteristics of corona-discharge ion generators are discussed at some length in the literature and will be treated only briefly here. The specific design of the unit used was developed by General Mills, Inc. personnel on another contract, and a detailed description may be seen in the associated reports.⁽³⁾ The corona point ion generator is shown schematically in the accompanying sketch.

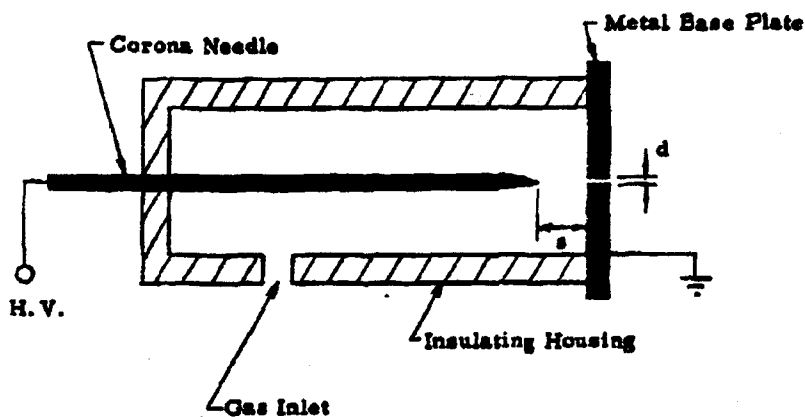


Figure 4.1 Corona-Point Ion Generator

When a voltage is applied to the corona needle, a high electric field is established at its point. The strength of this field is directly proportional to the applied voltage and inversely proportional to the radius of the needle's tip. For a suitable combination of tip radius and applied voltage, the electric field strength in the immediate neighborhood of the point is great enough to cause ionization of the gas molecules in that region. In the case where the needle is positive, the resulting negative ions (presumably free electrons) are collected at the needle after traveling a short distance. The positive ions drift toward the grounded base plate at a velocity governed by the electric field and the ion mobility. If a gas is admitted through the gas inlet, a "sink flow" of gas develops at the exit orifice. At sonic operation, the velocity of this flow is such that a large fraction of the positive ion current is swept out through the orifice and into the region beyond the base plate.

The ionizer used in the present work has a needle sharpened to a tip radius of about one micron. The needle spacing s is 1.8 mm, and the orifice diameter d is 0.79 mm. Dry nitrogen is used as the ionizing gas. We measured the free ion current output of the device by collecting the ion current in a 51-cm long by 1-cm ID copper tube mounted coaxially and spaced about 1/8 inch from the base plate. The results are shown in Figure 4.2, which also presents the gas-flow rate.

The ion gun is mounted in the chamber in a position diametrically opposite the dispersing gun, as shown in the following sketch. Both guns are exterior to the chamber. The base plate of the ion gun is electrically connected to the aluminum aerosol chamber, which in turn is connected to permanent ground. The ions that leave the gun are eventually collected on the chamber's walls. (See Figure 4.3.)

We have made measurements of current densities at equilibrium flow, a rough map of which is shown next. Note that a large fraction of the free ion output is collected on the floor of the chamber near the ionizer. Somewhat smaller current densities exist at other points in the chamber. (See Figure 4.4.)

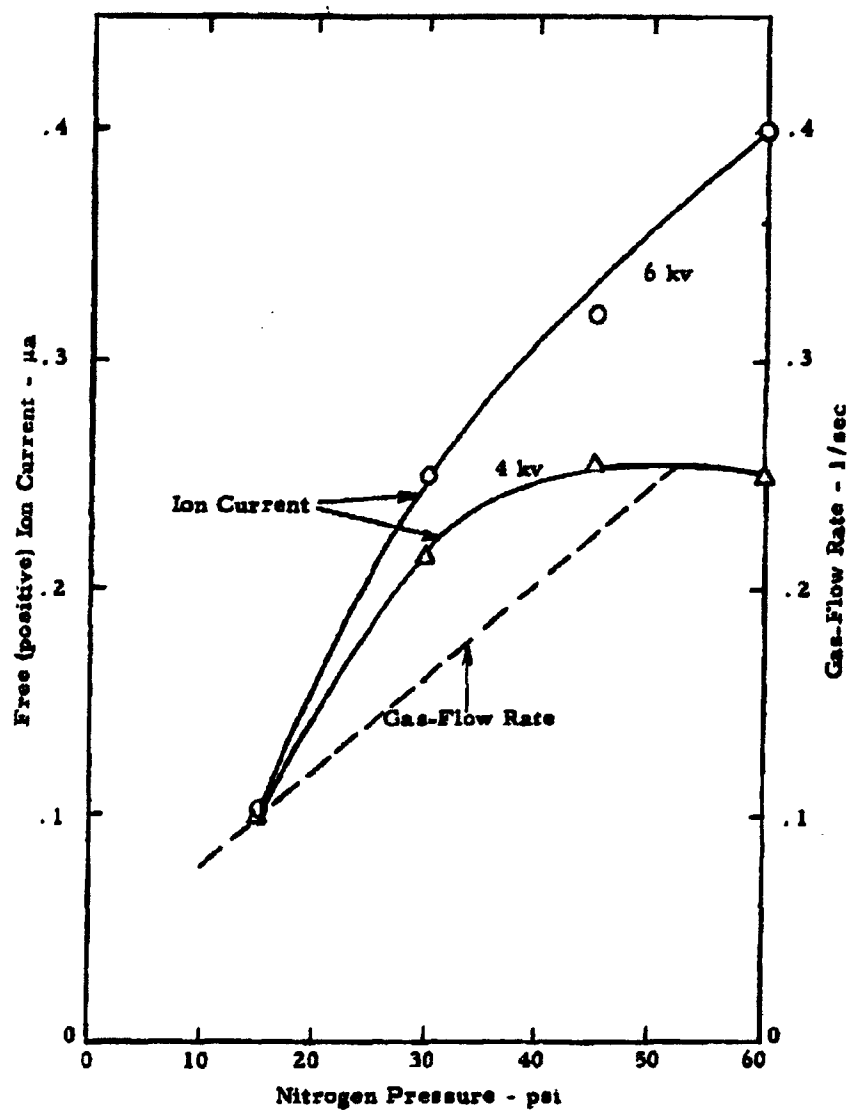


Figure 4.2 Characteristics of the Corona-Discharge Ion Generator

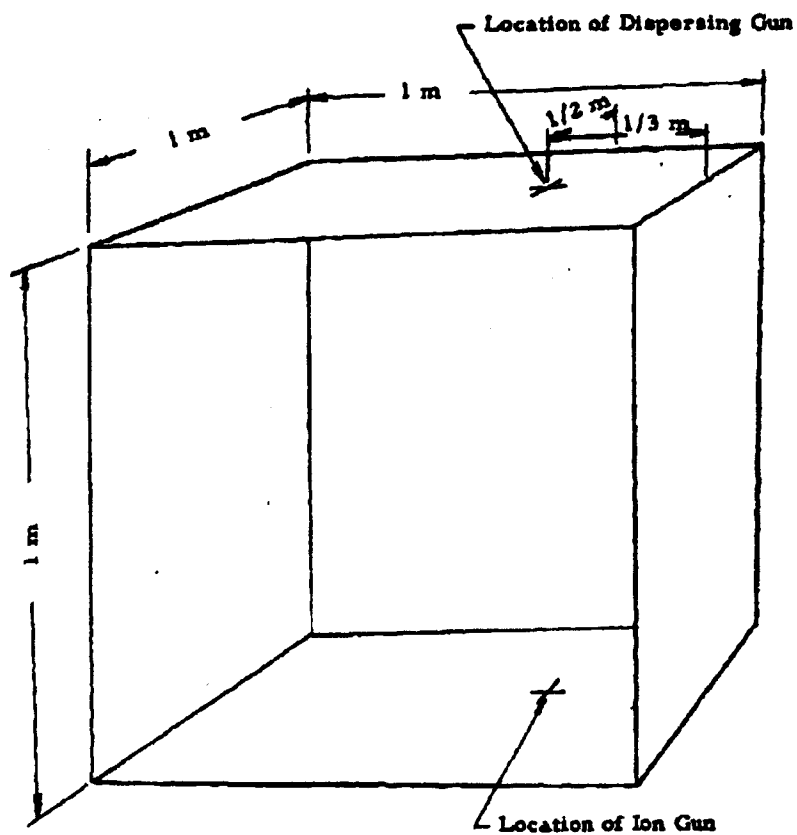


Figure 4.3 Position of Ion Gun with Respect to Dispersing Gun in the Aerosol Chamber

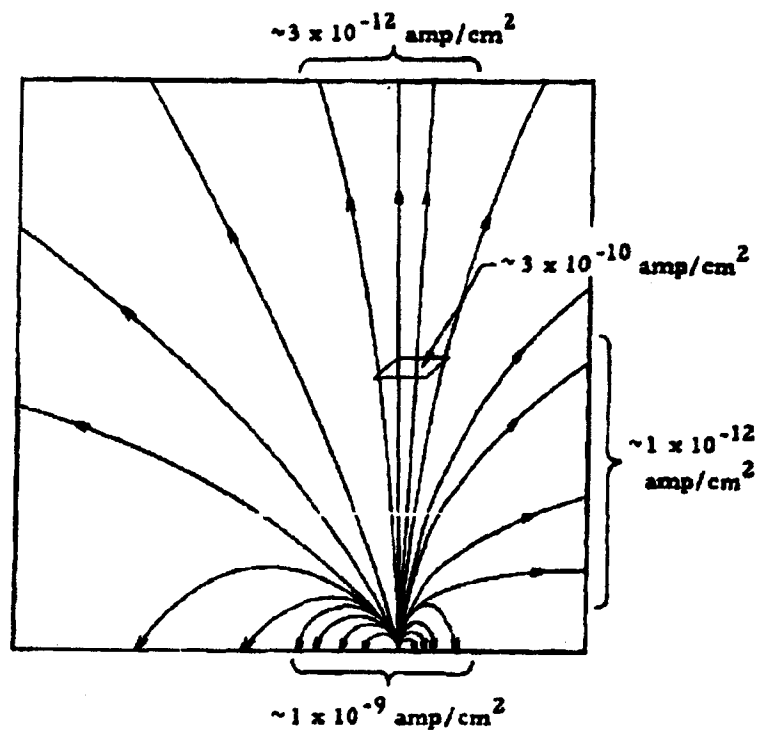


Figure 4.4 Map of Ion Current Densities in Aerosol Chamber

4.2 Procedure for Electrostatic-Charge Runs

The series of runs to be reported here all involved dispersing of 100 ± 5 mg of powder into the chamber with either simultaneous (Mode B) or subsequent (Mode C) injection of positive ions. These runs are to be compared to runs where no charge was injected (Mode A). The procedure for each of the series is indicated in the diagram. (Figure 4.5)

The time scale for each mode of operation is started when the ionizer gas is turned on. In each case, the swirl powder disperser was operated for a 5-second interval starting 10 seconds after the ionizer gas. The swirl disperser was operated at 60 psi. The difference between the modes of operation lies in the application of high voltage for the corona needle; it is this voltage which causes ion production. In Mode A no ions are injected; in Mode B ions are injected simultaneously with the powder for a 10-second interval; in Mode C ions are injected for 10-second intervals after powder injection (see Figure 4.5).

The gas pressure in the ionizer for the runs to be reported was 30 psi, and as the high voltage was set at 6000 volts, one can now see by referring to Figure 4.2 that the volume of gas admitted was 10.2 liters and that the total charge injected was about 2.5×10^{-6} coulombs (1.5×10^{13} uncharged ions). On the other hand, the powder disperser admitted 3.6 liters of gas and about 100 mg of powder ($\sim 10^9$ particles of $5\text{-}\mu$ diameter). The number of positive ions introduced per particle of powder is therefore approximately 10^4 .

We have, of course, no guarantee that there is actually a combination of powder particles and injected ions. One might expect some fraction of the powder particles that descend into the chamber bearing negative charge to be neutralized. The extent of this discharging is not known, however, at the present time. The experiment is to be viewed simply as one in which the aerosol particles are exposed to an abnormally large concentration of positive ions.

The aerosol experiments were carried out under conditions of room humidity, which remained relatively constant throughout a given series of runs.

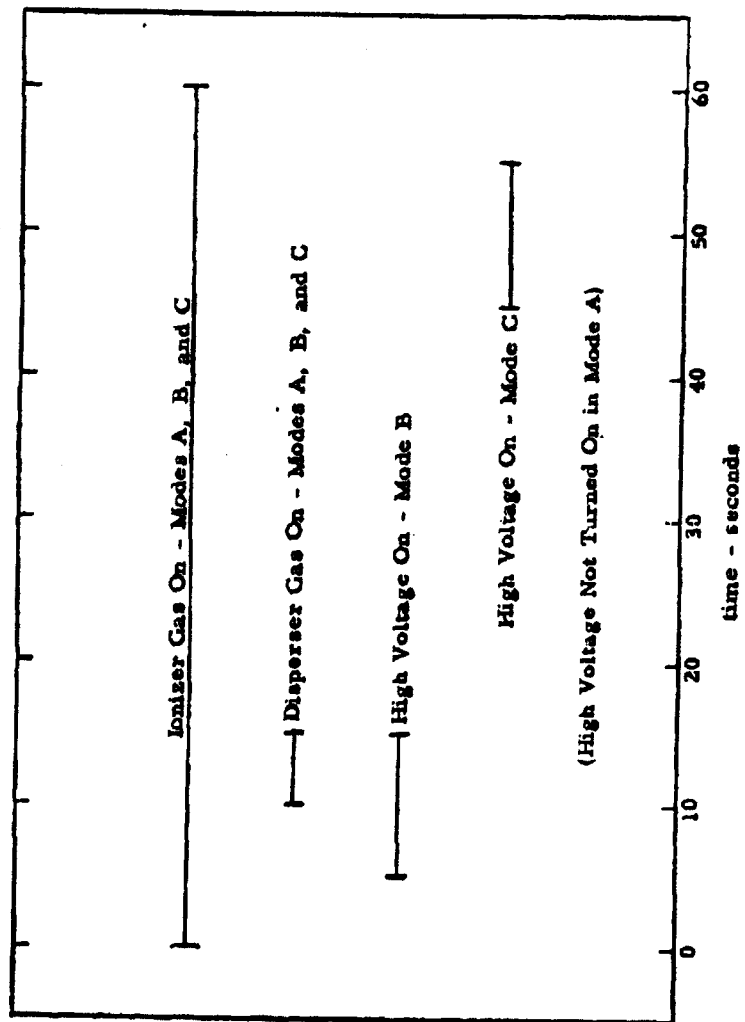


Figure 4.5 Modes of Ion Injection

4.3 Experimental Results

Electrostatic charge runs have been made on talc and saccharin. Each powder was run through the sequence of Modes A-B-C-A twice, the two series involving different humidity conditions. The light-scattering data from each run were reduced by the log-normal plot procedure explained previously. The half lives and initial amplitudes of the various aerosols are shown in Figures 4.6 and 4.7.

The data points in Figures 4.6 and 4.7 are collected into groups according to prevailing humidity. Each group of points represents 4 aerosol runs (only 3 in one of the saccharin series) carried out under "identical" prevailing humidity conditions. The fourth point in each group is a rerun of the no-charge conditions of the first point and is thus a check on reproducibility.

The data of Figures 4.6 and 4.7 can be summarized as follows:

4.3.1 Talc Aerosols

The injection of positive ions simultaneously with the injection of powder reduces aerosol longevity under the no-charge condition; the injection of positive ions after injection of the powder further reduces aerosol longevity.

4.3.2 Saccharin Aerosols

The injection of positive ions simultaneously with the injection of powder increases longevity, whereas ion injection after powder injection reduces longevity, under the no-charge injection condition.

It should be noted that there is an element of risk in drawing the above conclusions from the data available because the reproducibility is not as good as one might hope for. It is quite evident, however, that the stabilities of aerosols are affected by the radical atmosphere charge conditions employed here. In view of this, it may be necessary to modify certain statements advanced previously regarding the effect of electrostatic charge on aerosol decay.

The study will be continued during the next quarter.

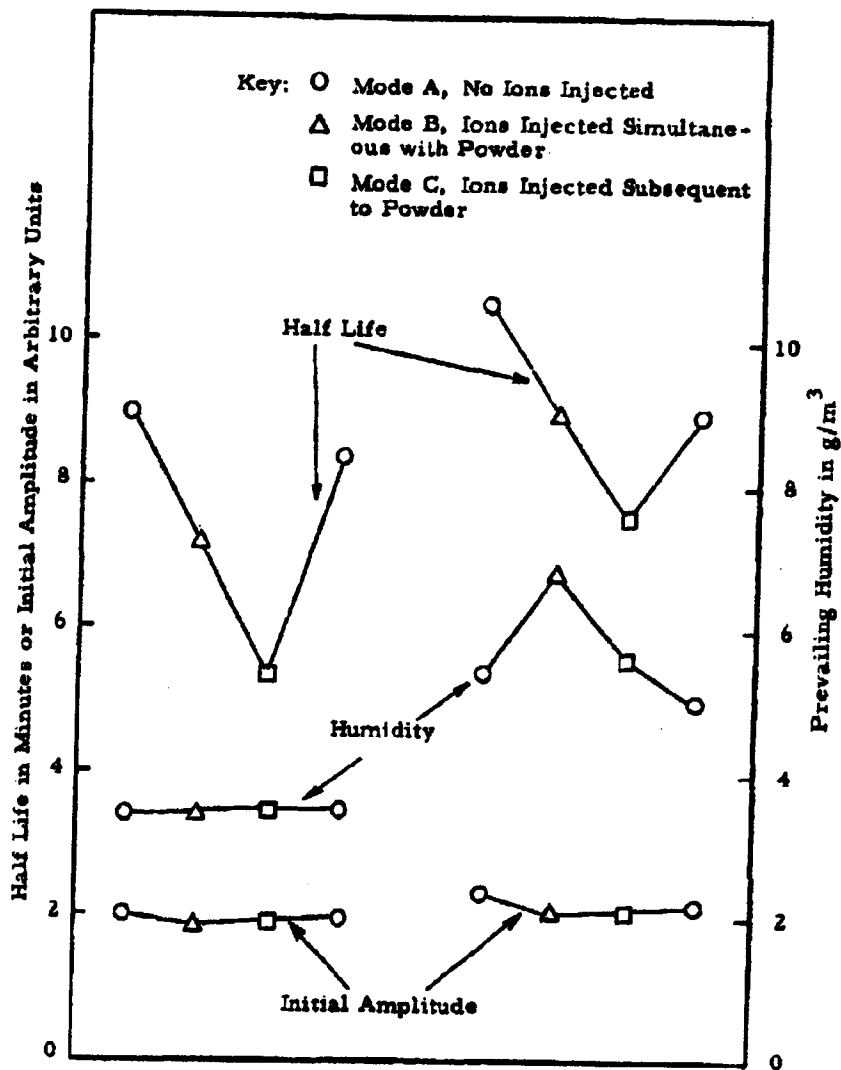


Figure 4.6 Half Lives, Initial Amplitudes, and Prevailing Humidity for Talc Aerosol Electrostatic Charge Runs

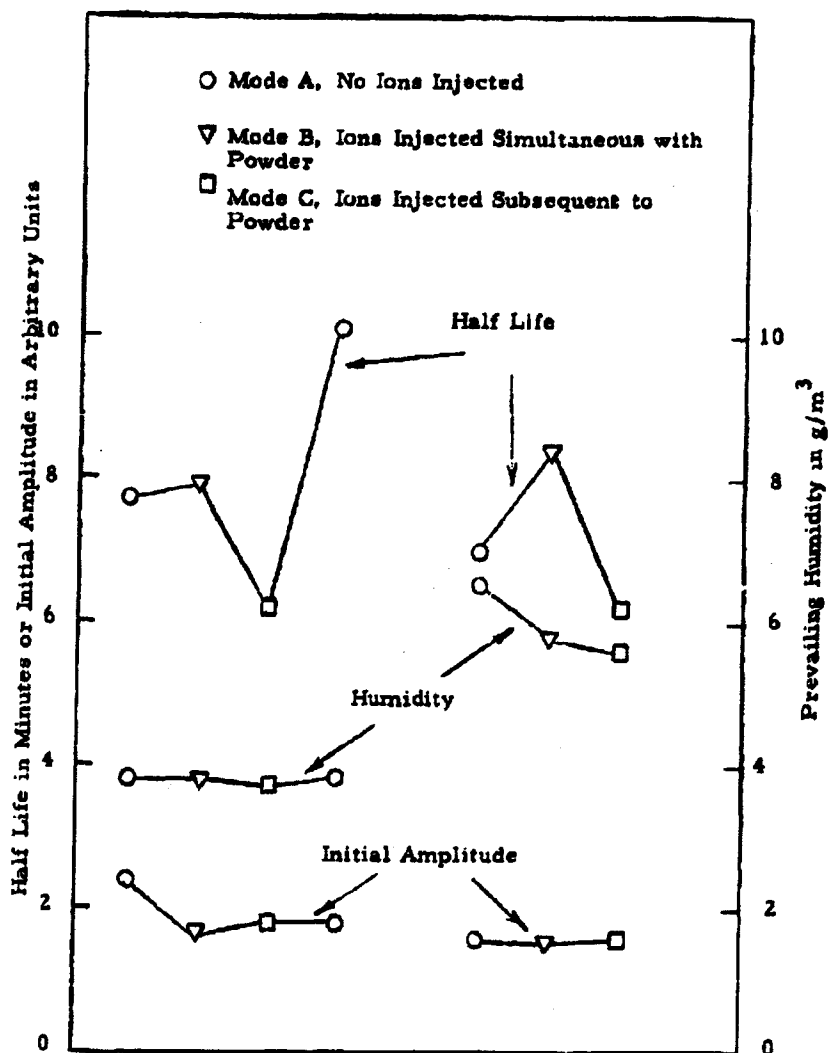


Figure 4.7 Half Lives, Initial Amplitude, and Prevailing Humidity for Saccharin Aerosol Electrostatic Charge Runs

4.4 Sampling of Swirl Dispenser's Output

One of the questions which has plagued the aerosol program for some time is whether grinding takes place in the dispersing process. During the past quarter, tests were made in which the entire output of the swirl dispenser was collected and submitted to Whitby sedimentation size analysis. The collection technique is discussed in Section 3.4 of this report. For the two powders tried--saccharin and powdered sugar--the size distributions of the swirl-dispersed samples were nearly identical to the size distributions of the stocks from which the samples were taken.

In another study of the swirl-dispenser performance, the dispersing gas-flow rate was measured by means of a capillary tube flowmeter. The results, somewhat higher than has been anticipated, are shown in Figure 4.8.

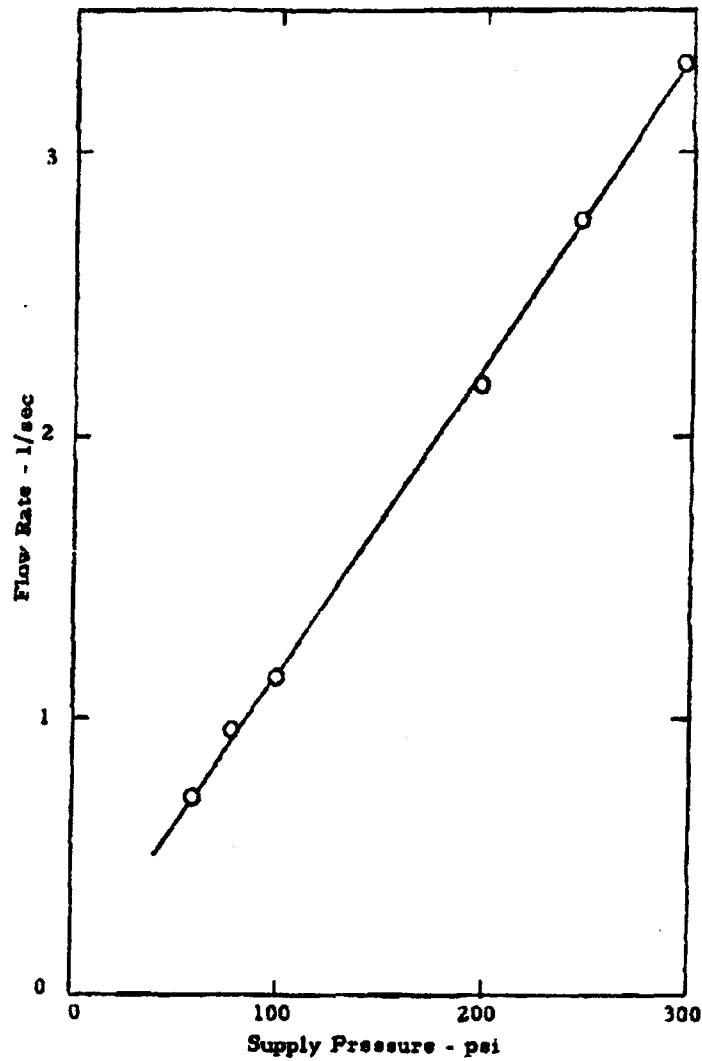


Figure 4.8 Gas Flow Characteristics of the Swirl Dispenser

5. EXPERIMENTS USING GRAPHITE TO REDUCE SIDE-WALL FRICTION OF COMPACTED POWDER SLIDING IN CYLINDERS

At the Fourth Coordination Meeting on Dissemination Research held at Fort Detrick in May, 1963, Mr. Eugene Flurie described some compacted powder experiments conducted at the Biological Laboratories in which graphite was used successfully on the walls of a small cylinder to reduce friction. Since side-wall friction is an important consideration in developing equipment to handle compacted dry-agent materials, an investigation of the use of graphite to reduce friction was started at General Mills, Inc. Most of our interest in lowering side-wall friction relates to the performance of the E-41 spray tank and its associated loading equipment. During the development of these items, a number of experiments were performed which provided data on the force required to move a mass of compacted powder out of the cylinder in which it was compacted. Some of these experiments were repeated during May and June using graphite as a lubricant on the cylinder's walls. The results were very gratifying. Use of graphite has lowered frictional force by approximately 50 percent. Experimental procedures employed and results obtained are discussed in the following paragraphs.

5.1 Procedure

The data reported herein were obtained in three sets of experiments: Two sets of tests were conducted in May and August, 1962, during a determination of the forces likely to be encountered in compacting and loading dry-powder charges into the E-41 spray tank. These tests provided data on density as a function of compactive pressure, and on the force required to push a body of compacted powder out of a cylinder as a function of compactive pressure and the cylinder's length-to-diameter ratio. A 6-inch diameter aluminum cylinder was used in tests with Mistron Vapor talc, and a 7.5-inch cylinder was used with powdered sugar, flour, and powdered milk.

For the third set of experiments, the tests with talc and powdered sugar were repeated in a 6-inch cylinder, using graphite to lubricate the cylinder's walls. These experiments were conducted during the latter part of May and early June, 1963. Their objective was to determine the effectiveness of graphite in lowering side-wall resistance to the sliding of compacted powder.

The experimental procedures were the same for all three sets of tests. The powder was pressed into the cylinder using the arrangement shown schematically in Figure 5.1. During compaction, force was applied for a sufficiently long period of time to allow entrapped air to pass through the felt pad and air holes incorporated in the compacting piston. The compactive force was measured on the platform scale. After completion of the filling operation, the cylinder was raised off the base plate with spacers so that the body of compacted powder could be pushed down out of the cylinder. The force required was measured on the platform scale, and the cylinder was kept vertical at all times.

When filling the cylinder, we added powder in increments and applied specified compactive force after each addition. One-half pound increments were used with talc, and one-pound measures with powdered sugar. The total amount of powder was varied so that different lengths of compacted powder specimens were obtained. The length-to-diameter ratios employed ranged from 0.7 to 2.5. The compactive pressures ranged from 3.5 to 13.1 psi.

The graphite used to lubricate the cylinder wall was wiped on with a piece of chamois skin when applied dry. This was the case for most of the experiments. A few trials were made in which the graphite was mixed with a liquid and sprayed on with a small spray can. The film was allowed to dry before we filled the cylinder with powder. Water, alcohol, and trichloroethylene were tried as vehicles for applying the graphite as a spray.

Two brands of finely-divided graphite were used. Their particle sizes were not known, but we plan to make size determinations. One brand was "620" powdered amorphous graphite from the American Graphite Company, Ticonderoga, New York. The other was "Microfyne" lubricating flake graphite from the Joseph Dixon Crucible Company, Jersey City, New Jersey. There was no discernible difference in performances of the two brands.

APR 15 2013

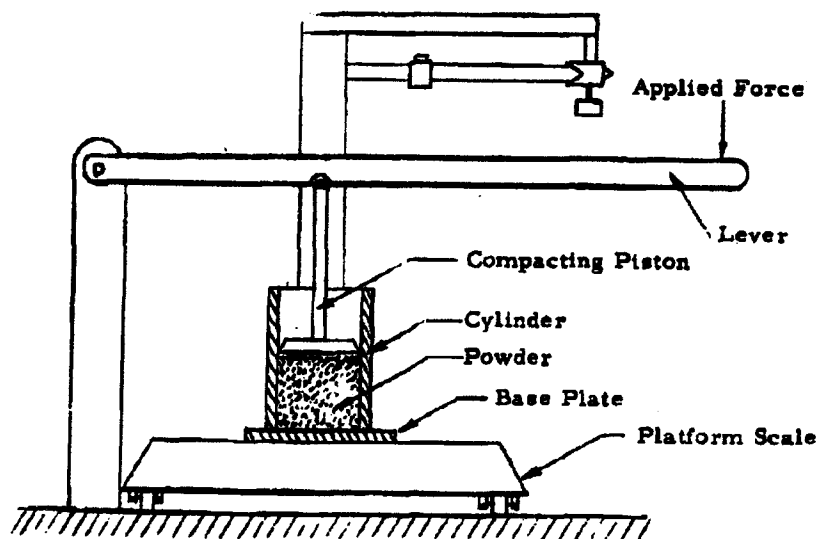


Figure 5.1 Schematic Diagram of Arrangement Used to Compact Powder into a Cylinder and to Determine the Force Required to Translate the Compacted Powder through the Cylinder

5.2 Results

The results of the experiments are presented in Figures 5.2, 5.3, and 5.4, where the force to eject the body of compacted powder is plotted against the length-to-diameter ratio of the body of powder. Although the ejection force was measured directly in pounds, it has been converted to pounds per square inch to permit a comparison of the results obtained with the 6-inch cylinder to those from the 7.5-inch cylinder. In both Figures 5.2 and 5.3 there are two sets of data plotted. The results from the plain aluminum cylinder are represented by dashed lines, and those from the graphite-coated cylinder are depicted with solid lines. Each point represents a single test.

The data from the trials with talc are presented in Figure 5.2. It is clearly evident that the use of graphite to lubricate the cylinder produces an appreciable reduction in side-wall friction. These data also indicate that the percentage of reduction is greater for the larger length-to-diameter ratios than it is for the smaller ratios. This was observed for both compactive pressures employed in the trials. For the 5.3 psi pressure, the percentage of reduction was 49 percent at a length-to-diameter ratio of 1.5, increasing to 55.7 percent at a length-to-diameter ratio of 2.3. For the 3.53 psi compactive pressure, the percentages of reduction at the respective ratios were 28.8 and 49.

It will also be observed that the percentage of reduction in ejecting pressure is greater at a higher compactive pressure than at a lower one. (This is undoubtedly related to the higher density produced by the higher compactive pressure.) For a length-to-diameter ratio of 2.3 and a compactive pressure of 3.53 psi, the use of graphite resulted in a 49 percent reduction in ejecting pressure whereas the percentage of reduction was 55.7 percent at a pressure of 5.3 psi.

An examination of the data presented in Figure 5.3 for powdered sugar shows the same general pattern. Here again, the use of graphite to lubricate the cylinder's walls before packing in the powdered sugar resulted in a significant reduction in the force required to push compacted powder out of the cylinder.

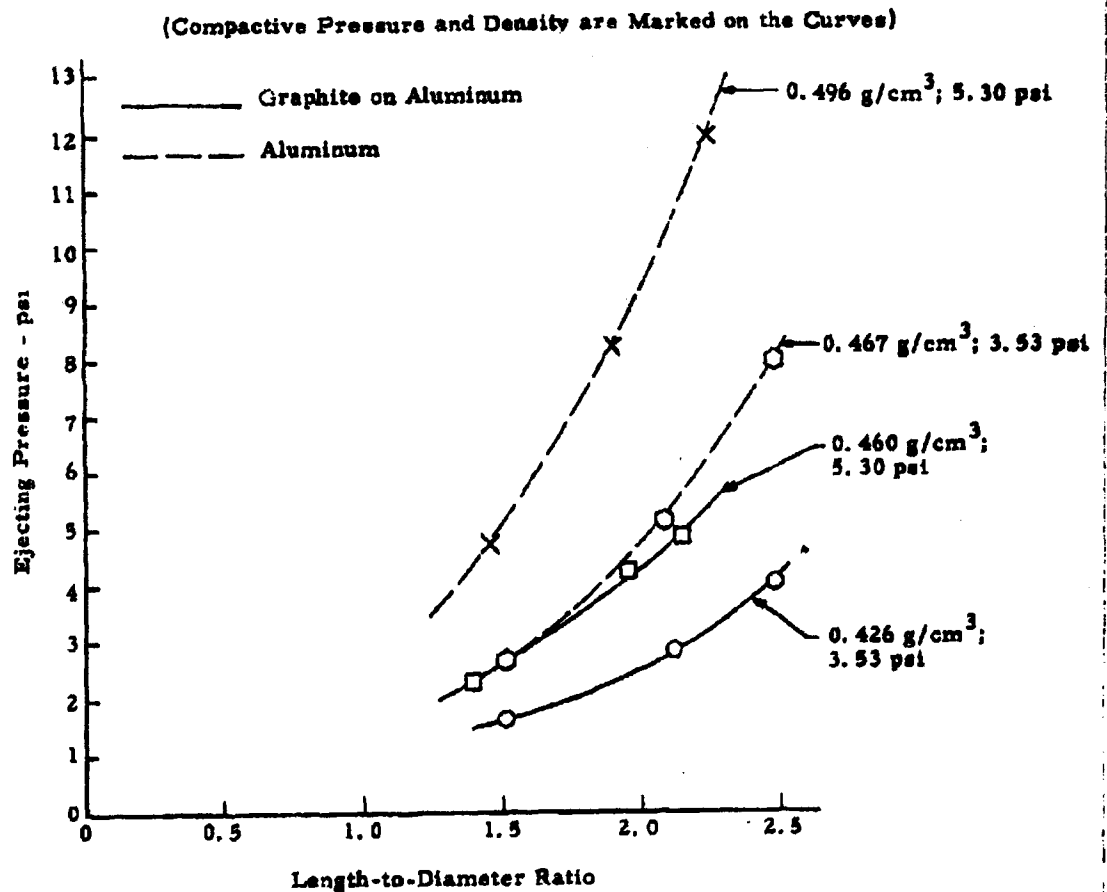


Figure 3.2 Comparison of Force to Eject Compacted Talc from a 6-inch Diameter Aluminum Cylinder with and without Graphite

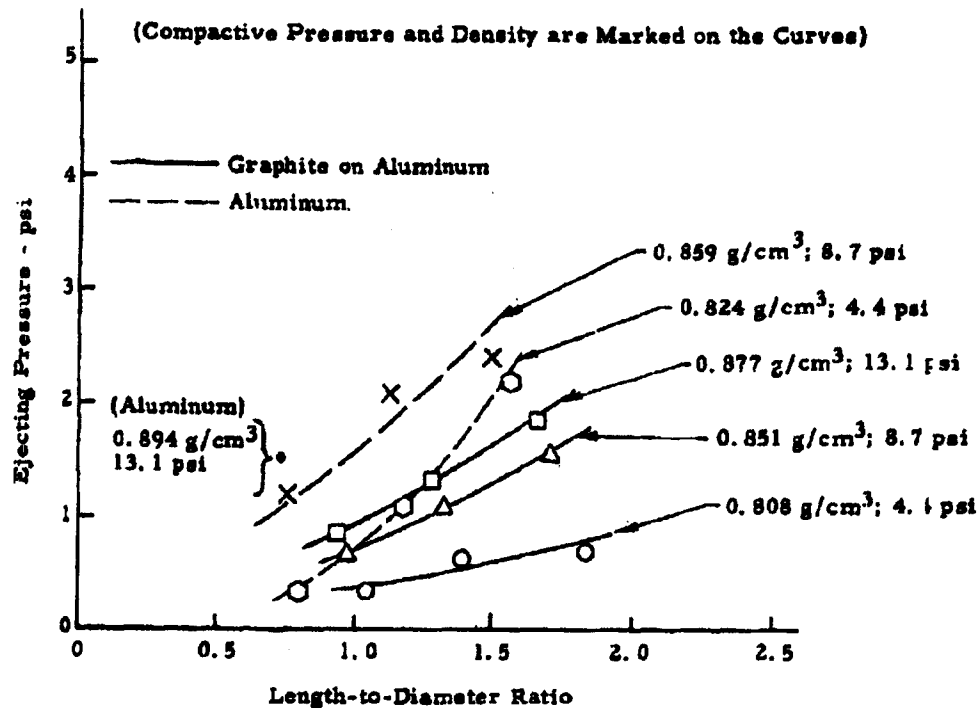


Figure 5.3 Comparison of Force to Eject Compacted Powdered Sugar from a 6-inch Diameter Aluminum Cylinder with Graphite and a 7.5-inch Diameter Aluminum Cylinder without Graphite.

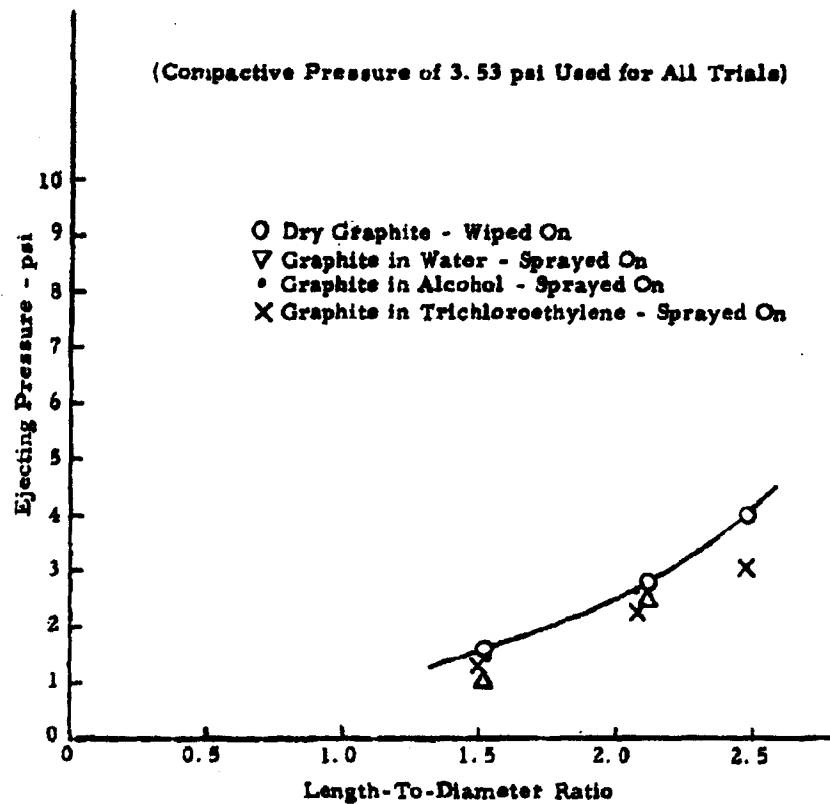


Figure 5.4 Comparison of Force to Eject Compacted Talc from a 6-Inch Diameter Aluminum Cylinder for Various Methods of Applying Graphite for Lubrication

The percentage of reduction in force was more for the large length-to-diameter ratios than for the small. The data for the graphite-lubricated cylinder showed less scatter than that for the plain aluminum cylinder. This could be interpreted as a further indication that frictional effects are alleviated by the use of graphite.

As was pointed out in the discussion on procedures, the graphite powder was applied dry with a chamois skin for most of the trials. This was the method of application employed for the data presented in Figures 5.2 and 5.3. A few trials were made in which the graphite was suspended in a liquid and then sprayed onto the surface. The liquid was then allowed to evaporate before filling the cylinder with powder (Mistron Vapor talc was used). Water, alcohol, and trichloroethylene were tried as vehicles. We found that all three systems deposited graphite satisfactorily on the cylinder's wall. Data from the trials using the spray technique are presented in Figure 5.4 with comparable data for dry trials with talc. All of the data points for the sprayed graphite trials were found to be slightly below the curve for the trials where the graphite was applied dry. The results obtained when trichloroethylene was used are especially encouraging and suggest that a technique for applying graphite may be discovered that will result in even lower side-wall friction.

In view of the encouraging results obtained with the 6-inch diameter cylinder, we decided to experiment with the loader used for filling the E-41 spray tank with compacted powder. This loader is described in the Ninth Quarterly Progress Report.⁽²⁾ The loading tube is 16-3/16 inches in diameter and 36-5/8 inches long. It contains sufficient material to fill one end of the E-41 spray tank in a single loading operation.

The loading tube is made of aluminum that has been hard-coat anodized and then coated with a dry-film lubricant. Experience has shown that an air pressure of from 30 to 35 psig behind the piston is required to force the compacted powder out of this tube.

In preparation for the experiment with graphite lubrication, the tube was cleaned of powder from previous loading operations by a light rubbing with steel wool. Then the graphite was wiped on with a chamois skin, and Mistron vapor talc was packed into the tube to an average density of 0.63 g/cm³.

The loading tube was then positioned horizontally, and the talc was pushed out and allowed to fall into a barrel. A pressure of 12 psig was sufficient to force the talc out of the tube. This particular experiment has not been repeated, but graphite lubrication was used subsequently in filling the E-41 spray tank with talc prior to shipment to Eglin Air Force Base. During this operation a pressure of 20 psig was observed on three occasions. Both the 12 psig and 20 psig pressures are substantial improvements over the 30 to 35 psig previously required.

5.3 Conclusions

Although only a limited amount of data has been obtained on the use of graphite to reduce side-wall forces associated with moving a charge of compacted powder in a cylinder, the results are significant enough to warrant reporting them at this time. The tests with the 6-inch cylinders showed a reduction in force of approximately 50 percent when graphite is used to lubricate the cylinder's wall. One test with the 16.5-inch cylinder showed a 60-percent reduction in the force (from 30 to 12 psi) required to push a charge of compacted talc out of this cylinder. Subsequent experience in loading for the Eglin tests indicates that a reduction of approximately 35 percent may be more reasonably expected.

As a consequence of the good results obtained thus far with graphite, further work in this area is planned. More tests with 6-inch cylinders will be conducted. One area of special interest is the influence of initial surface roughness on frictional forces when graphite is used as a lubricant. Full-scale tests with the experimental disseminator are also planned.

6. DISSEMINATION AND DEAGGLOMERATION STUDIES

6.1 General Approach

During this period, studies were continued on the deagglomeration of dry, finely divided Sm simulant. Wind-tunnel tests were conducted to investigate two factors: dissemination at low flight speeds, and dissemination of material stored in the compacted state.

6.2 Dissemination at Low Flight Speeds

Prior to this time, we have been concerned with the feasibility of deagglomerating finely divided Sm at flight speeds of Mach number 0.5 to 0.8 (330 to 528 knots). Results from wind-tunnel tests showed that the material could be mechanically disaggregated and disseminated with high physical efficiency at these speeds. Our study has now been extended to cover flight speeds below Mach number 0.5. We have determined the minimum speed for efficient dissemination of uncompacted material, and have conducted a thorough investigation at Mach number 0.3.

During these tests, we employed the same aerosol-sampling techniques described in an earlier report.⁽²⁾ Full-flow impactor tests provided a qualitative measure of the presence of very large agglomerates (100 to 500 microns in diameter) in the aerosol, whereas collection of fine highly deagglomerated material on membrane filters provided quantitative data from which the limiting bulk-density condition could be determined. For this purpose, the high-velocity sampling probe was located 0.5 inch from the bottom tunnel wall.

The Sm used in this study was taken from lot S1-Sm-342, the same lot used in our previous tests. The moisture content of this simulant has increased to 2.6 percent from a value of 1.7 percent which it had during many of our earlier tests. This change does not, however, appear to be affecting the deagglomeration efficiency.

The results of these tests at Mach number 0.3 are shown in Figure 6.1. The measurements indicate that the concentration of fine, deagglomerated aerosol is essentially independent of bulk density in the range 0.33 to 0.52 g/cm³. Above this range, however, the quantity of material in the fine aerosol cloud decreases. Conversely, the impactor results indicate that as the bulk density exceeds 0.52 g/cm³ an increasing percentage of the aerosol is comprised of large agglomerates that do not readily break up. This value, therefore, represents the limiting condition for a flight speed of Mach number 0.3.

With the uncompacted material, we found that very good break-up can be obtained at a flight speed of Mach number 0.25. As the air velocity was decreased below this value, the large agglomerates became increasingly prominent.

6.3 Efficient Deagglomeration with the E-41 Aircraft Disseminator

Results that have been obtained with the wind-tunnel apparatus are combined in this section to define more clearly the relationship between flight speed and compactive density for a disseminator of the E-41 type. The maximum bulk density that can be deagglomerated efficiently was determined from concentration curves such as that shown in Figure 6.1. Those for Mach number 0.5 and 0.8 were discussed in Reference 2. For this purpose, we determined the "break point" for each curve; break point is defined as the bulk density at which the fine aerosol concentration decreases to 95 percent of its maximum value for a particular series of tests. Figure 6.2 and Table 6.1 show the break points for runs at Mach numbers of 0.3, 0.5, and 0.8. At the break point, deagglomeration efficiency is approximately 90 percent--that is, 90 percent of the particles that originally had diameters in the 1- to 5-micron range are dispersed in the same size range by the disseminator. Microscopic analyses of filter samples and full-flow impactor collections have been used to determine this value of efficiency.

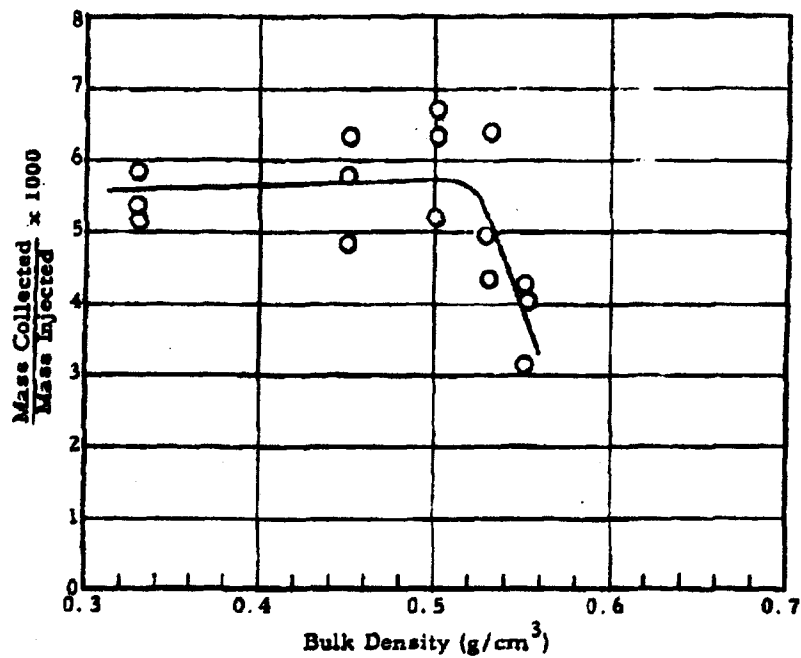


Figure 6.1 Concentration of Fine Sn Aerosol Cloud in Wind Tunnel as a Function of Bulk Density (Airstream Mach Number 0.3; Sampling Probe Positioned 0.5 Inch from Wall)

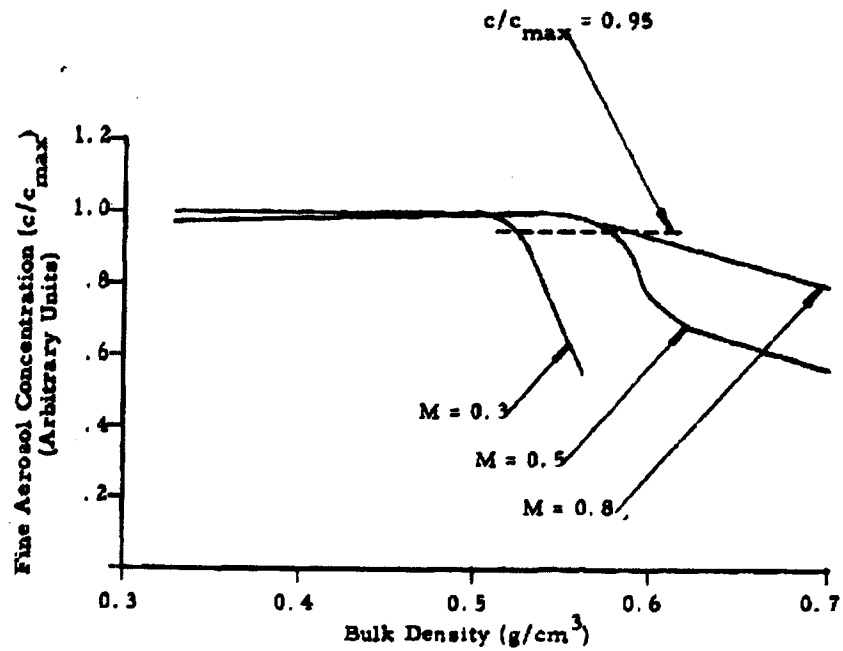


Figure 6.2 Concentration of Fine Sm Aerosol Cloud in Wind Tunnel as a Function of Bulk Density and Airstream Mach Number (Sampling Probe Positioned 0.5 Inch from Wall)

Table 6.1 Break Points for Dissemination Tests with Compacted Sm at Wind Tunnel Mach Numbers of 0.3, 0.5, and 0.8

<u>Mach Number</u>	<u>Bulk Density (g/cm³)</u>
0.30	0.52
0.50	0.58
0.80	0.59

In Figure 6.3 the break points are plotted against dissemination flight speed. Also, the minimum flight speed is shown for uncompacted Sm. This curve defines the operational region in which the E-41 is expected to be very effective in deagglomerating compacted materials. In the bulk density range 0.3 to 0.5 g/cm³, the curve is quite flat because the energy of compaction is low (see Figure 6.4). In mechanically disaggregating the compacted slug prior to dissemination, the material is essentially returned to its original condition. Consequently, dry Sm compacted to 0.5 g/cm³ is as easy to deagglomerate as the uncompacted material. As density increases above 0.5 g/cm³, the binding energy of the particles increases very rapidly, as shown in Figure 6.4. In this range the mechanical disaggregator produces material which consists of an increasing percentage of large, strong agglomerates with diameters in the 100 to 1000 micron size range. These are quite difficult to deagglomerate with fluid energy, and the flight speed requirement therefore increases very rapidly above a density of 0.55 g/cm³. For this material, the maximum density that can be disseminated with high efficiency is 0.59 g/cm³ at high subsonic flight speeds.

It is apparent that the curve shown in Figure 6.3 will shift somewhat for each agent. Different lots of Sm have been shown to be either more or less difficult to disseminate in the compacted state, depending greatly on the compaction energy-density relationship shown in Figure 6.4. We therefore believe that measurement of this parameter will be one method used to predict the flight-speed requirements for various agents. Both the shape of the resulting curves and their absolute values indicate the binding energy of compacted materials which must be overcome during the dissemination process.

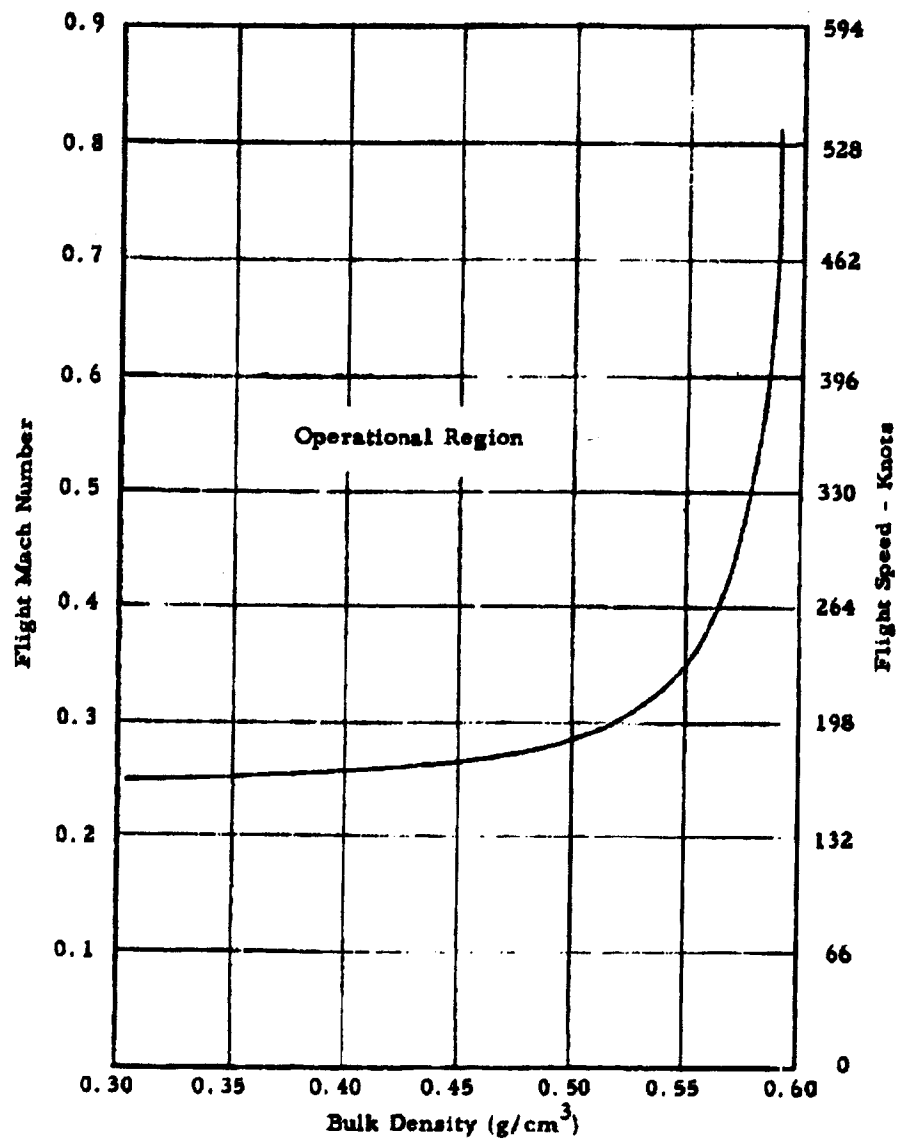


Figure 6.3 Flight Speed Required for Dissemination of Dry, Compacted Sm Simulant (Lot S1-Sm-342) at Approximately 90 Percent Deagglomeration Efficiency

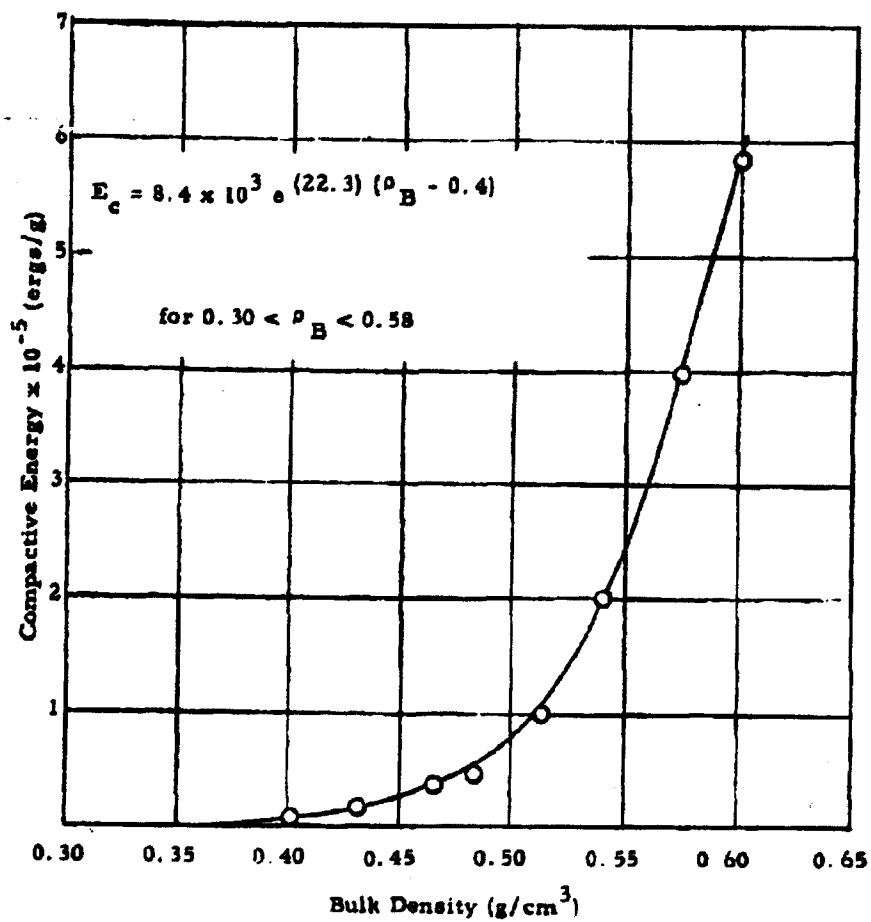


Figure 6.4 Energy Required to Compact Sm (Lot 51-Sm-342)

6.4 Dissemination of Stored Sm in the Compacted Condition

At an earlier date, dissemination tests were conducted on Sm simulant that had been stored in the compacted condition at -18 C for 10 weeks. The results indicated that this material was somewhat more difficult to deagglomerate than similar material, which had not been stored. Since storage is an important factor, a larger test program was planned and initiated during this period. The program is divided into two parts--namely, wind-tunnel deagglomeration tests, and viability tests.

6.4.1 Wind-Tunnel Deagglomeration Tests

The dissemination and deagglomeration test constitutes 2 x 3 x 6 factorial with duplicate runs for each treatment. The variables investigated include

Storage Temperature

-2 C
-23 C

Storage Bulk Density

0.33 g/cm³, uncompacted
0.57 g/cm³
0.61 g/cm³

Storage Period

0.04 day
1 day
7 days
30 days
91 days
182 days

We are using our standard methods for generating and assessing aerosols. They include the GMI-3 dissemination fixture, and the isokinetic sampling probe and full-flow impactor-collection systems.

For this series of tests Sm lots 61-26 and 61-28 are being used. The material has a MMD of 9.5 microns. In preparing the samples, Sm is compacted into storage cylinders of 0.75 inch diameter in a dry, controlled atmosphere. The containers are sealed securely during the storage period.

At the present time tests have been conducted for all time periods through 30 days. The results indicate that there is no significantly detrimental effect of storage on deagglomeration efficiency. Material that can be deagglomerated immediately after being compacted also can be effectively deagglomerated after storage at -2 C or -23 C.

6.4.2 Storage Viability Tests

The samples prepared for the above tests are also used in a study of the effect of storage on viability. The same variables are investigated, but the test has an additional seven time periods and therefore consists of a 2 x 3 x 13 factorial. The time variable includes

Storage Periods

0.04 day	30 days
1 day	61 days
3 days	91 days
5 days	122 days
7 days	152 days
14 days	182 days
21 days	

Samples of these tests are taken after the slugs have been mechanically disaggregated. Our standard method of biological assay is used, and a Waring blender is employed to break-up the compacted clusters of material. Each analysis has an uncompacted control, which is stored at -23 C.

As in the former case, the results to date do not indicate a significant decrease in viability after storage periods of 30 days. Detailed results of this program will be presented in the next progress report.

~~CONFIDENTIAL~~

7. E-41 SPRAY TANK

During the quarterly report period, work related to the E-41 Spray Tank continued in the Development Engineering Department. Considerable progress was made in the fabrication of the second unit. Minor design changes are being incorporated in this second unit as well as in the first air-borne E-41. Some of these modifications will make it possible to fill the unit with loose powder by inserting a filling tube through the end plate and piston. The arrangement of components within the discharge shroud has been modified to provide improved decontamination features. Plans were initiated for flight tests of the E-41 Spray Tank at Eglin Air Force Base on the F-100 and F-105 airplanes.

7.1 Fabrication of the Second E-41 Spray Tank

A second E-41 Spray Tank is being fabricated for use in future flight-test programs. In view of the high degree of success experienced with the first air-borne E-41, there will be no major design changes in the second unit. The minor modifications which are being incorporated in the second unit are of such a nature that they will also be made on the first unit. Thus, both E-41 Spray Tanks will be similar. Completion of the second unit is scheduled for June.

7.2 Improved Arrangement of Components within Discharge Shroud

The shroud surrounding the discharge tube on the bottom of the E-41 Spray Tank serves as an enclosure for components associated with the discharge valve's operation. The shroud also streamlines the discharge tube and separates the aerosol stream from the spray tank. The initial design for this area was somewhat deficient in that it was difficult to decontaminate. This area has been redesigned, and the improved features are being incorporated in both E-41 Spray Tanks.

~~CONFIDENTIAL~~

APR 15 2013

CONFIDENTIAL

In the revised design, all the electrical components such as the motor and limit switches are enclosed by a sealed cover or housing as shown in Figure 7. 1. All of the wiring leading from the disseminator proper to these components is contained in a single sealed cable assembly. The connector is mounted in the cover. The squib wires and the arming wire are connected by means of terminal strips mounted externally on the cover. Since the sealing assembly (which is missing in Figure 7. 1) on the discharge tube contains the squibs and arming wire and must be replaced after each mission, these wires can be disconnected at the terminal strips during the decontamination procedure.

7.3 Removal of Heater and Low-Pressure Switch

Experience with the E-41 Spray Tank has shown that the unit can be operated satisfactorily without the heating jacket on the high-pressure nitrogen tank. The heating jacket has been operating satisfactorily to date, but tests have shown that the tank has adequate capacity to supply a sufficient volume of nitrogen without heating. The heating jacket will therefore no longer be used on the nitrogen tank.

The Eleventh Quarterly progress report contains a discussion of the performance of the low-pressure switch during the flight trials at Dugway Proving Ground last January. An analysis of the spray tank's performance, taking into consideration the airplane's flight-altitude changes during the trials, led to the conclusion that the switch was operating untimely to cause a short delay in the start of dissemination. In as much as the jamming condition which this switch was intended to protect against has never occurred, a decision was made to eliminate the switch. The mounting holes for the switch in the end plate will be sealed with plugs.

7.4 Addition of Filling Holes in Pistons and End Plates

Because the E-41 Spray Tank is capable of disseminating dry agent material from the loose bulk state as well as the compacted state, there is justification for incorporating filling holes in pistons and end plates for loading loose

CONFIDENTIAL



Figure 7.1 Sealed Housing for Components within the
Discharge Shroud

7-3

CONFIDENTIAL

DECLASSIFIED IN FULL
Authority: EO 13526
Chief, Records & Declass Div, WHS
Date: 15 APR 2013

~~CONFIDENTIAL~~

powder. Filling holes have been added to the end plates of both E-41 Spray Tanks. Corresponding holes have been made in the pistons of the units so that a filling tube can be inserted into the tanks.

The holes in the pistons are three inches in diameter, and the holes in the end plates are 3.25 inches so that the plug for the pistons can be removed through the holes in the end plates. The closures in the end plates are sealed with two O-rings.

7.5 Flight Tests at Eglin Air Force Base

In May 1963 Detachment 4, ASD, Weapons Laboratory (ASQWC) Eglin Air Force Base requested that the E-41 Spray Tank be made available to them for flight tests on the F-100D and the F-105 airplanes. It was subsequently decided by Fort Detrick that an E-41 would be shipped from General Mills, Inc. to Eglin Air Force Base for this purpose. The tests are scheduled to begin during the latter part of June.

These flight trials are intended to demonstrate the compatibility of the spray tank with the F-100D and the F-105, and procedures for assaying ground coverage resulting from dissemination of simulants are not included in the plans. The unit will be loaded with talc, which will be disseminated during the trials.

7-4

~~CONFIDENTIAL~~

DECLASSIFIED IN FULL
Authority: EO 13526
Chief, Records & Declass Div, WHS
Date: 19 5 APR 2013

~~CONFIDENTIAL~~

8. PREPARATIONS FOR FLIGHT TESTS OF THE E-41 SPRAY TANK ON THE MOHAWK AIRCRAFT

On 11 March 1963 Mr. Gordon R. Whitnah of General Mills, Inc. visited Lt. Col. Vincent Ulery, Army Liaison Officer at the Navy Bureau of Weapons, and Mr. R. Groundwater at the Mohawk Project Office in Building T-7 to discuss plans for flying the E-41 Spray Tank on the AO-1 Mohawk airplane. On 28 March 1963 engineers from General Mills, Inc. met with Mr. John Coursen, Mohawk Project Engineer, and with several other Grumman personnel at the Grumman Aircraft Company, Bethpage, Long Island. During this visit General Mills, Inc. obtained engineering data pertaining to the installation of the E-41 on the Mohawk.

The weight and size of the E-41 present no apparent problems, but it will be necessary to carry two units or one E-41 and one 150-gallon fuel tank to obtain symmetrical loading. This decreases the maximum obtainable speed but is necessary for flight stability. The maximum dissemination velocity will be in the 200 to 240 knot range. Wind-tunnel experiments reported in Section 6 of this report indicate that BW agents can be successfully disseminated and aerosolized at this air speed.

The spray tank will be mounted on the Aero 65 A pylon at wing station 185. If only one unit is flown, it appears that the left-hand pylon (as viewed from the front) is the preferable location because of the tendency of the propwash to move from right to left.

A cruciform tail is used on the 150-gallon fuel tanks flown on the AO-1 Mohawk. The major reason for this is to stabilize the store when it is released from the pylon upon jettisoning. Because the empty weight of the E-41 is significantly greater than the empty weight of the fuel tank, it should not be necessary to use the cruciform tail. However, since the cruciform tail is the accepted design and there is no strong objection to using it on the E-41, a decision was made to provide an interchangeable aft section with cruciform tail for the E-41 Spray Tank when flown on the Mohawk airplane. Details of this four-finned tail section are shown in GMI drawing SK 29100-1305 in Appendix B.

8-1

~~CONFIDENTIAL~~

DECLASSIFIED IN FULL
Authority: EO 13526
Chief, Records & Declass Div, WHS
Date: 15 APR 2013

~~CONFIDENTIAL~~

Installation of the E-41 on any particular Mohawk aircraft will require rewiring of the wing, pylon, and control box. Since a free-fall jettison system is employed, a pig tail with quick-release connector is needed for the spray tank to insure positive separation from the pylon wiring. There is ample room for the E-41 control panel in the airplane's cockpit. Grumman expressed a willingness to perform the wiring modifications on the test airplane provided they are paid for their services.

Further progress on the Mohawk flight-test program is dependent upon the establishment of dates for the flights by the Mohawk Project Officer in Washington, D. C.

8-2

~~CONFIDENTIAL~~

DECLASSIFIED IN FULL
Authority: EO 13526
Chief, Records & Declass Div, WHS
Date: 11 5 APR 2013

~~CONFIDENTIAL~~

9. SUMMARY AND CONCLUSIONS

The improved multipurpose test unit is now being used to measure shear strength, tensile strength, and bulk density within the confines of a single isolator lab. The fact that reproducible results are being obtained with this unit is indicated by the data presented for several powders. "Rulon" slip agent and graphite have been tried on the mold used to form the "necked-down" specimens for the triaxial tensile test. Three supposedly identical Sm samples have been found to exhibit distinctly different compaction characteristics. Tests for particle size distribution, particle density, and moisture content are being conducted in an effort to explain the differences in the behavior of these Sm samples. Whitby particle-size determinations have shown that a change in size distribution toward a smaller MMD occurred when saccharin was compacted to a compressive stress of 2.84×10^4 dynes/cm². It has been found that the addition of 0.25 to 5.0 percent Cab-o-Sil to powders causes a significant increase in the compaction stress required to produce a given bulk density.

Experiments were performed to determine the time required for the fluid bed to equilibrate. Even though extensive agglomeration occurs, particle-size analyses performed on samples taken from different levels of the bed showed no evidence of segregation or attrition during the 75-minute runs. There was no loss of powder by carry-over at a fluid velocity of 4 cm/sec; but 2.8 percent was lost at 8 cm/sec, and 5.6 percent lost at 12 cm/sec (Section 2).

The BET gas-adsorption method was used to measure the total surface area of saccharin for comparison with similar data obtained for talc during the previous quarter. For saccharin, the BET specific surface area is $1.53 \text{ m}^2/\text{g} \pm 7$ percent, which is significantly less than the value of $15.9 \text{ m}^2/\text{g}$ determined for Mistron Vapor talc. The increased surface area for talc is attributed to its porosity. The rugosity, defined as

~~CONFIDENTIAL~~

DECLASSIFIED IN FULL
Authority: EO 13526
Chief, Records & Declass Div, WHS
Date: 11 5 APR 2013

~~CONFIDENTIAL~~

BET Surface Area

Surface Area from MMD (Whitby)

is 2.2 for saccharin. Micrographs that have been used to obtain particle-shape information are presented for talc, saccharin, egg albumin, powdered milk, Srn, powdered sugar, and cornstarch. Whitby size analyses made on saccharin and powdered sugar before and after their being dispersed by the swirl disperser for use in the aerosol chamber have shown that grinding does not occur in the disperser (Section 3).

A program was initiated to study the effects of atmospheric charge conditions on aerosol decay using the aerosol chamber. Ion concentration in the chamber is varied through introduction of positive ions by means of a corona-discharge ion generator. The injection of positive ions reduces the longevity of talc aerosols. For saccharin aerosols, the introduction of positive ions simultaneously with the introduction of the powder increases aerosol longevity, whereas ion injection after injection of the powder decreases longevity (Section 4).

Experiments were conducted to determine the effectiveness of powdered graphite in reducing side-wall friction of compacted powders sliding in cylinders. Data reported were obtained with three sizes of cylinders -- 6, 7.5, and 16.187 inches internal diameter. Graphite was applied dry and as a suspension in water, alcohol, and trichloroethylene. The latter showed a small improvement over the others. The force required to eject compacted talc and powdered sugar from a graphite-lubricated cylinder was found to be significantly below that for a plain aluminum cylinder. Although the results varied as the length-to-diameter ratio and the compactive pressure were changed, a reduction of 50 percent is representative of the decrease in ejection force observed during the tests. Further tests are planned. An area of particular interest is the effect of surface roughness on side-wall friction when graphite is used as a lubricant (Section 5).

~~CONFIDENTIAL~~

~~CONFIDENTIAL~~

Dissemination and deagglomeration studies with dry Sm using the blow-down wind tunnel have been conducted to extend the range of investigated air velocities down to Mach number 0.25. Tests run at various bulk densities have shown that the concentration of fine, deagglomerated aerosol is essential independent of bulk density in the range from 0.33 to 0.52 g/cm³. Consequently, 0.52 g/cm³ is the limiting bulk density for Sm for a speed of Mach number 0.3/ Wind-tunnel deagglomeration tests and viability tests on Sm stored in the compacted state have thus far demonstrated that storage at -2 C or -23 C for periods up to 30 days has no significant detrimental effect on either deagglomeration efficiency or viability (Section 6).

Fabrication of the second E-41 spray tank progressed significantly during the quarter. Minor design changes being incorporated in the E-41 tank include 1) improved sealing of components in the discharge tube region; 2) removal of the heating jacket from the nitrogen tank; 3) removal of the low-pressure switches from the gas supply system; and 4) the addition of filling holes in the pistons and end plates to facilitate loading loose powder. Plans were initiated to conduct flight tests at Eglin Air Force Base in which the E-41 will be flown on the F-100D and F-105 airplanes to demonstrate its airworthiness and compatibility (Section 7).

Personnel from General Mills, Inc. met with engineers at the Grumman Aircraft Company (Bethpage, Long Island) to discuss the problems of flying the E-41 spray tank on the AO-1 Mohawk airplane. Engineering and performance data were obtained. When the E-41 is flown on the Mohawk, it will be necessary to carry a spray tank (or a 150-gallon fuel tank) on each wing to maintain balanced loading. Maximum flight speed will be in the 200- to 240-knot range. Cruciform tails have been ordered for the E-41 spray tanks because this is the accepted design for the 150-gallon fuel tanks used on the Mohawk. Minor aircraft rewiring will be necessary to accommodate the E-41 (Section 8).

9-3

~~CONFIDENTIAL~~

DECLASSIFIED IN FULL
Authority: EO 13526
Chief, Records & Declass Div, WHS
Date:

11 5 APR 2013

10. REFERENCES

- 1) General Mills, Inc. Electronics Division. Report 2373. Dissemination of solid and liquid BW agents (U), by G. R. Whitnah. Contract DA-18-064-CML-2745. Tenth Quarterly Progress Report (September 4 - December 4, 1962). Confidential.
- 2) ----. Report 2344. Dissemination of solid and liquid BW agents (U), by G. R. Whitnah. Contract DA-18-064-CML-2745. Ninth Quarterly Progress Report (June 4 - September 4, 1962). Confidential.
- 3) ----. Report 2381. Fundamental studies of the dispersibility of powdered materials, by J. H. Nash et al. Contract DA-18-108-405-CML-824. Final Report (March 15, 1963).
- 4) Zenz, F. A. and D. F. Othmer. Fluidisation and fluid-particle systems. N. Y., Reinhold, 1960.
- 5) Matheson, G. L., W. A. Herbst and P. H. Holt. Characteristics of fluid-solid systems. Ind. Eng. Chem. 41: 1099-1104 (1949).
- 6) General Mills, Inc. Electronics Division. Report 2395. Dissemination of solid and liquid BW agents (U), by G. R. Whitnah. Contract DA-18-064-CML-2745. Eleventh Quarterly Progress Report (December 4 - March 4, 1963). Confidential.
- 7) Fries, R. J. The determination of particle size by absorption methods. In American Society for Testing Materials. Spec. Tech. Publ. No. 234. Symposium on particle size measurement. Philadelphia, The Society, 1959. pp. 259-78.
- 8) Whitby, K. T. Rapid general purpose centrifuge sedimentation method for measurement of size distribution of small particles. Heating, Piping Air Conditioning 27, 6: 139-45 (June 1955).
- 9) General Mills, Inc. Electronics Division. Report 2396, op. cit.
- 10) Flossdorf, E. W. and G. W. Webster. The determination of residual moisture in dry biological substances. J. Biol. Chem. 121: 353-59 (1937).
- 11) Ernsberger, F. M. Temperature coefficient of the McBain sorption balance. Rev. Sci. Instr. 24: 998-99 (1953).
- 12) Wilson, E. D. and H. C. Ries. Principles of chemical engineering thermodynamics. N. Y., McGraw-Hill, 1956. p. 238.

APPENDIX A
LOAD AND STRESS ANALYSIS, E-41 SPRAY TANK

Page determined to be Unclassified
Reviewed Chief, RDD, WHS
IAW EO 13526, Section 3.5
Date: **15 APR 2013**

REPORT NO. 43.300

DATED 9-12-62

FLETCHER aviation company

A DIVISION OF A. J. HUNTER, INC. LIVERMORE, CALIF. AND P.O. BOX 1000
SAN JOSE, CALIF. 95128 • TEL. (415) 285-1000 • CABLES: FLETCHER • CHICAGO 4700




LOADS & STRESS ANALYSIS
SOLID FUEL TANK

APPROVED


Chief Engineer


Project Engineer


Structures Engineer

MODEL Custom

COPY NO.

REFERENCE

ISSUED

FORM F 625

PREPARED	NAME R.W. Hill	DATE 9-12-62	FLETCHER AVIATION COMPANY		PAGE	TOTAL PAGES 1
CHECKED			TITLE LOADS & STRESS ANALYSIS SOLID FUEL TANK		Model Custom 43.300	
APPROVED					Report No.	

TABLE OF CONTENTS

Item	Page
INTRODUCTION	2
REFERENCES	4
NOMENCLATURE	5
MINIMUM MARGINS OF SAFETY.	7
BASIC LOADS SECTION	
General View of Tank.	8
Loading Assumptions	9
Unit Shear & Moment Data.	10
Design Conditions	12
Reactions to Design Loads	14
Airload Breakdown	22
Critical Shell Shear & Bending.	23
Critical Design Conditions.	27
STRESS ANALYSIS SECTION	
Nose Section - Shell	28
Center Section - Shell.	29
Aft Section - Shell	31
#4544419-501 Lug (Eye-bolt)	32
-20179 Casting.	34
Main Frames	36
-4679 Fin	41
Fin Attachments	44
APPENDIX A	A-1

IAC Form 7200

Page determined to be Unclassified
Reviewed Chief, RDD, WHS
IAW EO 13526, Section 3.5
Date: 5 APR 2013

PREPARED	NAME R.W.Hill	DATE 8-24-62	FLETCHER AVIATION COMPANY	PAGE	2
CHECKED			TITLE LOADS & STRESS ANALYSIS SOLID FUEL TANK	Model Custom	43.300
APPROVED				REPORT No.	1

INTRODUCTION

The following report covers the basic loads and stress analysis of a special tank built for the Electronics Division of General Mills Inc. The design is per their specification GMS-29100-610, and is covered by Purchase Order MD-84384 dated 6-4-62.

The basic loads for the tank design are developed from the requirements of Section #3.5.6 of MIL-T-7378A, dated 20 October 1958 and from airload data furnished by General Mills in their letter to F.A.C. dated July 27, 1962. Load factors for the catapult takeoff and arrested landing conditions, as well as for the flight conditions, are taken from Fig. 1 of the above Mil spec., which gives load factors for wing-mounted stores. Since the load requirements of MIL-A-8591B are the same as MIL-T-7378A, they are also met.

The reactions on the tank attach points are calculated and summarized on pages 20 and 21. Resultant shear and bending moment at critical stations along the tank are also calculated. See pages 23 to 24 inclusive. The foregoing data is then studied and a summary of design conditions critical for the various items of structure is presented on page 27. The choice of static test conditions is based on this summary.

The sign convention for both the inertia loads and airloads and the reactions to the loads is as follows:

- Z = Upward acting
- Y = Acting to the left (looking forward)
- X = Rearward acting

Positive moment vectors are in the same direction, using the left-hand rule.

In the case of the shear and bending moments in the tank shell, the sign of both the shear and bending moment agrees with the sign of the force on the end of the tank beyond the cut section.

PREPARED	NAME R.W. Hill	DATE	FLETCHER AVIATION COMPANY	PAGE	TOTAL PAGES
CHECKED			TITLE LOADS & STRESS ANALYSIS SOLID FUEL TANK	Model Custom	3
APPROVED				43.300	REPORT No.

Symbols and definitions used throughout this report are tabulated on page 4. All loads, reactions and all stress analysis are presented in terms of ultimate loads unless specifically noted to the contrary.

The results of the stress analysis of the critical structural items in the tank are summarized in the Table of Minimum Margins of Safety, page 7, which includes all margins of safety less than 20%.

PREPARED	NAME R.W.Hill	DATE 9-12-62	FLETCHER AVIATION COMPANY	PAGE	TOTAL 4
CHECKED			TITLE LOADS & STRESS ANALYSIS SOLID FUEL TANK	Model Custom	
APPROVED				43.300	
				Report No.	

REFERENCES

DRAWINGS

General Mills Drawing #SK 29100-612 "Prelim. Tank Assy. Drawing"

#21-150-48032 "Tank Assembly - G.M.I. Specs."
 " " 1342 "Nose Section Assm."
 " " 3372 "Bulkhead - Fin Support"
 " " 4232 "Beam - Fin"
 " " 4235 "Angle - Fin Support, Upper"
 " " 4236 "Angle - Fin Support, Lower"
 " " 4679 "Fin Assembly"
 " " 20179 "Casting - Center Section Support"
 " " 20181 "Ring Segment"

Douglas Aircraft Drawing #2550568 - "Insert"
 " " " 4544419-501 "Eye-bolt"
 " " " 4552066 "Forging Blank"

REPORTS, MANUALS, ETC.

General Mills Specification #GMS 29100-610.
 General Mills letter to F.A.C. dated 7-11-62.
 General Mills letter to F.A.C. dated 7-27-62.
 MIL-T-7378A - "External Fuel Tanks".
 MIL-A-8591B - "Airborne Stores & Equipment".
 MIL-HDBK-5 - "Strength of Metal Aircraft Elements".
 QQ-S-766C - "Corrosion Resisting Steel Sheet".
 F.A.C. Report #43.284 - "Loads & Stress Analysis, General Mills Tank".
 N.A.C.A. T.N. #427 - "Thin-walled Cylinders in Torsion".
 " T.N. #479 - "Thin-walled Cylinders in Bending".
 " T.N. #929 - "Circular Shell-Supported Frames".
 Lockheed Aircraft Stress Memo Manual

BOOKS

Alcoa Structural Handbook, 1958 ed.
 F.R. Shanley - "Basic Structures" 1944 ed.

Parpared	R.W. Hall	8-24-62	MITCHELL AVIATION COMPANY		Page	1	Rev.	1
Checked			TITLE		Model Custom			
Approved			LOADS & STRESS ANALYSIS SOLID FUEL TANK		43.300 Report No.			

NOMENCLATURE

SYMBOL

DEFINITION

A	Area (in ²)
E	Modulus of elasticity
F	Allowable stress (#/in ²)
f	Actual stress (#/in ²)
I	Moment of inertia (in ⁴)
I _m	Mass moment of inertia (slug-ft ²)
K	A factor; coefficient
L	A length (in.)
l	A length (in.)
M	Moment (in-lbs.)
M.S.	Margin of safety
n	Load factor
P	Load (lbs.)
R	Reacting force; hook load; radius;
r	Moment arm; radius (in.)
S	Shear load (lbs.); sway brace load (lbs.)
W	Weight (lbs)
w	Running load (lbs/in.)
X	Longitudinal reference axis, positive aft.
X̄	Tank station at center of gravity.
Y	Lateral reference axis, positive outb'd. to left.
Ȳ	Distance to center of gravity in Y direction.
Z	Vertical reference axis, positive upward.
Z̄	Section modulus (in ³)
z	Distance to center of gravity in Z direction.
Δ	Increment of change, as ΔF, change in force.
θ	An angle (Deg.)
θ̈	Pitching angular acceleration (Rad./sec. ²)
ψ̈	Yawing angular acceleration (Rad./sec. ²)
δ	Deflection (in.)

WHEN USED AS SUBSCRIPTS

A	Aft
b	Bending
br	Bearing
c	Compression
cr	Crippling
F	Forward
H	Horizontal
L	Left side

146 Form 0000

Page determined to be Unclassified
Reviewed Chief, RDD, WMS
IAW EO 13526, Section 3.5
Date:

15 APR 2013

PREPARED	NAME R.W. Hill	DATE 8-24-62	FLETCHER AVIATION COMPANY	PAGE	1. OF 1
CHECKED			TITLE LOADS & STRESS ANALYSIS SOLID FUEL TANK	MOOD	CUSTOM
APPROVED				43.300	Report No.

WHEN USED AS SUBSCRIPTS (contd)

M	Mass; moment	
R	Resultant; right side	
s	Shear	
t	Tension	
u	Ultimate	
v	Vertical	
x	X-axis	
y	Y-axis	See sign convention, page 2.
z	Z-axis	
Y	Yield	

MAC Form 1102

Page determined to be Unclassified
Reviewed Chief, RDD, WHS
IAW EO 13526, Section 3.6
Date: 15 APR 2013

PREPARED	R.W. Hill	DATE	9-12-62	FLETCHER AVIATION COMPANY		PAGE	7
ENGINEER		TITLE	LOADS & STRESS ANALYSIS SOLID FUEL TANK		Model	CUSTOM	
APPROVED					Report No.	43.300	

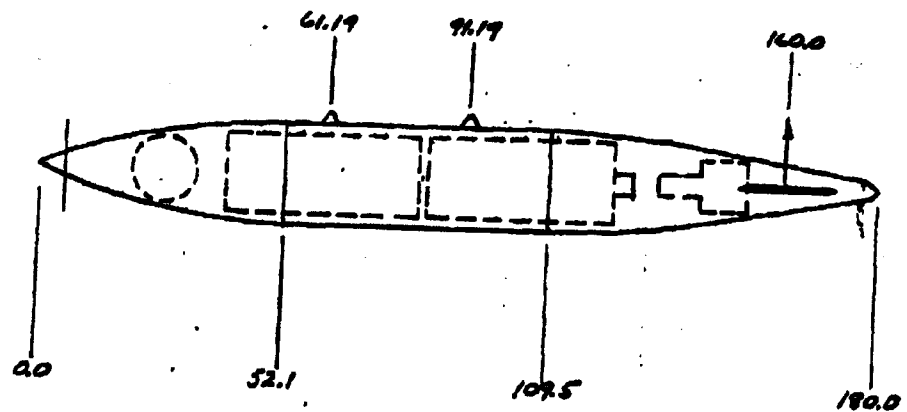
**TABLE SHOWING
MINIMUM MARGINS OF SAFETY ***

PAGE	DWG NO.	MATERIAL	CRITICAL IN.	M.S.
35	-20180	Type #304 Stainless Steel	Tension	.04
38	-20179	356-T6 Casting	Bending	.00
38	-20181	4130 Steel, h.t. 170,000	Bending	.04
41	-4232	2024-T4 Plate	Bending	.00
43	-4679	ΔT-106 Polyurethane	Shear	.18
46	-3372	6061-T6 Plate	Bearing	.03

* Includes all margins of safety less than 20%

PREPARED	NAME <i>R. W. Hill</i>	DATE <i>8-7-62</i>	FLETCHER AVIATION CORPORATION		PAGE	1.1	OF	1
CHECKED			TITLE		MODEL	<i>Custom</i>		
APPROVED					WEIGHT	<i>48,300</i>		
					REPORT NO.			

GENERAL MILLS TANK
(SOLID FUEL)



WEIGHT DATA

	W	\bar{X}	I_{mass}
Tank Empty	819.0 ²	82.0	260.3 slug-ft. ²
Tank Full	1168.0 ²	82.0	415.0 slug-ft. ²

PREPARED	R. W. Hill	DATE	8-24-62	FLETCHER AVIATION COMPANY		PAGE	1
CHECKED				TITLE Loads & Stress Analysis Solid Fuel Tank		MODEL Custom	
APPROVED						43.300	
						REPORT No.	

LOADING ASSUMPTIONS

The basic loads for the tank design are developed from the requirements of Section 3.5.6 of MIL-T-7378A, dated 20 October 1958 and from airloads furnished by General Mills in their letter to F.A.C. dated July 27, 1962. These loads and the necessary reactions from the hooks and sway-brace pads are distributed into the structure of the tank, using the following assumptions:

- (1) Reactions from the sway brace pads are always normal to the tank surface, at an angle of 26° from the vertical. (Ref. sk. on page 14).
- (2) Side loading is resisted by a hook vertical load and the sway brace acting at 26° from the vertical.
- (3) Each eye-bolt should be capable of carrying 60% of the total drag load.
- (4) Rolling moments (M_x) will be carried by a couple between the hook and sway brace, each force in the couple acting at the same 26° from the vertical as noted above. Each couple may be equal to 100% of the total rolling moment.
- (5) Pitching moments are resisted by a couple between an eye-bolt and the far pair of sway braces.
- (6) Yawing moments are resisted by a couple formed by the lateral components of load of the forward and aft sway braces. The resulting vertical components are resisted by vertical loads on the adjacent eye-bolts.
- (7) The analysis will ignore pre-loads in the attach fittings due to torquing the sway braces, because experience has shown that these pre-loads disappear before ultimate test loads are reached.
- (8) The effect of the various load components is linear (below the yield stress of all affected parts) and the reactions to them may therefore be superimposed on each other.

LOADED TANK UNIT SHEAR & MOMENT DATA

FLETCHER AVIATION CORPORATION											
PREPARED		NAME		DATE		TITLE		PAGE		FORM	
R. W. Hill				7-9-62				6		11	
CHECKED								Model		42-300	
APPROVED								Report No.			
1	2	3	4	5	6	7	8	9	10	11	
T.S.	W	L	L ²	Wn ²	$\frac{P}{10^3 M_{eq}}$	T.S.	$\frac{S}{n}$	$\frac{S}{10^3 M_{eq}}$	$\frac{M}{n}$	$\frac{M}{10^3 M_{eq}}$	
Vertical Loading											
10	61.8	-72.0	5184	320,370	-3.237	21.5	61.8	-3.237	670	-38	
33	78.8	-47.0	2401	189,200	-2.807	44.5	140.6	-6.046	3200	-145	
57	210.7	-26.0	676	142,430	-3.995	27.5	351.3	-10.031	8250	-330	
79	403.7	-3.0	9	3640	-0.894	90.5	765.2	-10.925	21380	-571	
102	225.6	+20.0	400	90240	+3.282	113.5	980.5	-7.643	41340	-785	
79	403.7	-3.0	9	3640	-0.894	27.5	816.7	10.031	25630	670	
102	225.6	+20.0	400	90240	+3.282	90.5	412.8	10.925	11470	429	
125	94.4	41.0	1849	174,540	2.963	113.5	187.2	7.643	4590	215	
148	76.8	66.0	4356	343,260	3.784	136.5	92.8	4.690	1370	74	
171	14.0	87.0	7921	110,870	.906	189.5	14.0	.906	140	9	
Lateral Loading											
8	53.8	-74.0	5476	294,610	-2.926	17.5	53.8	-2.926	530	-32	
31	66.3	-51.0	2601	172,450	-2.486	42.5	120.1	-5.412	2530	-128	
54	208.7	-28.0	784	163,620	-4.296	65.5	328.8	-9.708	7670	-301	
77	404.7	-5.0	25	10120	-1.495	88.5	733.5	-11.203	19900	-541	
100	227.1	+18.0	324	74230	+3.030	116.5	962.6	-8.173	39410	-764	
77	404.7	-5.0	25	10120	-1.495	65.5	839.2	9.708	27060	699	
100	227.1	+18.0	324	74230	+3.030	88.5	434.5	11.203	12410	459	
123	104.0	41.0	1681	174,820	3.134	116.5	205.4	8.173	6060	236	
146	85.5	64.0	4096	350,210	4.022	134.5	101.4	5.039	1530	84	
11	15.9	87.0	7569	120,850	1.017	157.5	15.9	1.017	180	15	
* $\Sigma Wn^2 = 1,374,560$ (Vert. loading) $= 1,360,410$ (Lat. loading)											

FAE Form 1000-1

Page determined to be Unclassified
Reviewed Chief, RDD, WHS
IAW EO 13526, Section 3.5
Date:

15 APR 2013

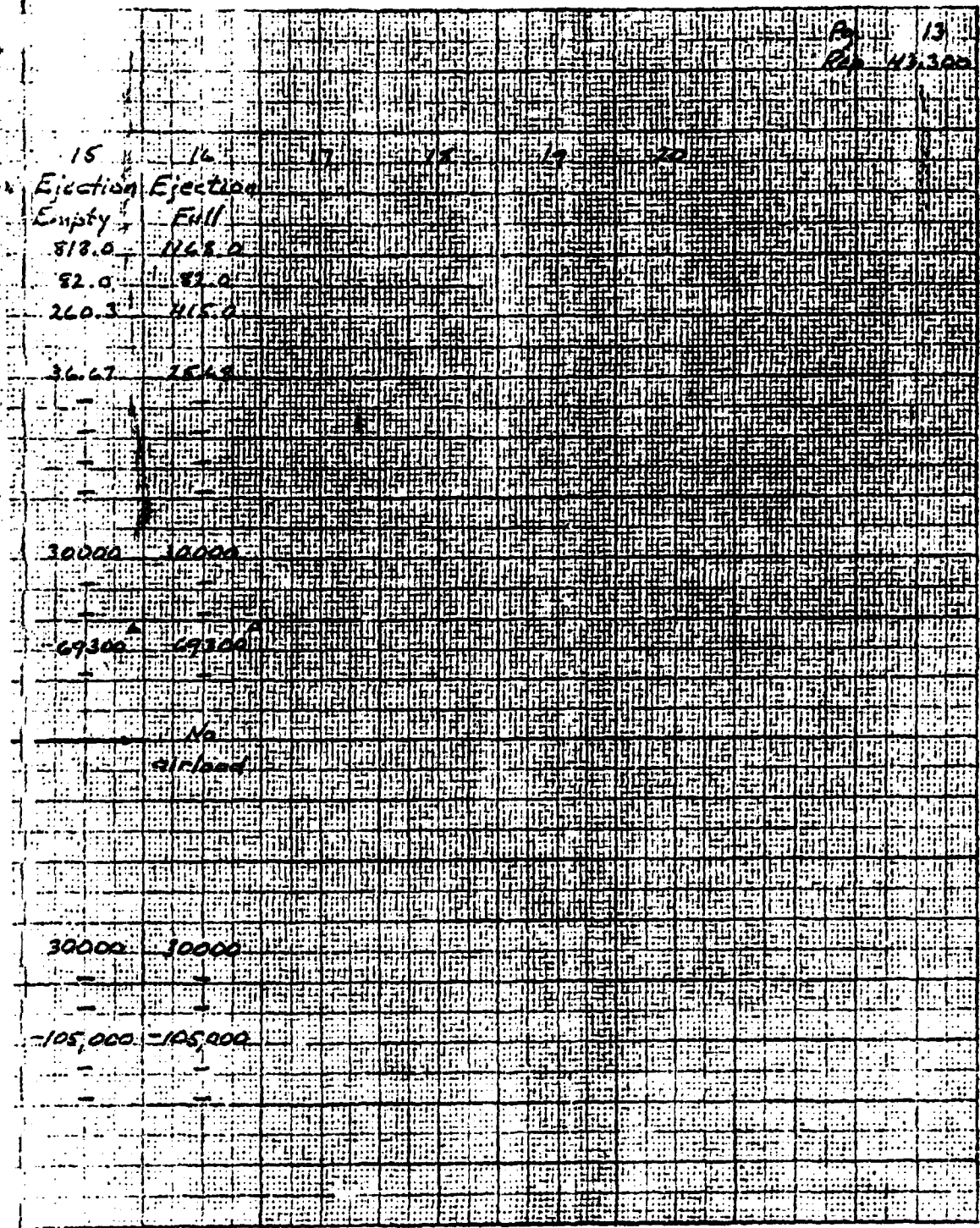
DESIGN CONDITIONS - GENERAL				
(MIL-T-7379A - Fig. 1)				
Gen'l Mills airloads, etc.				
Condition	1	2	3	4
1. <u>Wing</u>	Wing	Wing	Wing	Wing
2. <u>Roll</u>	Roll	Roll	Roll	Roll
3. <u>Yaw</u>	Yaw	Yaw	Yaw	Yaw
4. <u>Design Parameters</u>				
5. η_x	7.50	7.50	7.50	-9.00
6. η_y	2.25	2.25	2.25	9.75
7. η_z	2.00	3.00	3.00	3.00
8. δ (Pitch)	-9.00	-9.00	-9.00	-9.00
9. ψ (Yaw)	0	0	0	0
10. <u>Inertia loads at tank CG</u>				
11. P_x (1)	9700	1752	1752	-10512
12. P_y (1)	2225	11388	11388	11388
13. P_z (1)	3504	3504	3504	3504
14. M_x (2)	44820	44820	44820	44820
15. M_y (2)	0	0	0	0
16. <u>Airloads at E.T.S. T.S.</u>	(1)	(2)	(3)	(4)
17. P_x	-4095	-166	-4425	3360
18. P_y	330	345	345	345
19. P_z	720	555	750	450
20. M_x	79560	72120	194580	-79560
21. M_y	-26100	-79480	-78480	-78480
22. M_z	-520	-180	-2160	-1440
23. <u>Total load at ref point Δ</u>				
24. P_x (1) + (17)	4665	1587	-2883	-7352
25. P_y (2) + (18)	2055	11733	11733	12733
26. P_z (3) + (19)	-2784	4059	-2754	3954
27. M_x (4) + (20) + 5.8(11) + 3(12)	73750	17230	230660	-54350
28. M_y (5) + (21) + 5.8(12) + 3(13)	-6320	-12210	-12210	-12210
29. M_z (6)	-540	-180	-2160	-1440
Δ Loads ref point ~ to tank @ T.S. T.S.				

Age	12
Pop.	43,300

1 - Fig*1 and
air/cats dated 7-27-62

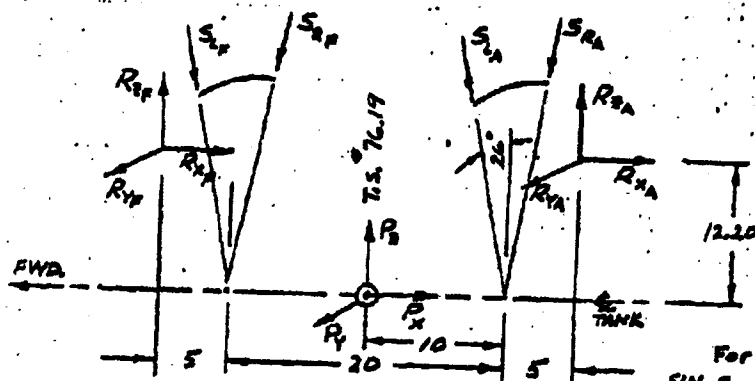
	4	5	6	7	8	9	10	11
	Att. Ing	Att. Ing	Att. Ing	Att. Ing	Att. Ing	Att. Ing	Att. Ing	Att. Ing
1								1169
2								1169
3								1169
4								1169
5								1169
6								1169
7								1169
8								1169
9								1169
10								1169
11								1169
12								1169
13								1169
14								1169
15								1169
16								1169
17								1169
18								1169
19								1169
20								1169
21								1169
22								1169
23								1169
24								1169
25								1169
26								1169
27								1169
28								1169
29								1169
30								1169
31								1169
32								1169
33								1169
34								1169
35								1169
36								1169
37								1169
38								1169
39								1169
40								1169
41								1169
42								1169
43								1169
44								1169
45								1169
46								1169
47								1169
48								1169
49								1169
50								1169
51								1169
52								1169
53								1169
54								1169
55								1169
56								1169
57								1169
58								1169
59								1169
60								1169
61								1169
62								1169
63								1169
64								1169
65								1169
66								1169
67								1169
68								1169
69								1169
70								1169
71								1169
72								1169
73								1169
74								1169
75								1169
76								1169
77								1169
78								1169
79								1169
80								1169
81								1169
82								1169
83								1169
84								1169
85								1169
86								1169
87								1169
88								1169
89								1169
90								1169
91								1169
92								1169
93								1169
94								1169
95								1169
96								1169
97								1169
98								1169
99								1169
100								1169

Condition		12	13	14	
Loading		Full	Full	Full	E
1	W	1168	1168	1168	
2	X	82.0	82.0	82.0	
3	T_{xx} & T_{yy}	415.0	415.0	415.0	
4	Ult. Design Parameters				
5	n_x	-12.00	1.50	-415.0	
6	n_y	2.25	2.25	2.25	
7	n_z	3.00	13.50	13.50	
8	$\ddot{\theta}$ (Pitch)	18.00	-18.00	-18.00	
9	$\ddot{\psi}$ (Yaw)	9.00	6.00	-6.00	
10	Inertia loads at C.G.				
11	P_x	-11416	1752	-5256	3
12	P_y	2628	2628	2628	
13	P_z	3504	15768	15768	
14	M_x	89640	-89640	-89640	
15	M_y	44320	29880	-29880	
16	Airloads at T.S. 76.5				
17	P_x	No			
18	P_y	airload			
19	P_z				
20	M_x				
21	M_y				
22	M_z				
23	Total load at ref. point				
24	P_x	-11416	1752	-5256	3
25	P_y	2628	2628	2628	
26	P_z	3504	15768	15768	
27	M_x	117070	-77820	-59100	-10
28	M_y	60090	45150	-14610	
29	M_z	0	0	0	
Ejection point 11.5" fwd. of rear hook					



PREPARED	NAME <u>R. V. L. Hill</u>	DATE <u>7-10-62</u>	FLETCHER AVIATION CORPORATION	PAGE	TAB	PERF.
CHECKED			TITLE <u>BASIC LOADS</u>			<u>14</u>
APPROVED				MODEL <u>Custom</u>		
				<u>43.300</u>		
				REPORT NO.		

REACTIONS TO LOADS AT TANK REF. PT.



For $26^\circ 0'$
 $\sin = .43837$
 $\cos = .89879$
 $\tan = .48773$

Ref. pg. 9 for assumptions made in equations for reactions to applied loads.

<u>Load</u>	<u>Reactions</u>
$+P_F$	$S_{LF} = S_{RF} = S_{LA} = S_{RA} = \frac{.25 P_F}{.89879} = .2782 P_F$
$-P_F$	$R_{LF} = R_{RF} = -.5000 P_F$
$+P_Y$	$S_{LF} = S_{LA} = \frac{.50 P_Y}{.43837} = 1.1406 P_Y$
	$R_{LF} = R_{LA} = \frac{.50 P_Y}{.48773} = 1.0252 P_Y$
$+P_X$	$R_{LF} = R_{LA} = -.6000 P_X$
	$R_{RF} = \frac{12.20 P_X}{25} = .4880 P_X$
	$S_{LA} = S_{RA} = \frac{50 \times .4880 P_X}{.89879} = .2715 P_X$
$-P_X$	$R_{RF} = R_{RA} = -.6000 P_X$
	$R_{RA} = -.4880 P_X$
	$S_{LF} = S_{RF} = -.2715 P_X$

PREPARED	NAME <i>R.W. Hill</i>	DATE <i>7-10-62</i>	FLETCHER AVIATION CORPORATION	PAGE	15
CHECKED			TITLE <i>Basic Loads</i>	MODEL	<i>Custom</i>
APPROVED				REPORT NO.	<i>43,300</i>

$$\begin{aligned}
 -M_x & \quad S_{R_F} = S_{R_A} = \frac{M_x}{5.25} = -19048 M_x \\
 & \quad R_{R_F} = R_{R_A} = \frac{.81979 M_x}{5.25} = -17119 M_x \\
 & \quad R_{R_F} = R_{R_A} = \frac{.43837 M_x}{5.25} = .08350 M_x \\
 +M_y & \quad R_{R_A} = M_y / 25 = .04000 M_y \\
 & \quad S_{L_F} = S_{R_F} = \frac{.040 M_y}{2 \times .89879} = .02225 M_y \\
 -M_y & \quad R_{R_F} = -.04000 M_y \\
 & \quad S_{L_A} = S_{R_A} = -.02225 M_y \\
 +M_z & \quad S_{R_F} = S_{L_A} = \frac{M_z}{20 \times .43837} = .11406 M_z \\
 & \quad R_{R_F} = R_{R_A} = \frac{M_z}{20 \times .48773} = .10252 M_z \\
 -M_z & \quad S_{L_F} = S_{R_A} = -.11406 M_z \\
 & \quad R_{R_F} = R_{R_A} = -.10252 M_z
 \end{aligned}$$

Adjustments for Final Reactions

Because of the manner of computing and superimposing the reactions to the various load components, it is possible for all four sway braces & both hooks to be loaded simultaneously. The reactions from the hooks and sway braces may be reduced in a proportion to maintain the static equilibrium. This will be done in two steps.

Step #1. Reduce the reactions in the hooks and sway braces simultaneously until one hook or one sway brace reaction becomes zero. If one reaction is already zero, this step is omitted. Because of the symmetry of the hooks and sway braces about the load reference axes, the following relationships

FAC Form F800-1

PREPARED	NAME <i>R.W. Hill</i>	DATE <i>7-12-62</i>	FLETCHER AVIATION CORPORATION		PAGE	16
CHECKED			TITLE <i>Basic Loads</i>		MODEL	<i>Custer</i>
APPROVED					REPORT NO.	<i>43.300</i>

REACTIONS, CONT.

are true when the reactions from both hooks or from all four sway braces are changed simultaneously.

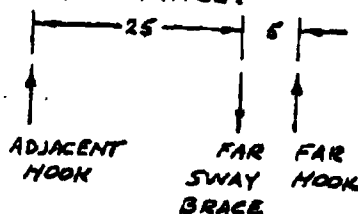
For hook $\Delta R_2 = 1.0^*$, the corresponding sway brace $\Delta R = \frac{5000}{.89879} = .5563^*$

And conversely,

For a sway brace $\Delta R = 1.0^*$, the corresponding hook $\Delta R_2 = 2 \times .89879 = 1.7976^*$

The above ΔR adjustments are shown as the 1st Reduction on pages 20 and 21.

Step #2. After one sway brace reaction reaches zero, the adjacent hook load may still be reduced if the moments are kept in balance.



For $\Delta R_2 = 1.0^*$ on adjacent hook,

Far sway brace $\Delta R = \frac{30 \times 5}{.89879} = 3.3378^*$

Far hook $\Delta R_2 = 6.0 - 1.0 = 5.0^*$

For $\Delta R = 1.0^*$ on a far sway brace,

Adj. hook $\Delta R_2 = \frac{5}{30} \times .89879 \times 2 = .2996^*$

Far hook $\Delta R_2 = 2 \times .89879 - .2996 = 1.4980^*$

10-10-10

NO. 10-10-10

10-10-10

PRELIM REACTIONS T.O. TA			
(Area TA rock with 30" hook)			
Location of tank ref. point (E. Tank @ T.S. *76.07)			
1 - F.P.	7665	1587	
2 - F.			-2893
3 - D.	2659	11733	11733
4 - E.		4059	
5 - D.	(Ref. previous tank)	-2784	-2754
6 - H.D.	(H.D. 10000)	173750	230660
7 - M.			
8 - M.			
9 - M.	-6320	-20110	-12210
10 - M.	-540	-180	-2160
Reaction in 10000			
R ₁ = 5000(2) + 10152(3) + 4880(4)	3465	15292	15092
- 17119(10) + 24000(6) + 10152(3)	-10252(9)		
R ₂ = 15350(8)	-45	-15	-180
R ₃ = 10000(4) - 6000(5)	1670	-2435	1670
R ₄ = 5000(2) + 10252(3) + 4880(3)	11774	14000	25662
- 17119(10) + 24000(6) + 10152(3)	-10207(9)		
R ₅ = 15350(8)	-45	-15	-180
R ₆ = 10000(4) - 6000(5)	1670	-2435	1670
S ₁ = 2782(1) + 11401(3) - 2715(5)	9672	15600	20655
+ 02225(6) - 11401(9)			
S ₂ = 2782(1) + 2715(3) + 02225(6)	6022	859	6291
+ 11401(8) - 19043(10)			
S ₃ = 2782(1) + 11401(3) + 2715(4)	4330	14926	13383
- 02225(7) + 11401(9)			
S ₄ = 2782(1) + 2715(4) - 02225(7)	2122	2970	1804
- 11401(9) - 19043(10)			
* (Ref. pgs. 14, 15, 16)			

PA 18							
LOADS							
25 5:00 (009)							
4	5	6	7	8	9	10	11
-7152	-10512	-14955	-17520	7575	7824	15014	-256
11733	11733	2658	2658	2658	2658	2658	2658
3954		3969		4089			
	-3009		-3009		-15114	-15748	-15165
	105890		146,610	3110	43030	49830	170182
-64350		-6280					60090
-12210	-12210	-6320	-6320	-6320	-24850	-24850	
-1440	0	-3060	0	-180	0	0	0
21606	18536	13522	12133	5397	5721	5724	11483
-120	0	-256	0	-15	0	0	0
-2372	1805	-2381	1805	-2453	7101	7461	7461
17103	24240	11374	19466	3528	7197	16190	13985
-120	0	-256	0	-15	0	0	0
-2372	1805	-2381	1805	-2453	7101	7461	7461
14775	17948	1752	7832	5929	10488	13165	9952
274	3173	583	4079	2211	4120	6797	13809
15888	13383	4249	3032	6249	5191	3972	9851
4172	1393	2521	721	3973	5564	4345	0

PRELIM. REACTIONS, CONTINUED

Pg. 19
Rep. 43.300

		12	13	14	15
<u>Loads at tank ref point</u>					
1	+R ₂		1752		
2	-R ₂	-14016		-5256	
3	+R ₂	2628	2628	2628	
4	+R ₂	3504	15768	15768	
5	-R ₂				
6	+M ₂	171070			
7	-M ₂		-9920	-59100	
8	+M ₂	60290	45150		
9	-M ₂			-14610	
10	+M ₂	0	0	0	
<u>Reactions to loads</u>					
R _{2F}		17572	19011	16879	
R _{2F}		0	0	0	
R _{2F}		-2102	-9461	-9461	
R _{2A}		22705	7323	6820	
R _{2A}		0	0	0	
R _{2A}		-2102	-9461	-9461	
S _{2F}		6804	3485	4664	
S _{2F}		10660	5637	0	
S _{2H}		10803	15137	8593	
S _{2A}		951	6989	7262	

ADJUSTMENTS & FINAL REACTIONS						
	Cond.	1	2	3	4	
	Reaction					
Prelim. Vertical Reactions (Pgs 18 & 19)	R_{2F}	3465	15292	15092	21096	1
	R_{2A}	11774	14000	25662	17103	2
	S_{1F}	9072	15600	20655	14775	1
	S_{1A}	6022	859	6291	274	
	S_{2A}	4330	14926	13383	15888	1
	S_{2F}	2122	2970	1804	4172	1
1 st Reduction (Ref. pg. 15)	ΔR_{2F}	-3465	-1544	-3243	-492	-
	ΔR_{2A}	-3465	-1544	-3243	-492	-
	ΔS_{1F}	-1728	-859	-1804	-274	-
	ΔS_{1A}					
	ΔS_{2A}	-1929	-859	-1804	-274	-
	ΔS_{2F}					
Adjusted Reactions	R_{2F}	0	13748	11849	21114	1
	R_{2A}	8309	12456	22419	16611	2
	S_{1F}	7744	14741	18851	14501	1
	S_{1A}	4094	0	4487	0	
	S_{2A}	2402	14065	11579	15614	1
	S_{2F}	194	2111	0	3878	
2 nd Reduction (Ref. pg. 16)	ΔR_{2F}	0	-632	-6722	-1168	-
	ΔR_{2A}		-3162	-1344	-5839	-
	ΔS_{1F}		0	-4487	0	-
	ΔS_{1A}		0	-4487	0	-
	ΔS_{2A}		-2111	0	-3878	-
	ΔS_{2F}	0	-2111	0	-3898	-
FINAL REACTIONS	R_{2F}	0	13116	5127	19946	1
	R_{1F}	-45	-15	-180	-120	
	R_{2A}	1670	-2435	1670	-2372	1
	R_{1A}	8309	9294	21075	10772	2
	R_{2A}	-45	-15	-180	-120	
	R_{1A}	1670	-2435	1670	-2372	1
	S_{1F}	7744	14741	14364	14501	1
	S_{1A}	4094	0	0	0	
	S_{2A}	2402	11954	11579	11116	1
	S_{2F}	194	0	0	0	

REACTIONS TO TANK LOADS								Pg.	20.
								Rep.	43.300
	4	5	6	7	8	9	10	11	
7	21206	18536	13562	12133	5379	5724	5724	12483	
6	17103	24240	11374	17466	3528	9187	16170	23985	
5	14775	17948	3752	7832	5929	10488	13165	7952	
4	274	3173	583	4079	2211	4120	6797	13809	
3	15288	13383	4249	3032	6249	5191	3972	9851	
4	4172	1393	2521	721	3973	5564	4345	0	
4	-492	-2504	-1048	-1296	-3528	-5724	-5724	0	
43	-472	-2504	-1048	-1296	-3528	-5724	-5724		
11	-274	-1393	-583	-721	-1763	-3184	-3184		
14	-274	-1393	-583	-721	-1763	-3184	-3184	0	
4	21114	16032	12514	10837	1871	0	0	11483	
17	16611	21736	10326	18170	0	3463	10466	23985	
5	14501	16555	3169	7111	3966	7304	9981	7952	
37	0	1780	0	3358	248	936	3613	13809	
7	15614	11790	3666	2311	4286	2007	788	7851	
	3878	0	1938	0	2010	2380	1161	0	
2	-1168	-2666	-581	-3462	0	0	0	-11483	
14	-5839	-533	-2903	-692				-2297	
37	0	-1780	0	-2311				-7666	
17	0	-1780	0	-2311				-7666	
	-3878	0	-1938	0				0	
	-3878	0	-1938	0	0	0	0	0	
7	19946	13366	11933	7375	1871	0	0	0	
2	-120	0	-256	0	-15	0	0	0	
0	-2372	1805	-2381	1805	-2453	2102	9461	9461	
15	10772	21203	7423	17478	0	3463	10466	21688	
1	-120	0	-256	0	-15	0	0	0	
0	-2372	1805	-2381	1805	-2453	2102	9461	9461	
4	14501	14775	3169	4800	3966	7304	9981	2286	
	0	0	0	1047	248	936	3613	6143	
9	11716	11990	1729	2311	4286	2007	788	9851	
	0	0	0	0	2010	2380	1161	0	

21
 43.300

ADJUSTMENTS & FINAL REACTIONS, C					
Cond.	12	13	14	15	16
Reaction					
R_{RF}	17573	19011	16879		
R_{RA}	27705	7323	6820		
S_{LF}	6804	3485	4664		
S_{RF}	10660	5637	0		
S_{LA}	10803	15137	8593		
S_{RA}	951	6989	7262		
ΔR_{RF}	-1710	-6265	0		
ΔR_{RA}	-1710	-6265			
ΔS_{LF}	-951	-3485			
ΔS_{RF}					
ΔS_{LA}					
ΔS_{RA}	-951	-3485	0		
R_{RF}	15863	12746	16879		
R_{RA}	20995	1058	6820		
S_{LF}	5853	0	4664		
S_{RF}	9709	2152	0		
S_{LA}	9852	11652	8593		
S_{RA}	0	3504	7262		
ΔR_{RF}	-8768	-212	-1364		
ΔR_{RA}	-1754	-1058	-6820		
ΔS_{LF}	-5853	0	0		
ΔS_{RF}	-5853	0	0		
ΔS_{LA}	0	-706	-4553		
ΔS_{RA}	0	-706	-4553		
R_{RF}	7095	12534	15515		
R_{RA}	0	0	0		
R_{XF}	-2102	-9461	-9461		
R_{RA}	19241	0	0		
R_{YA}	0	0	0		
R_{XA}	-2102	-9461	-9461		
S_{LF}	0	0	4664		
S_{RF}	3858	2152	0		
S_{LA}	9852	10946	4040		
S_{RA}	0	2798	2709		

FINAL
 ACTIONS

PREPARED	NAME	DATE	FLETCHER AVIATION CORPORATION		PAGE	7	22
CHECKED			TITLE		Model Custom		
APPROVED					43.300		
					REPORT No.		

TANK AIRLOAD BREAK-DOWN

Load Sta.	Vertical Loads					Load Sta.	Lateral Loads	
	1	2	3	4	6		1, 6, 7, 8	2, 3, 4, 5
10	-310	124	-361	372	276	8	44	185
33	-605	236	-707	726	576	31	106	413
56	-449	166	-521	550	427	54	73	314
79	-99	+16	-127	+137	+73	77	+4	+68
102	+91	-66	+96	-83	-92	100	-29	-79
125	231	-119	260	-253	-226	123	-55	-180
148	285	-138	313	-321	-276	146	-68	-218
171	196	-84	209	-215	-163	169	-45	-158
FIN (160)	-3135	-300	-3795	+2445	+1950		30	345
	-4095	-165	-4235	3360	2565			

Ref. G.M.I. letter
dated 7-27-62

FLC Form 1800-1

Page determined to be Unclassified
Reviewed Chief, RDD, WHS
IAW EO 13526, Section 3.6
Date: 15 APR 2013

NAME		DATE		FLETCHER AVIATION CORPORATION		PAGE	
PREPARED: R. W. Hill		9-14-62		TITLE		23	
CHECKED						MODEL: Custom	
APPROVED						REPORT NO. 43,300	

CRITICAL SHEAR & BENDING MOMENT		TANK STA. 51.2		3		4		6		7		9	
Item	Cond.	1	2	3	4	5	6	7	8	9	10	11	12
1	S ₁			202.0									
2	M ₁			4646									
3	S ₁₀ M ₁₀			7.207									
4	M ₁₀ M ₁₀			199									
5	N ₁			1.50									
6	N ₁₀			9.75									
7	10 ³ M ₁₀			44.82									
8	10 ³ M ₁₀			0									
9	R ₁ F												
10	S ₁₀												
11	S ₁₀												
12	P ₁ Perm												
13	P ₁ Perm												
14	S ₁₀												
15	M ₁₀												
16	S ₁₀												
17	M ₁₀												
18	S ₁₀												
19	M ₁₀												
20	S ₁₀												
21	M ₁₀												
22	M ₁₀												
23	M ₁₀												

FAE Form 1000-1

CRITICAL SHEAR & BENDING MOMENT

TANK STA * 41.0 +

PREPARED		NAME	DATE	FLETCHER AVIATION CORPORATION				PAGE	24
CHECKED				TITLE				MODEL 41.0 + 0.0	
APPROVED								REPORT NO. 43.300	
Item	Cond.	1	3	4	6	9	14		
1	S ₁	319.2							
2	M ₁ /n	7790							
3	S ₁₀ /M ₁₀	9.425							
4	M ₁₀ /M ₁₀	302							
5	n ₁	7.50	1.50	-7.00	-15.00	6.75	-4.50		
6	n ₂	2.25	9.75	9.75	2.25	2.25	2.25		
7	10 ³ M ₁₀	44.82	44.82	-44.82	-44.82	89.64	-89.64		
8	10 ³ M ₁₀	0	0	0	0	-44.82	-29.88		
9	R ₁ /F	0	5127	14946	11933	0	15515		
10	S ₁ /F	7794	14364	14501	3169	7304	4664		
11	S ₁ /F	4094	0	0	0	936	0		
12	P ₁ /F	-10640	-7783	6913	9085	-7406	11823		
13	P ₁ /F	-1200	-6297	-6357	-1389	-2792	-2044		
14	S ₁ /F	-1296	-1510	1564	1214	0	0		
15	M ₁ /F	-39210	-45720	47140	36290	0	0		
16	S ₁ /F	223	912	912	223	0	0		
17	M ₁ /F	6690	27130	27130	6690	0	0		
18	S ₁ /F	-9120	-8392	5182	5088	-4407	-9042		
19	S ₁ /F	-659	-2273	-2333	-4418	-1251	-1044		
20	S ₁ /F	9144	8694	5683	5108	4706	9102		
21	M ₁ /F	32750	-20500	-36500	-94150	79250	-62130		
22	M ₁ /F	24220	103080	103080	24220	31060	26850		
23	M ₁ /F	40730	105100	104350	97170	85490	67560		

CRITICAL SHEAR & BENDING MOMENT

TANK STA * 88.5 -

PREPARED		NAME	DATE	FLETCHER AVIATION CORPORATION		PAGE	25
CHECKED				TITLE		Model Custom	
APPROVED						43,300	
						Report No.	
Item	Cond.	3	7	11	13	12	
1	Sh	434.5				434.5	
2	M/n	12410				12410	
3	S/10 Mco	11.203				11.203	
4	M/10 Mco	459				459	
5	n	1.50	-15.00	-4.50	1.50	-12.00	
6	n	7.75	2.25	2.25	2.25	2.25	
7	103 M/co	44.82	44.82	89.64	-89.64	89.64	
8	103 M/co	0	0	44.82	29.88	44.82	
9	R ₂₀	21075	17478	21688	0	19241	
10	S ₂₀	11579	2311	9851	10946	9852	
11	S ₂₀	0	0	0	2798	0	
12	R ₂₀	10668	15401	12834	-12353	10386	
13	R ₂₀	-5076	-1013	-4318	-3572	-4319	
14	S ₂₀	-3029	0	0	0	0	
15	M ₂₀	-224,800	0	0	0	0	
16	S ₂₀	-635	-197	0	0	0	
17	M ₂₀	-32370	-9760	0	0	0	
Shell Loads							
18	S ₂₀	7789	8381	9875	-10297	4168	
19	S ₂₀	-1475	-232	-2838	-2260	-2839	
20	S ₂₀	7927	8384	10275	10933	5317	
21	M ₂₀	-226,760	-206,720	-96,990	59760	-190,060	
22	M ₂₀	58,230	18,160	48,490	41640	48,500	
23	M ₂₀	243,460	207,520	108,440	72840	196,150	

PREPARED		NAME	DATE	FLETCHER AVIATION CORPORATION		PAGE	TOTAL	PAGES
R. W. Hill		9-14-66		TITLE				26
CHECKED						Model Custom		
APPROVED						43.300		
						REPORT NO.		

Item	Cond.	3	4	6	7	12
1 S/n		216.6				
2 M/n	Ref. pg. 11	5490				
3 S ₁₀ M ₁₀		8.071				
4 M ₁₀ M ₁₀		243				
5 n ₁₀		1.50	-7.00	-15.00	-15.00	-12.00
6 n ₁₀ M ₁₀		9.75	9.75	2.25	2.25	2.25
7 10 ³ M ₁₀	Ref. pg. 12	44.82	-44.82	-44.82	44.82	89.64
8 10 ³ M ₁₀		0	0	0	0	44.82
9 R ₁₀						
10 S ₁₀	Ref. pg. —					
11 S ₁₀						
12 R ₁₀	⑨ - .89879(⑩ + ⑪)					
13 R ₁₀	.43837(⑩ + ⑪)					
14 S ₁₀	Ref. pg. 22	-3001	1645	1273	0	0
15 M ₁₀		-159,680	92300	73020	0	0
16 S ₁₀		-560	-560	-169	-169	0
17 M ₁₀		-19230	-19230	-5730	-5730	0
18 S ₁₀	Shell Loads					
19 S ₁₀	①⑤ - ③⑦ + ⑩ + ⑪	-3038	57	-1614	-3611	-3323
20 S ₁₀	①⑥ + ③⑧ + ④ + ⑫	1552	1552	318	318	849
21 M ₁₀	②⑤ - ④⑦ + ⑥	3411	1554	1645	3625	3430
22 M ₁₀	②⑥ + ④⑧ + ⑦	-12,340	53780	1560	-93240	-87660
23 M ₁₀	②⑦ + ④⑨ + ⑧	34300	34300	6620	6620	23240
	②⑧ + ④⑩ + ⑨	165,930	63790	6800	93470	90690

1AC Form 1100-1

Page determined to be Unclassified
Reviewed Chief, RDD, WHS
IAW EO 13526, Section 3.5
Date: 15 APR 2013

PREPARED	NAME R.W. Hill	DATE 9-6-62	FLETCHER AVIATION COMPANY	PAGE	27
CHECKED			TITLE LOADS & STRESS ANALYSIS SOLID FUEL TANK	Model	Custom
APPROVED					43.300
				REPORT No.	

CRITICAL DESIGN CONDITIONS

The following tabulation of the critical structural elements in the tank shows which design conditions produce the greatest loads on these items.

ITEM	CRIT. COND.	CRITERIA	PAGE
Eye-bolt (attach hook)	11	Max. R_z & R_x	
Central casting	(15), 5, 11	Bending	
Steel frames	(15), 4	Down ld., bending	
Fins & attachments	3	Max. fin load	
Tank shell	(15), 3, 11	Shear + moment, & max. drag load	

Condition #15 is an ejection condition. Since the loads to be experienced in the actual ejection may not reach the values assumed in design, static tests will be conducted of the next most critical design conditions in order to demonstrate an adequate strength level in the above items of structure.

It appears that static testing to Conditions #3, 4, 5, and 11 will prove out all the structural items. It appears also that the high sway brace load in Condition #5 (producing high local bending in the central casting) would be duplicated in Condition #3 if these loads were all increased by 2.9%. This would eliminate Condition #5 as a test condition.

REQUIRED STATIC TEST CONDITIONS

- Cond. #3 - Flight (with loads increased by 2.9%)
- Cond. #4 - Flight
- Cond. #11 - Arrested Landing

PREPARED	NAME <u>R.V. Hill</u>	DATE <u>8-29-62</u>	FLETCHER AVIATION CORPORATION	PAGE <u>1</u>	TEMP. <u>23</u>
CHECKED			TITLE	MODEL <u>Custom</u>	
APPROVED				43.300	
				REPORT No.	

STRESS ANALYSIS

Outer Shell Analysis

Nose Section (T.S. "0 - 52.1)

Ref drg. #21-150-49032 Tank Assembly
-1342 Nose Assembly

Critical section for combined shear & bending is just forward of sta. #52.1 joint. Highest loads are produced by the 30000^{lb} ejection force in the tank-empty condition.

$$W = 818.0 \text{ }^{\circ} \quad (\text{Pg. } 8)$$

$$\left. \begin{array}{l} P = 30000 \text{ }^{\circ} \\ M_{yc} = 69300 \text{ in-lbs} \end{array} \right\} \text{ Tank inertia loads} \\ \text{Cond \#15, pg. 13}$$

$$P_{eff} = \frac{30000}{818.0} = 36.67$$

$$S/n = 166.7 \text{ }^{\circ}$$

$$S/10^3 M_{yc} = 7.449 \text{ }^{\circ}$$

$$M/n = 4290 \text{ in-lbs}$$

$$M/10^3 M_{yc} = 222 \text{ in-lbs}$$

Pg. 10

$$\begin{aligned} S_{en} &= 166.7 \times 36.67 + 7.449 \times 69.30 \\ &= 6113 + 516 = 6629 \text{ }^{\circ} \end{aligned}$$

$$\begin{aligned} M_{en} &= 4290 \times 36.67 + 222 \times 69.30 \\ &= 157,310 + 15380 = 172,690 \text{ in-lbs} \end{aligned}$$

Section properties find. of T.S. #52.1

.063 6061-T4 shell

$$O.R. = 10.48 \text{ }^{\circ} \quad (\text{T.S. \#50, drg. \#21-150-1342})$$

$$A = .063 \pi \times 10.448 \times 2 = 4.136 \text{ in}^2$$

$$Z = \pi \times 10.448 \times .063 = 21.60 \text{ in}^3$$

$$\left(\frac{R}{Z} \right)^{1.25} = \left(\frac{10.448}{.063} \right)^{1.25} = 165.8^{1.25} = 991.8$$

PREPARED	NAME E W Hill	DATE 8-29-62	FLETCHER AVIATION CORPORATION	PAGE	2	TOTAL	29
CHECKED			TITLE	MODEL C-100			
APPROVED				43.300 REPORT NO.			

Nose Section, cont.

$$\frac{L}{R} = \frac{23.6}{10.448} = 2.26 \quad (-1342 \text{ Nose Assem.})$$

$$K_s = .90 \quad (\text{T.N. } ^\circ 427, \text{ Fig. 12})$$

$$F_s = \frac{K_s E}{(R/t)^{1.35}}$$

$$= \frac{.90 \times 10^7}{491.8} = 9070 \text{ } ^\circ/\text{in}^2$$

$$F_s = \frac{2 \times 6629}{4.136} \quad (\text{Prev. pg. } \times 2 \text{ for ratio of max. to avg. stress in thin sections.})$$

$$= 3206 \text{ } ^\circ/\text{in}^2$$

$$R_s = \frac{3206}{9070} = .3535$$

$$K_b = .00185 \quad (\text{T.N. } ^\circ 479, \text{ Fig. 5})$$

$$F_b = K_b E = .00185 \times 10^7$$

$$= 18500 \text{ } ^\circ/\text{in}^2$$

$$F_{cy} = 16000 \text{ } ^\circ/\text{in}^2 \quad (\text{Alcoa Structural Handb'k, table 4A, pg. 42, 6061-T4})$$

$$f_b = \frac{172,690}{21.60} \times 1.5 \quad (\text{Prev. pg. } 1.5 \text{ is arbitrary factor for stress concentration for bayonet-type joint.})$$

$$= 11990 \text{ } ^\circ/\text{in}^2$$

$$R_b = \frac{11990}{16000} = .7494$$

$$M.S. = \frac{1}{.3535 + .7494} - 1 = .21$$

Center Section (T.S. 52.1-109.5)

Ref. drg. 21-150-48032 Tank Assem.

Critical section for combined shear & bending is at sta. 88.5, in the tank-empty ejection condition. Load factor & pitching moment are same as shown on previous page. (Nose section analysis.)

PREPARED	NAME <u>R. N. Hill</u>	DATE <u>2-29-62</u>	FLETCHER AVIATION CORPORATION	PAGE <u>3</u>	TOTAL <u>30</u>
CHECKED			TITLE	MODEL <u>Custom</u>	
APPROVED				43.300	REPORT NO. 1

Center Section, cont.

$$\begin{aligned}
 S/n &= 288.3'' \\
 S/I^2M &= 9.993'' \\
 M/n &= 9840 \text{ in-lbs} \\
 M/I^2M &= 466 \text{ in-lbs}
 \end{aligned}
 \left. \begin{array}{l} \\ \\ \\ \end{array} \right\} \text{Pg } 10$$

$$\begin{aligned}
 S_{res.} &= 288.3 \times 36.67 - 9.993 \times 69.3 \\
 &= 10572 - 692 = 9880'' \\
 M_{res.} &= 9840 \times 36.67 - 466 \times 69.3 \\
 &= 360,830 - 32,290 = 328,540 \text{ in-lbs}
 \end{aligned}$$

Section properties

.063 6061-T6 shell

$$O.R. = 10.600''$$

$$A = 2\pi \times 10.468 \times .063 = 4.144 \text{ in}^2$$

$$Z = \pi \times 10.468^2 \times .063 = 21.69 \text{ in}^3$$

Since the section is nearly identical to that on pg. 28, the same allowable stresses will be used, but increased by 25% to allow for the stiffening effect of the foam filler. In addition, it may be assumed that the inner tank carries at least 10% of the actual shear and moment. (See also F.A.C. report #43,284, "Loads & Stress Analysis, General Mills Tank.")

$$f_s = \frac{2 \times 9880}{4.144} \times .9 = 4290 \text{ psi}$$

$$F_s = 1.25 \times 9070 \quad (\text{Prev. pg. 4 above})$$

$$= 11340 \text{ psi}$$

$$R_s = \frac{4290}{11340} = .3783$$

$$f_b = \frac{328,540}{21.69} \times .9 = 13630 \text{ psi}$$

PREPARED	NAME <i>R W Hill</i>	DATE <i>8-29-62</i>	FLETCHER AVIATION CORPORATION	PAGE	4	31
CHECKED			TITLE	MODEL	<i>Custom</i>	
APPROVED				REPORT NO.	<i>43.32</i>	

Center Section, cont.

$$F_b = 1.25 \times 16000 \quad (P_g \text{ 29 + 30. })$$

$$= 20000 \text{ } \frac{\text{lb}}{\text{in}^2}$$

$$R_b = \frac{12630}{20000} = .6315$$

$$M.S. = \frac{1}{.3783 + .6315} - 1 = .28$$

Aft Section (T.S. *109.5 - 159.5)

Ref. drg. *21-150-48032, sht. *2. Tank Assem.
Critical section for combined shear & bending
is just aft of sta. *109.5 joint. Highest loads
are again produced by Cond. *15, Tank-empty
Ejection. Section properties and material
are identical to those in the nose section,
just forward of sta. *52.1 joint. (See pg. 28.)

$$S/n = 176.5 \text{ } \frac{\text{in}^3}{\text{in}}$$

$$S/\bar{I}^3M = 8.104 \text{ } \frac{\text{in}^3}{\text{in}^4 \cdot \text{lb}}$$

$$M/n = 5091 \text{ in-lbs}$$

$$M/\bar{I}^3M = 275 \text{ in-lbs}$$

pg. 10

$$S_{a1ms} = 176.5 \times 36.67 - 8.104 \times 69.30 \quad (P_g \text{ 29. })$$

$$= 5911 \text{ } \frac{\text{in}^3}{\text{in}}$$

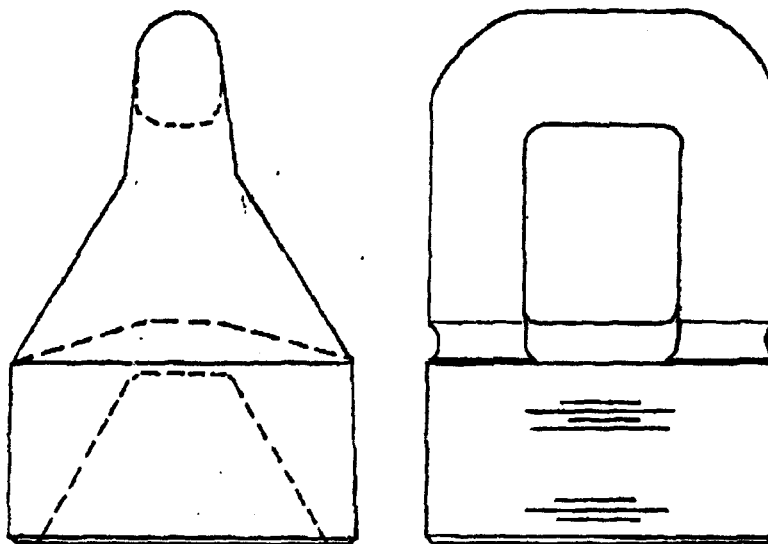
$$M_{g1ms} = 5091 \times 36.67 - 275 \times 69.30$$

$$= 167,630 \text{ in-lbs}$$

Since both the shear and moment at this
station are less than at T.S. *52.1 in the nose,
and since materials & section properties are
identical, the Aft Section, in shear & bending,
is safe by comparison.

PREPARED	NAME <i>P. V. Hill</i>	DATE <i>9-29-66</i>	FLETCHER AVIATION CORPORATION	PAGE <i>5</i>	PL. NO. <i>32</i>
CHECKED			TITLE	MODEL <i>Custom</i>	
APPROVED				43.300	REPORT NO.

*4544419-501 Lug (Eye-bolt)



Material : 4340 steel forging
Heat treatment : 180,000 - 200,000 $^{\circ}\text{F}/\text{in}^2$

Lug is critical for top section in double shear. Max. load occurs on aft lug in Cond. "II." (Pgs 20 & 21.)

$$\left. \begin{array}{l} R_{2A} = 21688 \text{ lb} \\ R_{1A} = 9461 \text{ lb} \end{array} \right\} \text{Ref. above.}$$

$$\text{Resultant } R_R = 23660 \text{ lb}$$

Shear area,

$A_s = .480 \text{ in}^2$ (Drgs. *4544419 & 4552066.)
"K" factor (form factor) for shear, for shape mid-way between circular & rectangular,
 $k = 1.42$ (Shanley, Sec. 17.4, pg. 282)

FAC Form 1808-1

PREPARED	NAME <u>R. Hill</u>	DATE <u>1-29-62</u>	FLETCHER AVIATION CORPORATION	PAGE <u>6</u>	FORM <u>33</u>
CHECKED			TITLE	MODEL <u>Custom</u>	
APPROVED				43.300	
				REPORT No.	

*4544419-501 Lug, cont.

$$f_s = \frac{442 \times 23660}{2 \times .480} = 35000 \text{ } \psi/\text{in}^2$$

$$F_{su} = 109,000 \text{ } \psi/\text{in}^2 \text{ (MIL-HDBK-5 table *2.2.2.0b)}$$

M.S. = High

Shear-out of threads in #21-150-20179 casting by 2 7/8-12N-3A threads on #2550562 insert, over an effective length of 1.10".

Shear area may be assumed conservatively,
 $A_s = \pi (P.D.) \times \frac{2}{3} L = \pi \times 2.82 \times \frac{2}{3} \times 1.10$
 $= 6.50 \text{ in}^2$

$$f_s = \frac{23660}{6.50} = 3640 \text{ } \psi/\text{in}^2$$

Casting material is 356-T6

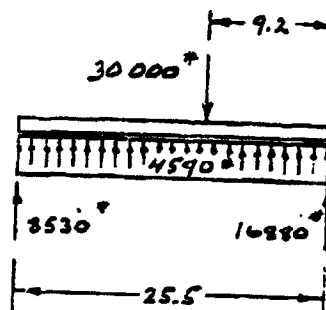
$$F_{su} = 25000 \text{ } \psi/\text{in}^2 \text{ (MIL-HDBK-5 table *3.2.15.0b)}$$

M.S. = High

*21-150-20179 Casting

Material : 356-T6 alum. casting

Critical bending stress occurs in Ejection Cond. #15. (Tank empty.)



Running load from weight of inner tank & equipment

$$W = 36.67 \times \frac{4.09}{83.2} \text{ (Pg. 25.)}$$

$$= 180.0 \text{ } \psi/\text{in}$$

$$M_{max} = \frac{9.2^2 \times 180.0}{2} + 9.2 \times 16880$$

$$= 162,700 \text{ in-lbs}$$

PAC Form 7808-1

15 APR 2013

PREPARED	NAME R. M. Hill	DATE 2-31-62	FLETCHER AVIATION CORPORATION		PAGE 1	PERM. 35
CHECKED			TITLE		MODEL Custom	
APPROVED					43.300	REPORT NO.

-20179 Casting, cont.

Moment of inertia,

$$I = (5.009 + 33.622 - 14.065 + 2.0566) \times 2$$

$$= 19.41 \text{ in}^4$$

Tension stress in inner tank shell,
.078 type 304 stainless steel, annealed.

$$f_T = \frac{162,900 (10.500 - 2.057 - 2.33 \cos 49^\circ 44')}{19.41} \times \frac{28}{10}$$

$$= 71900 \text{ psi} \quad (\text{Ref. prev. 2 pages})$$

$$F_{TV} = 75000 \quad (\text{QQ-5-766C, table II})$$

$$M.S. = \frac{75000}{71900} - 1 = .04$$

Tension in flange of casting (Item "7")

$$f_T = 162,900 \times \frac{2.193}{19.41} \quad (\text{Ref. prev. 2 pages})$$

$$= 18400 \text{ psi}$$

$$F_{TV} = 30,000 \text{ psi} \quad (356-T6 \text{ sand casting, MIL-HDBK-5, table 3.2.15.06})$$

$$M.S. = \frac{30,000}{1.33 \times 18400} - 1 = .22$$

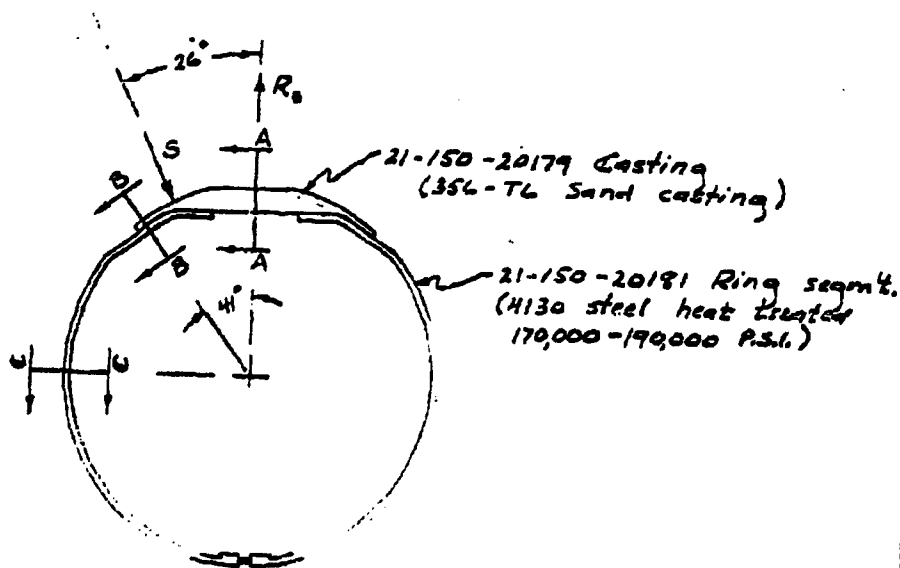
Compression side of casting, with a moment arm of only 1.776" from C.G. of section, is safe by comparison.

See pg. 36 for analysis of casting as part of main frames of tank support structure.

PREPARED	NAME K. W. Hill	DATE 7-4-62	FLETCHER AVIATION CORPORATION	PAGE	36
CHECKED			TITLE	MODEL	Custom
APPROVED				43.340	REPORT NO.

Main Frames

The forward and aft main frames are composite frames consisting of two semi-circular steel straps connected across the top by -20179 aluminum casting, which effectively forms the upper segment of the frame, and at the bottom by a jack screw. The forward and aft frames are identical.



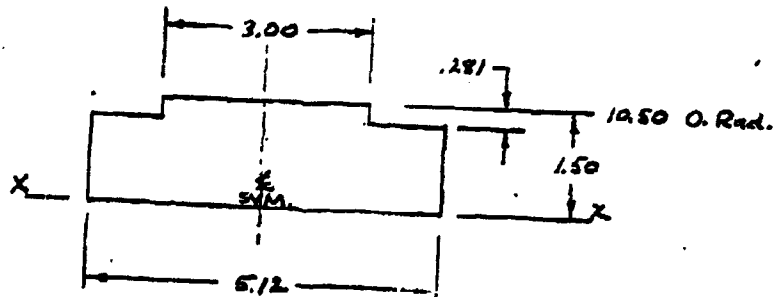
Bending moments in the ring are calculated from the coefficients in N.A.C.A. T.N. "929, "Analysis of Circular Shell-Supported Frames," and conservatively use a "d" value of zero. Sections B-B and C-C are taken on the same side of the frame as the sway brace load, for maximum

PREPARED	NAME <u>E. W. Hill</u>	DATE <u>9-4-62</u>	FLETCHER AVIATION CORPORATION	PAGE	1 OF 37
CHECKED			TITLE	MODEL	<u>Custom</u>
APPROVED				REPORT NO.	<u>43.300</u>

Main Frames, cont'

bending moment.

Section A-A



$$A = 1.50 \times 5.12 - .281 \times 2.12$$

$$= 7.680 - .596 = 7.084 \text{ in}^2$$

$$\bar{y} = \frac{7.5 \times 7.680 - 1.360 \times .596}{7.084} = .699'' \text{ (Above X-X)}$$

$$I = \frac{5.12 \times 1.50^3}{12} - \frac{2.12 \times .281^3}{12} + .051 \times 7.680 - .661 \times .596$$

$$= 1.440 - .004 + .020 - .260$$

$$= 1.196 \text{ in}^4$$

Moment coefficients for R_2 (on $\frac{1}{2}$) and S (26" away), per Fig. 11, T.N. "929"

$$\text{For } R_2, C_m = .238$$

$$\text{For } S, C_m = .041$$

Critical loads are from Cond. "11" (Pg. 20)

$$R_{2A} = 21688''$$

$$S_{4A} = 9851''$$

$$M_{A-A} = (9.00 + .699) \times (.238 \times 21688'' - .041 \times 9851'')$$

$$= 46100 \text{ in-lbs}$$

$$f_b = \frac{46100(1.500 - .699)}{1.196}$$

$$= 30870 \text{ psi}$$

1AC Form 800-1

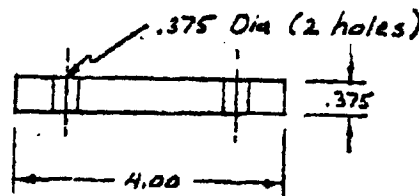
PREPARED	R. N. Hill	DATE	7-5-62	FLETCHER AVIATION CORPORATION	PAGE	11	28
CHECKED				TITLE	MODEL	Custom	
APPROVED					43.360	REPORT NO.	

Main Frames, cont.

$$F_{bu} = 41000 \text{ } \psi/\text{in}^2 \text{ (L.A.C. Stress Memo } ^\circ 53, \text{ fig. } ^\circ 1e.)$$

$$M.S. = \frac{41000}{1.33 \times 30870} - 1 = .00$$

Section B-B



Material: 4130 steel
h.t. 170,000 - 190,000 ψ/in^2

Moment coefficients for

$$\left. \begin{array}{l} R_s @ 41^\circ \text{ away, } C_m = -.033 \\ S @ 15^\circ \text{ away, } C_m = .117 \end{array} \right\} \text{ T.N. } ^\circ 929, \text{ fig. } ^\circ 11.$$

Critical bending moment is from Cond. "4"

$$\left. \begin{array}{l} R_{sp} = 19946 \text{ } \\ S_{sp} = 14501 \text{ } \end{array} \right\} \text{ Pg. } 20$$

$$M_{B-B} = (10.50 - .19 - .50)(.117 \times 14501 + .033 \times 19946)$$

$$= 23100 \text{ in-lbs}$$

$$Z = \frac{3.25 \times .375^2}{6} = .0762 \text{ in}^3$$

It can be assumed that the support from the heavy inner tank and the structural foam filler will reduce bending deflection (and consequently, bending stresses) by at least 20%.

$$f_b = \frac{.80 \times 23100}{.0762} = 242,500 \text{ } \psi/\text{in}^2$$

$$F_{bu} = 252,000 \text{ } \psi/\text{in}^2 \text{ (L.A.C. Stress Memo } ^\circ 53, \text{ fig. } 1f.)$$

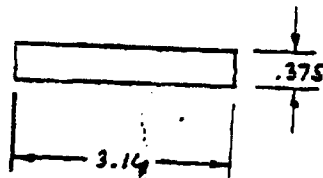
$$M.S. = \frac{252,000}{242,500} - 1 = .04$$

FAI Form 7100-1

PREPARED	NAME R. W. Hill	DATE 9-5-62	FLETCHER AVIATION CORPORATION	PAGE	12	39
CHECKED			TITLE	MODEL	Custom	
APPROVED				REPORT No.	43.340	

Main Frames, cont.

Section C-C



Same material as
Sect. B-B.

Moment coefficients for

$$\left. \begin{array}{l} R \text{ @ } 90^\circ \text{ away} \\ S \text{ @ } 64^\circ \end{array} \right\} \begin{array}{l} C_m = -.091 \\ C_m = -.095 \end{array} \quad \text{T.N. 729, fig. 11.}$$

Critical bending plus compression is from
Ejection Cond. #15.

Referring to sketch on pg. 33, the max. load
is on the aft frame.

$$R_{2A} = 16880 \text{ lb}$$

$$M_{C-C} = (10.50 - .19) \times .091 \times 16880 = 15840 \text{ in-lbs}$$

$$A = .375 \times 3.14 = 1.185 \text{ in}^2$$

$$Z = \frac{3.14 \times .375^2}{6} = .07406 \text{ in}^3$$

It can be assumed again (as for Sect. B-B)
that support from the heavy inner tank
and the structural foam filler will reduce
the bending loads on the section by 20%.

$$f_c = \frac{16880}{2 \times 1.185} = 7120 \text{ psi}$$

$$F_{cy} = 168,000 \text{ psi} \quad (\text{MIL-HDBK-5, table 2.2.2.06})$$

$$R_c = \frac{7120}{168,000} = .0424$$

$$f_b = \frac{.80 \times 15840}{.07406} = 171,100 \text{ psi}$$

PREPARED	NAME <i>R. W. Hill</i>	DATE <i>9-5-62</i>	FLETCHER AVIATION CORPORATION		PAGE	13	REV. 10
CHECKED			TITLE		MODEL <i>Custom</i>		
APPROVED					43,300		
					REPORT NO.		

Main Frames, cont.

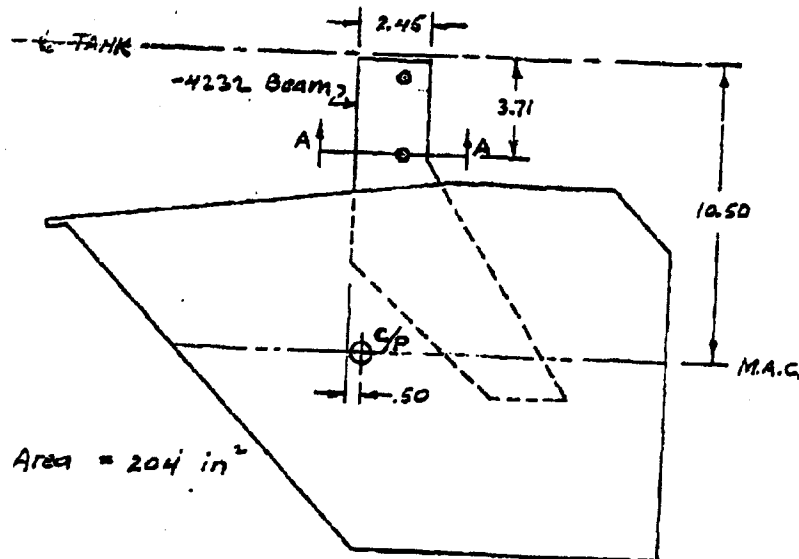
$$F_{by} = 252,000 \text{ "in}^2 \quad (\text{Pg. } 38)$$

$$R_b = \frac{171,100}{252,000} = .6790$$

$$M.S. = \frac{1}{.0424 + .6790} - 1 = .39$$

PREPARED	NAME A. Hill	DATE 9-10-62	FLETCHER AVIATION CORPORATION		PAGE	11	TOTAL	21
CHECKED			TITLE		MODEL	H3.340		
APPROVED					REPORT No.			

*21-150-4679 Fin

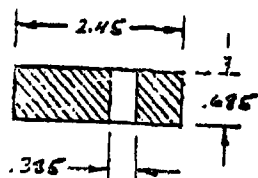


Max. fin load, (Cond. #3 ~ Flight)

$$P_{max} = 1.5 \left(\frac{2530}{2} + \frac{12 \times 120}{2 \times 10.50} \right) \text{ Ref. G.M.I letter to F.A.C. dated 7-27-62.}$$

$$= 2000$$

Section A-A



Material: 2024-T4 plate

$$M = (10.50 - 3.71) 2000$$

$$= 13580 \text{ in-lbs}$$

Net section modulus,

$$Z = (2.45 - .385) .485 / 6$$

$$= .1615 \text{ in}^3$$

$$f_b = \frac{13580}{.1615} = 84100 \text{ psi}$$

$$f_{bu} = \frac{12 \times 84900}{2} = 84100 \text{ psi}$$

(L.A.C. S.M. #53, fig. 1e)

$$M.S. = \frac{84100}{84100} - 1 = 0$$

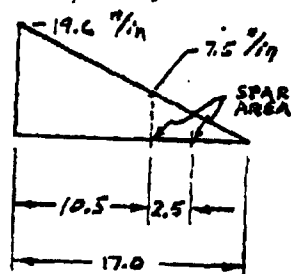
F. C. Form F202-1

PREPARED	NAME <u>R. W. Hill</u>	DATE <u>9-11-66</u>	FLETCHER AVIATION CORPORATION	PAGE	15	42
CHECKED			TITLE	MODEL	<u>Custom</u>	
APPROVED				REPORT No.	<u>43.300</u>	

-4679 Fin, cont.

Foam Filler

The airload on the surface of the fin is transferred into the 204-T4 beam (spar) by shear in the rigid polyurethane foam filler, and by tension or compression of the .040 2024-T3 Al. skins. Since the center of pressure at T.S. #1600 is very close to $\frac{1}{3}$ of the chord length, a triangular airload distribution may be assumed. Critical shear stress in the foam filler will be found along the front edge of the spar.



Typical section near tip of spar, parallel to M.A.C.

Total fin area,

$$A = 204 \text{ in}^2 \text{ (Prev. pg.)}$$

$$W_{avg} = \frac{2000}{204} = 9.80 \text{ lb/in}^2$$

$$W_{max} = 2 \times 9.80 = 19.60 \text{ lb/in}^2$$

Total shear at front edge of spar

$$S = \frac{10.5}{2} (19.6 + 7.5) = 142 \text{ lb}$$

Total moment at front edge of spar,

$$M = \frac{7.5 \times 10.5^2}{2} + \frac{12.1 \times 10.5^2}{3} = 353 \text{ in-lbs}$$

The over-all taper of the fin forward from the spar will reduce the shear load on the core material by the component of load in the sheet material normal to the fin \perp .

PREPARED	R. V. Hill	DATE	9-11-62	FLETCHER AVIATION CORPORATION	PAGE	1	13
CHECKED				TITLE	MODEL	43.340	REPORT NO.
APPROVED							

-4679 Fin, cont.

The total fin thickness varies from .387" to .120" in 10.0" distance. (Ref -4232 Beam and Sect. E-E of -4679 Fin drg., above)

$$\tan\left(\frac{\theta}{2}\right) = \frac{(.387 - .120)}{2 \times 10.0} = .01335$$

For 1" width of sheet

$$P_H = \frac{858}{.387 - .040} = \pm 2473 \text{ "}$$

$$P_N = .01335 \times 2473 = 33 \text{ "}$$

Remaining shear to be carried in core,

$$S_R = 142 - 2 \times 33 = 76 \text{ "}$$

Correcting for the shear area presented by a 47° sweep-back of the front face of the fin spar, the actual core shear stress,

$$f_{sc} = \frac{76 \cos 47^\circ}{.307} = \frac{76 \times .6820}{.307} = 169 \text{ "/in}^2$$

Foam is AT-106 (6" foam, foamed to 12"/ft³ density). Conservatively use strength properties for 10"/ft³ density.

$$F_{su} = 200 \text{ "/in}^2 \text{ (Test by AT Products, using MIL-STD-401 test methods.)}$$

$$M.S. = \frac{200}{169} - 1 = .18$$

Tension stress in .040 2024-T3 Alc sheet:

$$f_T = \frac{(2473 + 33) \cos 47^\circ}{.040} = 42700 \text{ "/in}^2$$

$$F_{Tux} = 59000 \text{ "/in}^2 \text{ (MIL-HDBK-5 Table 3.2.3.0 d)}$$

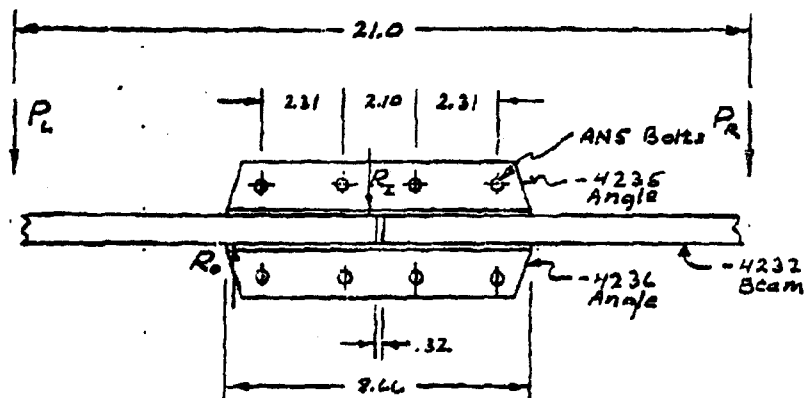
$$M.S. = \frac{59000}{42700} - 1 = .38$$

PREPARED	NAME <i>R. M. Hill</i>	DATE <i>9-11-62</i>	FLETCHER AVIATION CORPORATION	PAGE <i>17</i>	TOTAL <i>14</i>
CHECKED			TITLE	MODEL <i>Custom</i>	
APPROVED				43.300	REPORT No.

Fin Attachments

The two fins are mounted on -3372 bulkhead (T.S. #159.5) by sandwiching the inbd. ends of their spars between two angles which are bolted to this bulkhead. The fins are also stabilized against twisting by clipping the inbd. end of the leading edge to the adjacent tail cone.

As for the fin itself, the attachments will also be critical under the airloads of Cond. #3 - Flight.



Fin loads

$$P = \frac{1.5 \times 2530}{2} \pm \frac{1.5 \times 12 \times 12.2}{2 \times 10.50} \quad (P_q = 41)$$

$$= 1897.5 \pm 102.5$$

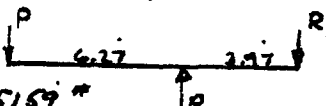
$$P_L = 2000 \text{ "}$$

$$P_R = 1795 \text{ "}$$

PREPARED	NAME R. L. Hill	DATE 9-11-62	FLETCHER AVIATION CORPORATION	PAGE	12	45
CHECKED			TITLE	MODEL	Auclem	
APPROVED				REPORT NO.	43.300	

Fin Attach, cont.

The inbd. & outbd. reactions on the spar (R_L & R_o) create the loads on the upper and lower attach angles. Assume these reactions are .10' away from edge of angle and end of spar. (Sk., prev. pg.)

For $P_L = 2000$ 

$$R_o = \frac{10.24 \times 2000}{3.97} = 5159 \text{ *}$$

$$R_L = 5159 - 2000 = 3159 \text{ *}$$

For $P_A = 1795$ *

$$R_o = \frac{10.24 \times 1795}{3.97} = 4630 \text{ *}$$

$$R_L = 4630 - 1795 = 2835 \text{ *}$$

Attachments for lower angle are critical.

Load on bolt pattern

$$P = 5159 + 4630 = 9789 \text{ *}$$

$$M = 4.23(5159 - 4630) = 2238 \text{ in-lbs}$$

Moment of inertia of bolt pattern.

$$I = 2(3.36^2 + 1.05^2) = 24.78$$

Max. bolt load,

$$P_{max} = \frac{9789}{4} + 2238 \times \frac{3.36}{24.78}$$

$$= 2447 + 303$$

$$= 2750 \text{ *}$$

Load is taken by an AN5 bolt bearing in .120' 6061-T6 plate.

Bolt allowable shear,

$$P_s = 5750 \text{ *} \text{ (MIL-HDBK-5, table *8.1.1.1(a))}$$

PREPARED	NAME <i>R. N. Hill</i>	DATE <i>9-11-62</i>	FLETCHER AVIATION CORPORATION	PAGE	11	16
CHECKED			TITLE	MODEL	<i>Custom</i>	
APPROVED					<i>43 300</i>	
				REPORT No.		

Fin Attach, cont.

Allowable bearing load by AN5 in .120
6061-T6 plate,

$$P_{br} = 1.5 \times 58000 \times .120 \times \frac{5}{16} \quad \text{(MIL-HDBK-5 table *8.1.1.1 f)}$$

$$= 3262 \text{ "}$$

$$M.S. = \frac{3262}{1.15 \times 2750} - 1 = .03$$

NAME	DATE	FLETCHER AVIATION COMPANY	PAGE	TEMP.	REVISION
PREPARED R. W. Hill	10-16-62				A-1
CHECKED		TITLE	Model Custom		
		APPENDIX "A"	43.300		
APPROVED			REPORT NO. 1		

INTRODUCTION

On October 4, 1962, a revised set of airloads was received from General Mills to use in conjunction with the inertia loads derived from MIL-T-7378A. This meant a revision of Flight Conditions #4, 5, 6 and 7 basic loads, as shown on the following pages. New attach point reactions are calculated, and resultant shears and moments are found at four stations along the tank shell, as before.

From the above data it was found that Condition #4 is no longer a critical condition requiring static testing. It will be replaced by Condition #5 and 7. (See discussion on page A-10) This means a total of four design conditions will require static tests.

Starting on page A-11, a review of the effects of the new loads on the previous stress analysis is made. It is shown that all structural items affected by the new loads still have positive margins of safety.

NAME		DATE	FLETCHER AVIATION CORP.		Page	72
Prepared	P. N. Hill	10-8-62	TITLE		1	72
Checked					Model	43.300
Approved			Appendix "A"		Report No.	

REVISED DESIGN CONDITIONS					
(Per revised G.M. airloads dated 9-17-62)					
Condition	4	5	6	7	
Flight	Flight	Flight	Flight	Flight	
Loading	Full	Full	Full	Full	
1. W	1168	1168	1168	1168	
2. \bar{X}	82.0	82.0	82.0	82.0	
3. $I_{yy} = I_{zz}$ (sq. ft.) $P_{y,z}$	415.0	415.0	415.0	415.0	
4. Ult. Design Parameters					
5. n_z	-7.00	-7.00	-15.00	-15.00	
6. n_y	9.75	9.75	2.25	2.25	
7. n_x	3.00	-3.00	3.00	-3.00	
8. δ (Pitch)	-9.00	9.00	-9.00	9.00	
9. ψ (Yaw)	0	0	0	0	
10. Inertia Loads at C.G.					
11. P_z (15)	-10512	-10512	-17520	-17520	
12. P_y (16)	11389	11388	2628	2628	
13. P_x (17)	3504	-3504	3504	-3504	
14. M_y (12)(8)	-44820	44820	-44820	44820	
15. M_z (12)(9)	0	0	0	0	
16. Airloads at T.S. "76.5"					
17. P_z	2085	-2250	1350	-2250	
18. P_y	345	345	30	30	
19. P_x	510	600	490	600	
20. M_y	26620	121260	39060	127260	
21. M_z	-78480	-78480	-21600	-21600	
22. M_x	-360	-4360	0	-180	
23. Total Load at Ref. Pt.					
24. P_z (11) + (17)	-2427	-12762	-11170	-11170	
25. P_y (12) + (18)	11733	11733	2658	2658	
26. P_x (13) + (19)	4014	-2904	3764	-2904	
27. M_y (10) + (20) - 5.51 (11) - 31 (17)	112430	235850	95610	274570	
28. M_z (3) + (21) + 5.31 (12) + 31 (18)	-12210	-12210	-6320	-6320	
29. M_x (22)	-360	-4860	0	-180	

14E Form FBCB-1

Prepared	E. Hill	DATE	10-8-62	FLETCHER AVIATION CORP.		PAGE	2	REV.	A-3
Checked				TITLE		Model Custom			
Approved				Appendix 'A'		43.300			
Report No.									

PRELIM. REACTIONS TO REVISED LOADS					
		4	5	6	7
Loads at Tank Ref. Pt.					
1	+ P ₂				
2	- P ₂	-2427	-12762	-16170	-19770
3	+ P ₄	11783	11733	2658	2658
4	+ P ₄	4014		3984	
5	- P ₂		-2704		-2704
6	+ M ₂	42430	233,850	95610	274,570
7	- M ₂				
8	+ M ₂				
9	- M ₂	-12210	-12210	-6320	-6320
10	- M ₂	-360	-4860	0	-180
Reactions to Loads					
R _{2F}		19514	20493	13402	13289
R _{4F}		-30	-406	0	-15
R _{2F}	Same	-2408	1742	-2390	1742
R _{2A}	Operations	19253	31204	15282	25639
R _{4A}	as on	-30	-406	0	-15
R _{2A}	pg. 18	-2408	1742	-2390	1742
S _{2F}		15719	20767	5880	10650
S _{4F}		1013	6917	2127	6932
S _{2A}		14472	18533	1113	3000
S _{4A}		2551	2318	1702	75

1AC Form 1802-1

Prepared		NAME	DATE	FLETCHER AVIATION CORP.		PAGE	OF
G. W. Hill			10-8-62			3	4
Checked		TITLE				Head	
						Custom	
Approved		Appendix "A"				Report No.	
						43.350	

		4	5	6	7
Prelim. Vertical Reactions (Pg. A-3)	R_{2F}	19574	20493	13402	13289
	R_{2A}	19253	31264	15282	25689
	S_{2F}	15717	20767	5880	10650
	S_{2A}	1013	6917	2127	6932
	SL_A	14472	13383	4113	3032
1 st Reduction (Ref. pg. 15)	SR_A	2551	2318	1802	755
	ΔR_{2F}	-1920	-4167	-3239	-1357
	ΔR_{2A}	-1920	-4167	-3239	-1357
	ΔS_{2F}	-1013	-2318	-1802	-755
	ΔS_{2A}	-1013	-2318	-1802	-755
Adjusted Reactions	R_{2F}	17694	16326	10163	11932
	R_{2A}	17433	27097	12043	24332
	S_{2F}	14706	18449	4078	9875
	S_{2A}	0	4599	325	6177
	SL_A	13459	11065	2311	2277
2 nd Reduction (Ref. pg. 16)	SR_A	1538	0	0	0
	ΔR_{2F}	-461	-6889	-487	-9253
	ΔR_{2A}	-2304	-1378	-97	-1851
	ΔS_{2F}	0	-4599	-325	-6177
	ΔS_{2A}	0	-4599	-325	-6177
FINAL REACTIONS	ASL_A	-1538	0	0	0
	ΔSR_A	-1538	0	0	0
	R_{2F}	17233	9427	9676	2679
	R_{2A}	-30	-406	0	-15
	R_{2F}	-2408	1742	-2340	1742
	R_{2A}	15129	25719	1946	22431
	R_{2A}	-30	-406	0	-15
	R_{2A}	-2408	1742	-2340	1742
	S_{2F}	14706	13560	0753	3718
	S_{2F}	0	0	0	0
SL_A	11921	11065	2311	2277	
SR_A	0	0	0	0	

TAC Form F80e-1

PREPARED	NAME <i>C. W. Hill</i>	DATE <i>10-9-62</i>	FLETCHER AVIATION CORPORATION		PAGE <i>4</i>	TOTAL PAGES <i>5</i>
CHECKED			TITLE <i>Appendix "A"</i>		MODEL <i>distam</i>	
APPROVED					43300 REPORT NO.	

REVISED AIRLOAD BREAK-DOWN

Ref. G.M.I. letter
dated 1 Oct, 1962.

Vertical Loads				Lateral Loads			
T.S.	4	5	6	7	T.S.	4+5	6+7
10	372	-128	276	-128	8		
33	726	-244	576	-244	31	Same	Same
56	550	-172	427	-172	54	45	45
79	+139	-17	+93	-17	77	pg. 22	pg. 22
102	-93	+68	-92	+68	100		
125	-253	123	-226	123	123		
148	-321	143	-276	143	142		
171	-215	87	-163	87	169		
FIN (140)	+1170	-2115	+750	-2115			
	2035	-2255	1365	-2255		345	30

PREPARED	NAME J. Hill	DATE 10-9-62	FLECHER AVIATION CORPORATION	PAGE 5	REV. A-6
CHECKED			TITLE Appendix "A"	MODEL 43.300	REPORT NO.
APPROVED					

CRITICAL SHEAR & BENDING MOMENT

TANK STA. *SL2

Item	Cond.	4	5	6	7
1 S _h		202.0			
2 M ₁₂		4646			
3 S ₁₀ M ₁₂		7.207			
4 M ₁₀ M ₁₂		199			
5 n ₁₂		-9.00	-7.00	-15.00	-15.00
6 n ₁₂		9.75	9.75	2.25	2.25
7 10 ³ M ₁₂		-44820	44820	-44820	44820
8 10 ³ M ₁₂		0	0	0	0
9 R ₁₂					
10 S ₁₂					
11 S ₁₂					
12 R ₁₂					
13 R ₁₂					
14 S ₁₂		1258	-422	976	-422
15 M ₁₂		29075	-9882	22270	-9882
16 S ₁₂		717	717	178	178
17 M ₁₂		16850	16850	4360	4360
18 S ₁₂					
19 S ₁₂					
20 S ₁₂					
21 S ₁₂					
22 S ₁₂					
23 S ₁₂					
24 S ₁₂					
25 S ₁₂					
26 S ₁₂					
27 S ₁₂					
28 S ₁₂					
29 S ₁₂					
30 S ₁₂					
31 S ₁₂					
32 S ₁₂					
33 S ₁₂					
34 S ₁₂					
35 S ₁₂					
36 S ₁₂					
37 S ₁₂					
38 S ₁₂					
39 S ₁₂					
40 S ₁₂					
41 S ₁₂					
42 S ₁₂					
43 S ₁₂					
44 S ₁₂					
45 S ₁₂					
46 S ₁₂					
47 S ₁₂					
48 S ₁₂					
49 S ₁₂					
50 S ₁₂					
51 S ₁₂					
52 S ₁₂					
53 S ₁₂					
54 S ₁₂					
55 S ₁₂					
56 S ₁₂					
57 S ₁₂					
58 S ₁₂					
59 S ₁₂					
60 S ₁₂					
61 S ₁₂					
62 S ₁₂					
63 S ₁₂					
64 S ₁₂					
65 S ₁₂					
66 S ₁₂					
67 S ₁₂					
68 S ₁₂					
69 S ₁₂					
70 S ₁₂					
71 S ₁₂					
72 S ₁₂					
73 S ₁₂					
74 S ₁₂					
75 S ₁₂					
76 S ₁₂					
77 S ₁₂					
78 S ₁₂					
79 S ₁₂					
80 S ₁₂					
81 S ₁₂					
82 S ₁₂					
83 S ₁₂					
84 S ₁₂					
85 S ₁₂					
86 S ₁₂					
87 S ₁₂					
88 S ₁₂					
89 S ₁₂					
90 S ₁₂					
91 S ₁₂					
92 S ₁₂					
93 S ₁₂					
94 S ₁₂					
95 S ₁₂					
96 S ₁₂					
97 S ₁₂					
98 S ₁₂					
99 S ₁₂					
100 S ₁₂					

CRITICAL SHEAR & BENDING MOMENT

TANK STA * 64.0 +

PREPARED		DATE	FILE	CHER AVIATION CORPORATION	PAGE	7	7
2		2/11/11	11-7-62				
CHECKED							
APPROVED							
				TITLE	Appendix "A"		
					Model	62-73m	
					43.300		
					REPORT NO.		
Item	Cond.	4	5	6	7		
1 S _h		317.2					
2 M _h		779.0					
3 S ₁₀ M ₁₀₀	Ref. pg. 11	9.425					
4 M ₁₀ M ₁₀₀		302					
5 n _h		-9.00	-7.00	-15.00	-15.00		
6 n _h		9.75	9.75	2.25	2.25		
7 10 ³ M ₁₀₀	Ref. pg. 12 + 13	-44.82	44.82	-44.82	44.82		
8 10 ³ M ₁₀₀		0	0	0	0		
9 R _h		17233	9437	9676	2679		
10 S _h	Ref. pg. A-4	14706	13850	3753	3718		
11 S _h		0	0	0	0		
12 P _h	① - 87079(⑩ + ⑪)	4015	-3011	6303	-623		
13 P _h	② 43831(⑩ - ⑪)	-6447	-6071	-1245	-1250		
14 S _h		1564	509	1214	509		
15 M _h	Ref. pg. A-5	47140	15812	36290	15812		
16 S _h		912	912	223	223		
17 M _h		27130	27130	6690	6690		
18 S _h		2283	-4952	2307	-4520		
19 S _h	① + ② + ③ + ④ + ⑤ + ⑥ + ⑦ + ⑧ + ⑨ + ⑩ + ⑪ + ⑫ + ⑬ + ⑭ + ⑮ + ⑯ + ⑰ + ⑱ + ⑲ + ⑳ + ㉑ + ㉒ + ㉓ + ㉔ + ㉕ + ㉖ + ㉗ + ㉘ + ㉙ + ㉚ + ㉛ + ㉜ + ㉝ + ㉞ + ㉟ + ㊱ + ㊲ + ㊳ + ㊴ + ㊵ + ㊶ + ㊷ + ㊸ + ㊹ + ㊺ + ㊻ + ㊼ + ㊽ + ㊾ + ㊿	-2423	-2047	-704	-689		
20 S _h			5358				
21 M _h	① + ② + ③ + ④ + ⑤ + ⑥ + ⑦ + ⑧ + ⑨ + ⑩ + ⑪ + ⑫ + ⑬ + ⑭ + ⑮ + ⑯ + ⑰ + ⑱ + ⑲ + ⑳ + ㉑ + ㉒ + ㉓ + ㉔ + ㉕ + ㉖ + ㉗ + ㉘ + ㉙ + ㉚ + ㉛ + ㉜ + ㉝ + ㉞ + ㉟ + ㊱ + ㊲ + ㊳ + ㊴ + ㊵ + ㊶ + ㊷ + ㊸ + ㊹ + ㊺ + ㊻ + ㊼ + ㊽ + ㊾ + ㊿	-36500	-40760	-94100	-87500		
22 S _h		103080	103080	24220	24220		
23 S _h		109350	110850	97170	24720		

CRITICAL SHEAR & BENDING MOMENT

TANK STA *88.5-

CRITICAL SHEAR & BENDING MOMENT

TANK STA 88.5-

PREPARED		NAME	DATE	FLECHER AVIATION CORPORATION		PAGE	7	OF	9
CHECKED				TITLE		Moore, Custom			
APPROVED				Appendix "A"		43-300			
						Report No.			
Item	Cond.	4	5	6	7				
1 S/h		434.5							
2 M/h		12410							
3 S/h-M/h	Ref. pg. 11	11.203							
4 M/h-M/c		459							
5 N		-9.00	-9.00	-15.00	-15.00				
6 N		9.75	9.75	2.25	2.25				
7 10 ³ M/c	Ref. pg. 12	-44.82	44.82	-44.82	44.82				
8 10 ³ M/c		0	0	0	0				
9 R/h		15129	25719	11946	22481				
10 S/h	Ref. pg. A-4	11921	11065	2311	2277				
11 S/h		0	0	0	0				
12 R/h	④ - 89879(②+③) .42837(②-③)	4414	15774	9849	20434				
13 R/h		-5226	-4850	-1013	-998				
14 S/h		310	-1695	1	-1695				
15 M/h		36475	-13013	14272	-13013				
16 S/h		-635	-635	-197	-197				
17 M/h		-32370	-32370	-9760	-9760				
18 S/h	Ref. pg. A-5	1316	9666	3835	11719				
19 S/h	①③ - ③⑦ + ③ + ④ ①③ + ③⑤ + ④ + ③ ④ + ④	-1625	-1249	-232	-217				
20 S/h					11721				
21 M/h	②④ - ①⑦ + ②⑤ ②④ + ④③ + ② + ④ ② + ④	-54640	-745280	-151300	-219740				
22 M/h		88630	88630	18160	18160				
23 S/h					220490				

PREPARED	NAME R. J. Hill	DATE 10-9-62	FLETCHER AVIATION CORPORATION	PAGE 2
CHECKED			TITLE Appendix "A"	MODEL 43.300
APPROVED				REPORT NO.

CRITICAL SHEAR & BENDING MOMENT
TANK STA * 110.5

Item	Cond.	4	5	6	7
1 S ₁₂		214.6			
2 M ₁₂		5470			
3 S ₁₀ M ₁₀	Ref. pg. 11	8.071			
4 M ₁₀ M ₁₀		243			
5 R ₁		-9.00	-7.00	-15.00	-15.00
6 M ₁		9.75	9.75	2.25	2.25
7 10 ³ M ₁₀	Ref. pg. 12	-44.82	44.82	-44.82	44.82
8 10 ³ M ₁₀		0	0	0	0
9 R ₂					
10 S ₂	Ref. pg.				
11 S ₂					
12 P ₂ (sum)	⑨ - .89879(⑩ + ⑪) .43837(⑩ - ⑪)				
13 P ₂ (sum)					
14 S ₂ air		370	-1753	73	-1753
15 M ₂ air		29185	-92270	13620	-92270
16 S ₂ air	Ref. pg. A-5	-560	-560	-169	-169
17 M ₂ air		-19230	-19230	-5730	-5730
18 S ₂ air		-1218	-4064	-2814	-6364
19 S ₂ air	⑬ - ⑬ + ⑬ + ⑬	1552	1552	318	318
20 S ₂ air	⑬ - ⑬ + ⑬ + ⑬			6373	6373
21 S ₂ air	⑬ - ⑬ + ⑬ + ⑬	-9320	-152,570	-57840	-185,510
22 S ₂ air	⑬ - ⑬ + ⑬ + ⑬	34300	34300	6620	6620
23 S ₂ air	⑬ - ⑬ + ⑬ + ⑬				185,630

Shell loads

NAME	DATE	FLITCHER AVIATION COMPANY	PAGE	1-10
PREPARED: R.W. Hill	10-10-62			
CHECKED		TITLE	Model	Custom
		APPENDIX "A"		43.300
APPROVED			Report No.	

CRITICAL DESIGN CONDITIONS

A comparison of the data on the preceeding pages for revised Conditions #4, 5, 6 and 7 with the corresponding data for all the other design conditions in the earlier original part of this report indicates a need for a new Summary of Critical Design Conditions. As on page 27 of this report, the following tabulation of the critical structural elements in the tank shows which design conditions produce the greatest loads on these items.

Item	Critical Load	Criteria
Eye-bolt (attach hook)	5	Max. $R_z + R_x$
Central casting	(15), 2 & 5	Bending
Steel frames	(15), 5	Dr. ld., bending
Fins & attachments	3	Max. fin load
Tank shell	(15), 7 & 11	Shr. + mom., ∇ max. drag load

Condition #15 is an ejection condition, to be proved by an actual ejection test. (See page 27.) Condition #2, critical for the bending produced in the central casting by the highest away brace reaction, may be replaced by Condition #3 with its loads increased by 2.6%. This eliminates Condition #2 as a test condition. Since Condition #3 test loads and data have already been prepared on the basis of loads increased by 2.9%, testing will be conducted to these latter loads. (See page 27)

It now appears that all structural items will be proved out by conducting static tests of four design conditions.

REQUIRED STATIC TEST CONDITIONS

- Condition #3 - Flight (with loads increased by 2.9%)
- Condition #5 - Flight
- Condition #7 - Flight
- Condition #11 - Arrested Landing

PREPARED	NAME E. W. Hill	DATE 10-15-67	FLETCHER AVIATION CORPORATION	PAGE	TEMP.	GR.
CHECKED			TITLE	10		A-11
APPROVED			APPENDIX "A"	Model	43.300	REPORT No.

STRESS ANALYSIS

Two new design conditions create critical loads on some items of structure, as has been shown on the previous page. To substantiate the structural integrity of the tank, an item by item review of all affected parts will be made. Reference page numbers are to the original load and stress analysis sections of this report.

Nose Section (T.S. #0.0 - 52.) (Pg. 28)

Design loads, $S = 6629$ #

$M = 172,690$ in-lbs

Loads from revised flight condition, Cond. #5.

$S = 3300$ #

$M = 75450$ in-lbs } Pg. A-6

New loads are \therefore not critical

Center Section Shell (T.S. #52.1 - 109.5) (Pg. 29)

Design loads, $S = 9880$ #

$M = 328,540$ in-lbs

Loads from revised flight condition, Cond. #7

$S = 11721$ #

$M = 220,490$ in-lbs } Pg. A-8

$f_s = \frac{2 \times 11721}{4.144} = 5660$ #/in² (Pg. 30)

$R_s = \frac{5660}{11240} = .4991$

$f_b = \frac{220,490}{21.69} = 10170$ #/in²

$R_b = \frac{10170}{20000} = .5085$

PREPARED	R. N. Hill	DATE	10-15-62	FLETCHER AVIATION CORPORATION	PAGE	11	REV.	1-12
CHECKED				TITLE			MODE	41.300
APPROVED				APPENDIX "A"			REPORT NO.	

Center Section, cont.

$$M.S. = \frac{1}{.4991 + .5085} - 1 = .40$$

∴ with an original M.S. = .28, the original design condition is still the more severe. New loads are not critical.

Aft Section (T.S. #109.5 - 159.5) Pg. 31

As noted on pg. 31, the materials and section properties are identical to those of the more highly loaded nose section. The critical design loads were

$$\left. \begin{array}{l} S = 6629 \text{ #} \\ M = 172,690 \text{ in-lbs} \end{array} \right\} \text{Prev. pg. \& pg. 28}$$

Loads from revised flight condition, Cond. 7

$$\left. \begin{array}{l} S = 5373 \text{ #} \\ M = 185,630 \text{ in-lbs} \end{array} \right\} \text{Pg. A-9}$$

$$f_s = \frac{2 \times 5373}{4.136} = 2600 \text{ #/in}^2 \text{ (Pg. 29)}$$

$$R_s = \frac{2600}{9070} = .2866$$

$$f_b = \frac{185,630 \times 1.5}{21.60} = 12900 \text{ #/in}^2$$

$$R_b = \frac{12900}{16000} = .8062$$

$$M.S. = \frac{1}{.2866 + .8062} - 1 = .17$$

∴ shell structure is still adequate for new loading conditions.

PREPARED	K. W. Hill	DATE	10-15-62	FLITCHER AVIATION CORPORATION	PAGE	12	REV.	A13
CHECKED				TITLE	MODEL	dustan		
APPROVED				APPENDIX "A"	REPORT NO.	43.300		

#4544419-501 LUG

Design loads

$$\left. \begin{array}{l} R_{EA} = 21688 \text{ *} \\ R_{XA} = 9461 \text{ *} \end{array} \right\} \text{Pg. 32}$$

Loads from revised Cond. "5"

$$\left. \begin{array}{l} R_{EA} = 26719 \text{ *} \\ R_{XA} = 1742 \text{ *} \end{array} \right\}$$

Since the original M.S. in the steel lug and in the threaded portion of the casting are both "High" (i.e. - over 100%), these items are still satisfactory.

-20179 casting (Pg. 36, 37, 38)

The above casting is critical in bending at Sect. A-A, from the high hook & sway brace loads of Cond. "5". In computing the bending moment at this section, an unnecessarily conservative value of $d = 0$ for the relative-stiffness parameter was chosen for the original analysis. Considering the added support afforded by the inner tank shell and foam filler bonding, a value of $d = 30$ may safely be used in finding the required bending coefficients.

Moment coefficients for R_z (on ϵ) and S (2L away), per Fig. 11, T.N. "927,

$$\text{For } R_z, \quad c_m = .193$$

$$\text{For } S, \quad c_m = .019$$

PREPARED	NAME <u>R. M. Hill</u>	DATE <u>10-11-62</u>	FLETCHER AVIATION CORPORATION	PAGE	1 of 1
CHECKED			TITLE <u>APPENDIX "A"</u>	MOEST. <u>11514</u>	
APPROVED				43.300	REPORT No.

-20179 Casting, cont.

Critical loads from Cond. "5", pg. A-4

$$R_{2A} = 25719 \text{ *}$$

$$S_{2A} = 11065 \text{ *}$$

$$M_{A-A} = (9.00 + .699)(.193 \times 25719 - .019 \times 11065)$$

$$= 46100 \text{ in-lbs} \quad (\text{Pg. 37})$$

$$f_b = \frac{46100 (1.500 - .699)}{1.196}$$

$$= 30870 \text{ *in}^2$$

$$F_{bu} = 41000 \text{ *in}^2 \quad (\text{Pg. 38})$$

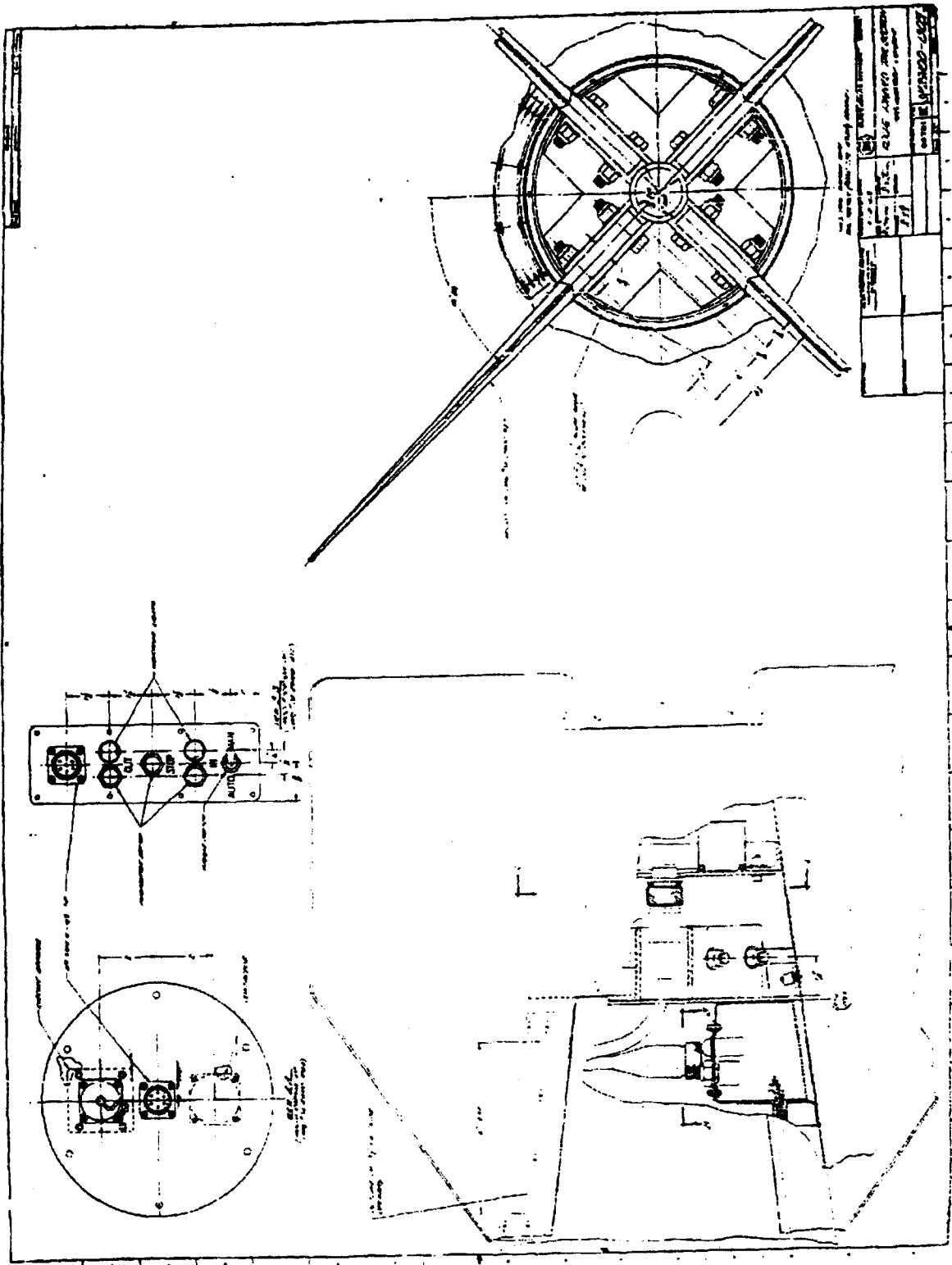
$$M.S. = \frac{41000}{1.33 \times 30870} - 1 = .00$$

APPENDIX B

Optional Four-Fined Tail Section

Drawing SK 29100-1305

Page determined to be Unclassified
Reviewed Chief, RDD, WHS
IAW EO 13526, Section 3.5
Date: 15 APR 2013



~~AD- 346750~~
~~SECURITY REMARKING REQUIREMENTS~~
~~DOD 5200.1-R, DEC 78~~
~~REVIEW ON 24 OCT 83~~

Page determined to be Unclassified
Reviewed Chief, RDD, WHS
IAW EO 13526, Section 3.5
Date: 11 5 APR 2013